UNIVERSIDAD CARLOS III DE MADRID

DOCTORAL THESIS

TRANSIENT STABILITY CONSTRAINED OPTIMAL POWER FLOW: IMPROVED MODELS AND PRACTICAL APPLICATIONS

Author:

Ignacio Antonio Calle

Advisors:

Dr. Edgardo Daniel Castronuovo

Dr. Pablo Ledesma Larrea

Department of Electrical Engineering

Leganés (Madrid), March 2015

DOCTORAL THESIS

TRANSIENT STABILITY CONSTRAINED OPTIMAL POWER FLOW: IMPROVED MODELS AND PRACTICAL APPLICATIONS

Author: Ignacio Antonio Calle

Advisors: Dr. Edgardo Daniel Castronuovo

Dr. Pablo Ledesma Larrea

Tribunal:

Signature

President: George Kariniotakis

Member: Gumersindo Queijo García

Secretary: Mª Ángeles Moreno Lopez de Saá

Qualification:

Leganés (Madrid), March 2015

"O somos capaces de destruir con argumentos las ideas contrarias, o debemos dejar que se expresen. No es posible destruir ideas por la fuerza, porque esto bloquea cualquier desarrollo libre de la inteligencia."

Frase atribuida a Ernesto "Che" Guevara.

Agradecimientos

Ante todo, y como no deseo olvidarme de nadie, vaya mi agradecimiento a todos aquellos que día tras día me han dado su apoyo y han contribuido a generar un ambiente de trabajo ameno en esta universidad que, poco a poco, se ha ido convirtiendo en mi segunda casa.

En particular quiero dar las gracias:

A Edgardo y Pablo, por darme la posibilidad de realizar los estudios de doctorado que concluyen con este trabajo y que, sin su ayuda, no habría podido culminar.

A Álvaro, Dianita, Sandra y Lorenzo, amigos cosechados durante estos años en Europa y que, seguramente, me acompañarán toda la vida.

A mis amigos en Argentina, a quienes he postergado durante todos estos años y que, sin embargo, en cada vuelta a la Pacha Mama han estado ahí para compartir una charla mate mediante.

En especial quiero agradecer a mi familia, Papo, Viejita y Mary que, a la distancia, me han dado su apoyo incondicional. Este logro es para ellos.

Summary

Transient Stability Constrained-Optimal Power Flow (TSC-OPF) is a useful tool to calculate the optimal operating point of a power system, while ensuring its stability after severe disturbances. The aim of this thesis is to advance in the development of an effective tool for economic and dynamic power system security assessment. Starting from the TSC-OPF models presented in the literature, the goal is to improve the representation of the dynamics of the systems in practical situations, implementing similar models to those used in dynamic simulations as usually performed by power system operators.

In order to achieve these objective, a synchronous generator dynamic transient *dq* axes model is implemented, with an excitation system and a turbine governor. The dynamic trajectories of all generators are retained in the optimization process. In addition, a model of High Voltage Direct Current (HVDC) link is implemented, modelling the dynamic response of the device to disturbances in the AC network. Conventional solvers are used to obtain the solution of the TSC-OPF.

The models of TSC-OPF include equations for conventional power flow, operation technical constraints, technical limitations of the power system equipment and a set of differential equations describing the system model for transient stability analysis. For discretizing these differential equations, the trapezoidal rule is used.

Several studies are performed: optimal economic dispatch ensuring the transient stability of the system; maximum loadability of the system; optimization of the dynamic response of the HVDC link; and economic effect of fault clearing time on the generation cost.

The application of the proposed TSC-OPF to various cases of study shows the effectiveness of the formulation and the feasibility of its application to real problems.

Resumen

Esta tesis aborda el problema del Flujo de Potencia Óptimo con Restricciones de Estabilidad Transitoria (TSC-OPF, en inglés), una herramienta útil para determinar el punto de operación óptimo de un sistema de potencia a la vez que se garantiza su estabilidad frente a grandes perturbaciones. El propósito de esta tesis es colaborar en la obtención de una herramienta útil para la evaluación económica y de seguridad dinámica del sistema de potencia. A partir de los modelos de TSC-OPF existentes en la literatura, el objetivo propuesto es mejorar la representación de la dinámica de los sistemas, implementando modelos similares a los utilizados en las simulaciones dinámicas realizadas habitualmente por los operadores del sistema de potencia.

Para conseguir estos objetivos se ha implementado un modelo dinámico transitorio de generador síncrono en ejes *dq*, en el que se incluye un sistema de excitación y un control de velocidad de la turbina, reteniendo las trayectorias dinámicas de todos los generadores durante el proceso de optimización. Además, se ha implementado un modelo de enlace de alta tensión en corriente continua, representando el comportamiento dinámico de dicho dispositivo frente a perturbaciones en la red de corriente alterna. Se han utilizado programas convencionales para calcular la solución del TSC-OPF.

Los modelos propuestos de TSC-OPF incluyen las ecuaciones del flujo de potencia convencional, las restricciones técnicas de operación, las limitaciones técnicas de los equipos de un sistema de potencia y el conjunto de ecuaciones diferenciales que describen el modelo del sistema para análisis de estabilidad transitoria, discretizadas por medio de la regla trapezoidal.

Varios estudios son realizados: despacho económico óptimo que asegure la estabilidad transitoria del sistema; cálculo de la máxima carga del sistema; optimización de la respuesta dinámica del enlace en continua; y efecto económico, sobre el despacho de generación, del tiempo de actuación de las protecciones.

La aplicación de los modelos propuestos de TSC-OPF a diversos casos de estudio muestran la eficacia de la formulación y la viabilidad de usar este tipo de algoritmos en problemas reales.

Contents

List of figures

List of tables

Chapter 1.

Introduction

In this chapter, the objectives that motivate the study and development of this work are presented. Also, the organizational structure of the thesis is introduced.

Contents

1.1 Motivation

Currently, electricity markets determine solutions for the dispatch of generators based on economic dispatch models that, generally, do not explicitly consider transient stability constraints. However, the system operator must ensure its safety during operation in real time, so it should study the feasibility of the operation also considering dynamic criteria. The increasing competition between producers in electric systems leads to operate near the operational limits of the equipment. In this scenario, dynamic analyses have become essential for secure operation of the system.

Possible stability problems may involve modifications in the market solutions, changing the power delivered by the generator, adjusting power flow control devices, and acting on the load consumption by shedding it. Today, dynamic studies are performed in all electric systems before authorizing the real operation. At least, heuristic trial-and-error methods, based on engineering experience, are used to guarantee the stability of the operation [1], [2]. Generally, it is expected that the security analysis modifies as little as possible the solution of the original economic dispatch. To ensure that the security settings minimally impact on the solution provided by the market, it would be desirable to model jointly the system behaviour and the security constraints, solving these problems in only one step.

Until recently, the dynamic of a power system could not be incorporated into a mathematical optimal power flow (OPF) formulation using a transient stability model, mainly due to the capacity of computers and mathematical solvers. However, the advance in computing resources and the consolidation of

optimisation methods for the solution of large-scale nonlinear problems, today allow the representation of the system dynamics in optimisation models [3]. The aforementioned advances and the necessity of obtaining transparent markets are the basis for the Transient Stability Constrained-Optimal Power Flow (TSC-OPF) methods, which are optimization problems that simultaneously include both static and dynamic constraints in the same formulation. TSC-OPF has received growing interest in the last decade as a tool for preventing transient instability at a low cost, thanks to the combination of economic objectives, steady-state equations and dynamic simulations into a unique model [4]-[6].

In the present work, two of the most applied approaches on electricity markets and stability analysis are combined. Firstly, a complete OPF formulation is used to calculate the economic dispatch of generators, including voltage, current and power flow constraints. The optimal operating point is calculated depending on the economic parameters of the generation. Secondly, the transient stability is studied using traditional methods, such as time-domain simulations. The dynamic equations are discretized using the trapezoidal method, and the resulting security constraints are explicitly included into the full OPF formulation as equality and inequality constraints. Moreover, the applicability of the proposed methods is a main concern, leading to the use of realistic systems, well-established models of generators and off-the-shelf programming solvers in the progress of the work.

1.2 Purpose and objectives

The purpose of this thesis is to obtain a useful tool for economic-dynamic security assessment. Starting from the existing TSC-OPF models in the literature, the aim is to improve the representation of the dynamics of the systems, implementing models close to those used in dynamic simulations routinely performed by transmission system operators.

To accomplish the work, the following specific objectives are defined:

- Perform an actualized review of the state-of-the-art related to the TSC-OPF problem.
- Develop an innovative algorithm to calculate the optimal operation of a system, explicitly taking into account transient stability constraints and using the classic dynamic model of synchronous generator.
- Improve the nowadays conventional TSC-OPF formulations, implementing more advanced models of the main elements of the power system. In particular:
  - Include transient *dq*-axes dynamic model of the synchronous generator into the TSC-OPF. This model makes it possible to represent the electromagnetic transients in the rotor, and represents a major improvement in dynamic model accuracy.
  - Include a turbine governor and an excitation system in the model.
  - Model a HVDC link, and study its effect on the TSC-OPF.
  - Include multiple contingencies in the analysis.
- Apply the previous models to different realistic cases, studying the problems of:
  - Optimal economic dispatch, ensuring the transient stability of the system.
  - Maximum loadability of the system, simultaneously considering both steady-state and stability constraints.
  - Economical effect on the dispatch of the fault clearing time.

1.3 Thesis structure

In Chapter 2, a brief introduction to the phenomenon of transient stability and optimal power flow is presented. A review of the state-of-the-art of the most

important researches carried out in relation to the TSC-OPF problem is included in this chapter.

Chapters 3, 4, 5 and 6 have been written as independent articles with its own abstract, introduction, notation and bibliography, and can be independently read. Each one corresponds to results obtained sequentially in the development of this thesis, and these have been published or submitted to journals indexed. Chapters 5 and 6 are still in revision process by the journals.

In Chapter 3, an algorithm to calculate the optimal operation of a system with different load levels and fault clearing times is proposed. The algorithm simultaneously considers both economic and stability constraints. The proposed formulation is evaluated on the Majorca and Minorca islands power system, a small, isolated system with low inertia. A conventional optimisation tool is used to solve the proposed optimisation problem. Results of this chapter were published in [7].

Chapter 4 presents an optimization model to calculate the maximum loadability of a system, when subjected to severe faults. The model simultaneously considers steady-state and dynamic constraints, with the dynamics of the generators explicitly included in the optimization formulation. The armature current and the field current heating limits of the synchronous generators are also included. Results of this chapter were published in [8].

Chapter 5 presents improved models from those used in the algorithm of the previous two chapters. The classic model of the synchronous generators is replaced by the transient *dq*-axes model, which makes it possible to represent the transient electromagnetic rotor machine. Furthermore, it is proposed a dynamic model of the HVDC-LCC link, seen from the inverter AC bus, to analyze the effects of the dynamic response of this device on the transient stability of the system.

Chapter 6 proposes a new TSC-OPF model that includes a transient synchronous generator *dq*-axes model. This improvement makes it possible to represent the electromagnetic transients in the rotor. The proposed optimization

model includes also an excitation system and a turbine governor, and can perform multi contingency analysis. The model is solved using a non-heuristic Interior Point algorithm on GAMS.

Finally, the main conclusions, contributions and publications are found in Chapter 7.

1.4 References

[1] D. Chattopadhyay and D. Gan, "Market dispatch incorporating stability constraints", International Journal of Electrical Power & Energy Systems, vol. 23, no. 6, pp. 459–469, Aug. 2001.

[2] H. R. Cai, C. Y. Chung and K. P. Wong, "Application of Differential Evolution Algorithm for Transient Stability Constrained Optimal Power Flow", IEEE Transactions on Power Systems, vol. 23, no. 2, pp. 719–728, 2008.

[3] C. F. Moyano and E. Castronuovo, "Non-Linear Mathematical Programming Applied to Electric Power Systems Stability", in Optimization advances in electric power systems, Nova Science Publishers, Inc, 2009.

[4] Y. Xu, Z. Y. Dong, Z. Xu, R. Zhang and K. P. Wong, "Power system transient stability-constrained optimal power flow: A comprehensive review", in 2012 IEEE Power and Energy Society General Meeting, 2012, pp. 1–7.

[5] F. Capitanescu, J. L. Martinez Ramos, P. Panciatici, D. Kirschen, A. Marano Marcolini, L. Platbrood and L. Wehenkel, "State-of-the-art, challenges and future trends in security constrained optimal power flow", Electric Power Systems Research, vol. 81, no. 8, pp. 1731–1741, Aug. 2011.

[6] Yue Yuan, J. Kubokawa and H. Sasaki, "A solution of optimal power flow with multicontingency transient stability constraints", IEEE Transactions on Power Systems, vol. 18, no. 3, pp. 1094–1102, 2003.

[7] I. A. Calle, E. D. Castronuovo and P. Ledesma, "Optimal re-dispatch of an isolated system considering transient stability constraints", International Journal of Electrical Power & Energy Systems, vol. 44, no. 1, pp. 728–735, Jan. 2013.

[8] I. A. Calle, E. D. Castronuovo and P. Ledesma, "Maximum loadability of an isolated system considering steady-state and dynamic constraints", International Journal of Electrical Power & Energy Systems, vol. 53, pp. 774–781, Dec. 2013.

Chapter 2.

Literature review

This section contains a review of the literature and the state-of-the-art of some topics related to the Thesis. The evolution of the problem of TSC-OPF is specially considered, with emphasis on the techniques used for representing the transient restrictions, the methods used to solve the problem, and the mathematical and computational advances implemented to achieve a more efficient resolution.

Contents

2.1 Stability of power systems

The stability of power systems was recognized as a problem since (approximately) 1920, when the structure of the systems consisted of generating plants located at relatively large distances from the load centres. These early stability problems, often as a result of insufficient synchronizing torque, gave rise to the first cases of transient instability [1].

The stability is a property of an electrical system, which depends on the operating point and on the disturbance to which it is subjected. The same electric network, subject to the same disturbance, can be stable at an operational point and unstable at another. Similarly, a network in an operating point can be stable after a perturbation and unstable after another. That is why stability studies often require the analysis of a large number of cases, to simulate a set of disturbances of interest at different points of the system and in different states of operation [2], [3].

Despite the different categories of stability that have emerged in power systems, transient stability remains a basic and important issue in the design and operation of the grid. While the operation of many power systems is limited by phenomena such as voltage stability or small-signal angular stability, most of

the systems are prone to transient instability in certain conditions or contingencies and, therefore, the understanding and analysis of the transient stability of a system is significant [4].

At first, it is necessary to define the stability for a power system:

> *"Power system stability is the ability of an electric power system, for a given initial operating condition, to regain a state of operating equilibrium after being subjected to a physical disturbance, with most system variables bounded so that practically the entire system remains intact."* [1].

A modern power system is a system whose dynamic behaviour is influenced by a wide range of devices with different characteristics and responses. The system operation experiences a constant imbalance, depending on the network topology, the status of the system and the type of disturbance to which it is (or it can be) subjected, leading to different forms of instability.

Essentially, the stability of the power system is a unique problem. However, the different forms of instability that the system may suffer cannot be correctly understood and effectively treated if they are considered jointly, due to the high dimension and complexity of the problem. This results on the need for a classification of stability problems, which helps to a) create simplifying hypothesis; b) analyze the specific types of problems using an appropriate level of detail in the representation of the systems; and c) use adequate analytical techniques to each one of the stability problems [2].

This classification has been generally established based on the following considerations [1], [2]:

- *"The physical nature of the resulting mode of instability, as indicated by the main system variable in which instability can be observed."*
- *"The size of the disturbance considered, which influences the method of calculation and the prediction of stability."*

- *"The devices, processes, and the time span that must be taken into consideration in order to assess stability."*

Fig. 2.1 presents an overview of stability problems in power systems, with identification of categories and subcategories [1].

To simplify the calculations, in all transient stability studies the following assumptions are usually used:

1. Only currents and voltages at the grid frequency in the stator windings and in the power system are considered. Therefore, DC components, electromagnetic transients and harmonics are not considered.
2. Symmetrical components, to represent unbalanced faults, are used when necessary.
3. It is assumed that the voltage in generators is not affected by any variation in the speed of the machine.

These assumptions make it possible the use of phasorial algebra and power flow techniques to calculate the electrical variables at the transmission network, using parameters calculated at the grid frequency [5].

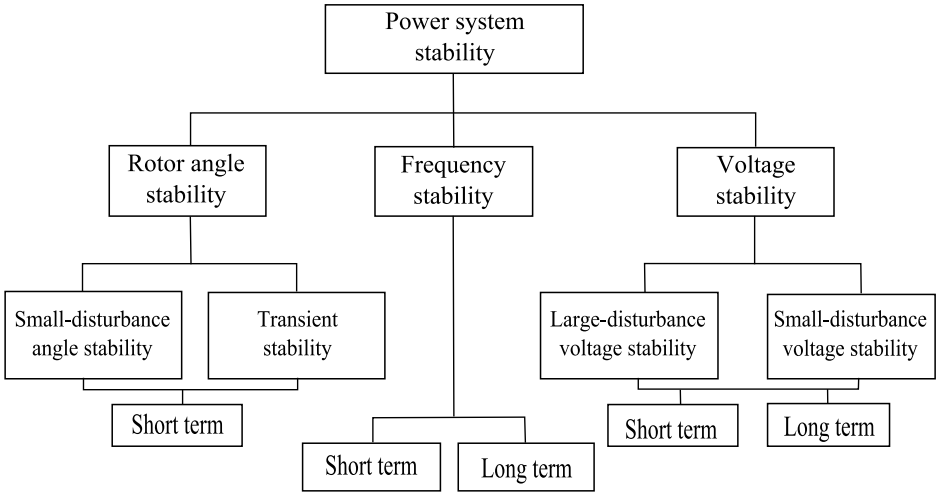

Fig. 2.1. Classification of power system stability problems [1].

The rotor angle stability, related to transient stability, is briefly considered below.

2.1.1 Rotor angle stability

Rotor angular stability refers to the ability of synchronous machines of an interconnected power system, to remain in synchronism after being subjected to a disturbance. This type of stability depends on the ability to maintain or restore the balance between electromagnetic and mechanical torques at each synchronous machine. The instability is often manifested as increasing angular oscillations of one or more than one generators, leading to the loss of synchronism with the other system generators.

The problem of angular stability of the rotor involves the study of the electromechanical oscillations. The most important factor of this problem is how the electrical power output of the synchronous machines varies with the angle of their rotor. In steady state conditions, there is equilibrium between the input mechanical torque and the output electromagnetic torque, and the speed remains constant. When a disturbance is applied to the system, this balance is disrupted, causing the deceleration or acceleration of the rotors of the machines. If a generator temporarily rotates slower than the other, the angular position of its rotor will be delayed with respect to the faster machine, and the resulting angular difference will transfer part of the load from the slow to faster machine. This effect depends on the power-angle relationship, and tends to reduce the speed difference and, thus, the angular separation [1], [2].

After a disturbance, the change in the electromagnetic torque of a synchronous machine can be decomposed into:

- A synchronizing torque component, in phase with the angular deviation of the rotor.
- A damping torque component, in phase with the speed deviation.

The stability of the system depends on the existence of the two torque components in each one of the synchronous machines. An insufficient synchronizing torque results in aperiodic instability, while the lack of damping torque results in oscillatory instability [2].

2.1.2 Transient stability

Transient stability is the ability of a power system to maintain synchronism when it is subjected to a severe disturbance, such as a fault in the transmission system, loss of generation or loss of a significant amount of load. In these circumstances, the power system can respond with large excursions of the rotor angle of the generators. These large excursions, together with the high nonlinearity of the relation between electromagnetic torque and rotor angle, makes it not possible the linearization of the system equations [1], [2].

Transient stability depends on both the initial state of system operation and the severity of the disturbance. Instability is usually visible in the first oscillation, associated with a local mode. However, in large power systems, instability could be the result of the superposition of slow inter-area oscillation modes and local modes, which can cause a large excursion of the rotor angles after the first oscillation [1].

Normally, transient stability analysis is performed using one of the following techniques, being the first one the technique used in the present work:

- Time-domain simulation: is the resolution of the differential-algebraic equations (DAE) that represent the dynamics of the system using numerical methods.
- Direct Methods: such as those based on Lyapunov functions or the equal area criterion.
- Hybrid methods: the problem is solved by including the calculation of Lyapunov functions in time-domain simulations.

Time-domain simulations make it possible to observe the evolution of the system variables over time. A common practice to detect loss of synchronism is to check if the rotor angle deviation, or angular speed deviation, between machines remains within a specific range during the simulation. This range is usually established using heuristics and may depend on the system size.

Graphically, the responses of a stable system to a disturbance can be seen, for example, in Fig. 2.2 and Fig. 2.3. In the first one, it can be observed how the rotor angles of the generators oscillate, but remain bounded. During the fault, angles grow and rotor speeds increase. After the fault clearance, it is observed that the angles oscillate, showing a trend to recovery the initial (or other) equilibrium state.

Fig. 2.3 shows angles jointly growing indefinitely. The reason for this increase is that, once recovered the synchronism between the generators, the system frequency is not the same as the original one.

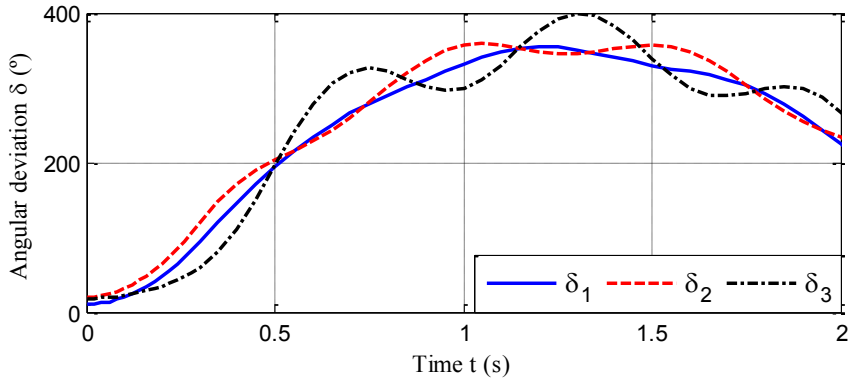

Fig. 2.2. Stable case.

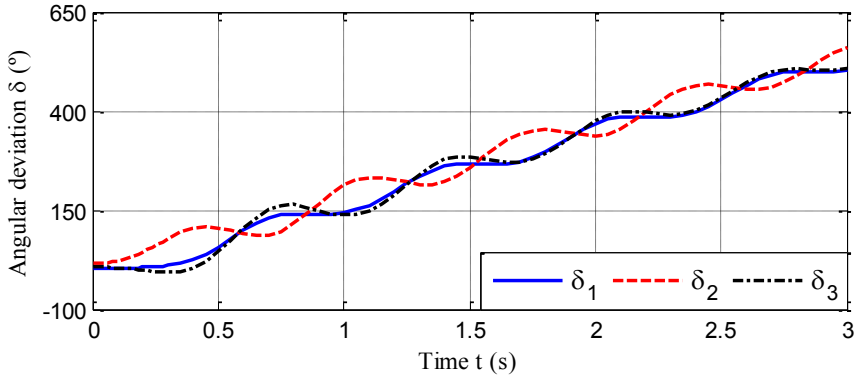

Fig. 2.3. Stable case with frequency deviation.

In Fig. 2.4, an unstable case can be seen. Generator 3 loses synchronism with respect to 1 and 2, after about 0.5 s from the fault clearance.

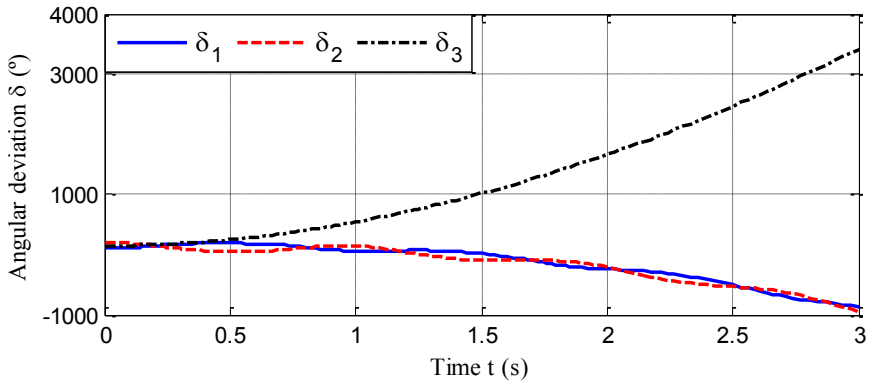

Fig. 2.4. Unstable case.

In transient stability studies, the time frame of interest is generally 3 to 5 s, after the disturbance. It may be extended to 10 or 20 s for very large systems with dominant inter-areas oscillations. In this case, the effects of the control systems of generating units must be considered, because they may change their dynamic behaviour [1], [2], [5].

In practice, the most common method for transient stability analysis of power systems is the representation of the set of differential- algebraic equations governing the dynamics of the elements of the system, followed by its numerical integration with the help of computer tools.

2.1.3 Numerical integration methods

In transient stability analyses, the power system is represented by a set of differential-algebraic equations that can be written in the form:

$$\begin{bmatrix} \dot{\mathbf{x}} \\ 0 \end{bmatrix} = \begin{bmatrix} F(\mathbf{x}) \\ G(\mathbf{x}) \end{bmatrix} \tag{2.1}$$

where $\mathbf{x}$ is the vector containing the temporal variables $\mathbf{x}_t$, algebraic variables $\mathbf{x}_s$ and control variables $\mathbf{x}_c$; $\mathbf{x} \in \Re^{n_x}$. Function F is a nonlinear function associated with vector $\mathbf{x}$, representing differential equations (e.g., those associated with the dynamics of synchronous generators and loads and their controls), $F : \Re^{n_x} \to \Re^{n_x}$; and function G represents the set of algebraic

equations, (e.g., power balances in the transmission network and algebraic equations of the synchronous machines).

The first part of system (2.1) results in a set of nonlinear ordinary differential equations, with initial conditions $\mathbf{x}_0$ at t_0 determined in the pre-disturbance steady state [2]. They can be written as:

$$\frac{d\mathbf{x}}{dt} = F(\mathbf{x}) \quad \text{with } \mathbf{x}(t_0) = \mathbf{x_0} \tag{2.2}$$

In the method used in this Thesis, the initial conditions are calculated in the TSC-OPF simultaneously with the integration of the nonlinear differential equations (2.2). The methods used to solve (2.2) are generally classified in two categories: explicit and implicit methods.

Explicit methods make it possible to calculate the vector of variables at each instant, depending on the value of the variables in previous moments. The simplest explicit method is due to Euler; however, this method has unsatisfactory properties of accuracy and numerical stability. In practice, other more advanced explicit methods, such as Runge-Kutta of second, third or fourth order, are used. Runge-Kutta methods approximate the solution of (2.2) using a Taylor series expansion of the original equations. In general, these algorithms do not require the explicit evaluation of derived equations higher than the first order. Explicit methods are easy to implement, but they are considered not numerically stable [6], [7].

Numerical stability is related to the stiffness of the set of differential equations representing the system and it is associated with the range of the time constants. Thus, when simultaneously representing fast and slow phenomena, small time constants require small integration steps to preserve the stability of the numerical integration. The presence of large time constants forces to simulate long periods of time to observe the response of the system. The simultaneous presence of small and large time constants leads to mathematically stiff systems, which consume large computational resources [2], [3], [8].

Implicit methods emerge as a response to the problem of representation of mathematically stiff systems. These methods use interpolation functions for the solution of (2.2), requiring the equations to be evaluated in future time steps in order to calculate the state variables. The solution of (2.2), for **x** at $t = t_1 = t_0 + \Delta t$, can be expressed in integral form as:

$$\mathbf{x_1} = \mathbf{x_0} + \int_{t_0}^{t_1} F(\mathbf{x})\, d\tau \tag{2.3}$$

One of the simplest and more effective methods of implicit integration for solving (2.3) is the trapezoidal rule, consisting in the resolution of (2.3) by using its approximation by trapezoids of a wide Δt. In this way, the value of $\mathbf{x}_1$ is calculated as:

$$\mathbf{x_1} = \mathbf{x_0} + \frac{\Delta t}{2}\left[F(\mathbf{x_0}) + F(\mathbf{x_1})\right] \tag{2.4}$$

In implicit methods state variables are not explicit, as shown in (2.4). Iterative processes are often applied to solve the equations. Implicit methods are particularly suitable for TSC-OPF problems, because the latter are usually iteratively solved. The stiffness of the system does not affect the stability of these integration methods [2], [3], [8].

2.2 Optimal Power Flow

The concept of Optimal Power Flow (OPF) was introduced in the ‘60s [9], [10], and is today considered one of the most powerful tools for planning and operation of electrical power systems. In operation studies, OPF makes it possible to determine optimal control actions and optimal operation points, considering operating restrictions. In planning stages, OPF is used to determine optimal scenarios for future developments of the power system [11].

In general, OPF is a problem of nonlinear programming that calculates the optimal system solution, minimizing a desired objective function and subject to equality and inequality constraints [12].

In a standard form, OPF can be formulated as

$$\min \quad f(\mathbf{x}) \tag{2.5}$$

$$\text{subject to} \quad G(\mathbf{x}) = 0 \tag{2.6}$$

$$H(\mathbf{x}) \leq 0 \tag{2.7}$$

where $f(\mathbf{x})$ is the objective function; $G(\mathbf{x})$ are equality constraints; $H(\mathbf{x})$ are inequality constraints.

The most common objective functions include minimizing the generation cost, minimize the loss of active power, minimize generation emissions, maximize system security, etc. [13], [14].

The restrictions of an OPF model are divided into equality and inequality constraints, (2.6) and (2.7). As examples, the set of equality constraints can include active and reactive power flow balances at each bus of the grid, while inequality constraints can represent technical and operating limits in the system.

The OPF was expanded in the '70s to include safety criteria [15]. The resulting optimization problem includes additional restrictions related to the operating conditions of the system when is disturbed. In this case, the objective is to ensure that the system operates properly under the pre and post-disturbance conditions [11].

Twenty years ago, the meeting "*Challenges to OPF*" (organized by IEEE, in 1995 [16]) proposed the challenge of including stability restrictions into the OPF formulation, a necessary objective for future optimal system operation.

2.3 Transient Stability Constrained-Optimal Power Flow

The Transient Stability Constrained-Optimal Power Flow (TSC-OPF) can be used in the operation of the system to determine a stable operating point facing one or more than one given disturbances. In power system planning, for example, it can be used to calculate the best way to ensure stability facing demand increases, or to obtain the stability limits of the system dealing with disturbances.

In general, the difficulties related to TSC-OPF can be classified in two groups:

1 How to include the differential equations that represent the transient stability in a conventional OPF. On this field, basically the following alternatives are found:

   a. Evaluation of transient stability in the traditional way, such as representing the system dynamics through the rotor swing equation, and solution of the resulting problem through time-domain simulations;

   b. Use of direct methods for transient stability assessment, such as the Equal Area Criterion, by applying them to an equivalent system consisting only in two rotating machines. Another alternative direct method that has been used is the representation of the problem of transient stability by energy functions such as Lyapunov;

   c. Application of hybrid methods combining the previous two to assess the transient stability of the system.

2 How to solve the optimization problem after the transient stability constraints are included, being found the following:

   a. Classic programming algorithms, such as linear programming (LP), interior point methods (IPM), etc.;

   b. Modern heuristic programming techniques based on evolution algorithm, such as particle swarm optimization (PSO); genetic algorithms (GA); and differential evolution (DE).

Based on these two groups, here it is presented a review of the main proposals found in the literature to include transient stability constraints in the OPF, as well as the methods to solve the resulting TSC-OPF model.

2.3.1 Traditional methods

In [17], (2.1) is rewritten to include the boundaries of the system equipment by using inequality constraints. It is obtained:

$$\dot{\mathbf{x}}(t) = F(\mathbf{x}) \tag{2.8}$$

$$G(\mathbf{x}) = 0 \tag{2.9}$$

$$H(\mathbf{x}) \leq 0 \tag{2.10}$$

where $H(\mathbf{x})$ represents operating conditions, such as upper and lower limits of generator powers, voltages, etc.

In (2.8)-(2.10) it is assumed that the first order partial derivatives of all functions exist, and that they are continuous. To study transient stability for a given k^{th} disturbance, the power system represented in (2.8)-(2.10) is subject to configuration changes, which can be represented in three stages:

- The pre-fault stage at $t = t_0$, with all circuits in service, which is used to calculate the initial conditions of the dynamic variables and the optimal point for the algebraic variables.

$$F(\mathbf{x}_0) = 0 \tag{2.11}$$

$$G(\mathbf{x}_0) = 0 \tag{2.12}$$

$$H(\mathbf{x}_0) \leq 0 \tag{2.13}$$

- The fault stage, at $t \in (0, t_{ccf}^k]$, in which the voltage at the fault point is zero.

$$\dot{\mathbf{x}}^k = F_1^k(\mathbf{x}^k) \quad \text{with initial value } \mathbf{x}_0 \tag{2.14}$$

$$G_1^k(\mathbf{x}^k) = 0 \tag{2.15}$$

$$H_1^k(\mathbf{x}^k) \leq 0 \tag{2.16}$$

- The post-fault stage, for $t \in (t_{ccf}^{k}, t_{sim.}]$, in which the disturbance has been cleared by protection systems.

$$\dot{\mathbf{x}}^{k} = F_2^{k}\left(\mathbf{x}^{k}\right) \quad \text{with initial value } \mathbf{x}_{ccf}^{k} \tag{2.17}$$

$$G_2^{k}\left(\mathbf{x}^{k}\right) = 0 \tag{2.18}$$

$$H_2^{k}\left(\mathbf{x}^{k}\right) \leq 0 \tag{2.19}$$

where $\mathbf{x}_0$ is defined as the operation point of the power system, being that point that satisfies (2.8) and (2.9), complying with the operating conditions (2.10); k is a parameter indicating the k^{th} event of disturbance; t_{ccf}^{k} is the time to clearance by the k^{th} disturbance; $t_{sim.}$ is the study period.

Equations (2.11)-(2.19) represent the model of transient stability for a power system proposed in [17]. Thus, the TSC-OPF can be defined as a nonlinear optimization problem in the functional space, with algebraic and differential constraints, as follow:

$$\min \quad f\left(\mathbf{x}_0\right) \tag{2.20}$$

$$\text{subject to } \; G^{0}\left(\mathbf{x}_0\right) = 0 \tag{2.21}$$

$$H^{0}\left(\mathbf{x}_0\right) \leq 0 \tag{2.22}$$

$$\dot{\mathbf{x}}^{k} = F^{k}\left(\mathbf{x}^{k}\right) \quad \text{with initial value } \mathbf{x}_0^{k} \tag{2.23}$$

$$G^{k}\left(\mathbf{x}^{k}\right) = 0 \tag{2.24}$$

$$H^{k}\left(\mathbf{x}^{k}\right) \leq 0 \tag{2.25}$$

with $\mathbf{x}_0$, $\mathbf{x}_t^{k}$ as variables, and for all $k = 1 \ldots m$ and $t \in [0, t_{sim.}]$.

G^0 and H^0 are the system equations for the pre-fault state; F^k, G^k and H^k are the functions corresponding to the equality and inequality constraints during

the transient period (during and after disturbance), for the k^{th} state of disturbance.

The proposed TSC-OPF is not easy to solve. The simulation interval $[0, t_{sim.}]$ can be discretized in infinite points, resulting in infinite dimensional variables $\left(\mathbf{x}_t^k\right)$ and infinite equality and inequality constraints, (2.24) and (2.25) respectively. In practice, the simulation interval is discretized into a finite number of points, making it possible the resolution of the problem.

The problem (2.20)-(2.25) implies that, at least, a disturbance is present. Usually, stability constraints include variations in the rotor angle and deviations in the angular velocity of the generators, although other restrictions can be also considered, such as over-voltages and sags, power flow limits by lines, power swings, etc.

In [17]-[19], the previous TSC-OPF is transformed from the functional space to the Euclidean space, through a transcript of constraints by techniques of functional transformation. This technique reduces the dimension of the problem. In [17], this transformation is justified because the purpose of the TSC-OPF is finding an optimal operating point ($\mathbf{x}_0$) with finite dimensions that satisfy all constraints at the end of the simulation frame. Therefore, the authors do not calculate in detail the trajectories of the variables for the perturbation, making it impossible to evaluate the intermediate behaviour of the variables. Applying the technique of transcription detailed in [17] to (2.20)-(2.25), an optimization problem in the Euclidean space is obtained, expressed as:

$$\min \quad f\left(\mathbf{x}_0\right) \tag{2.26}$$

$$\text{subject to} \quad G^0\left(\mathbf{x}_0\right) = 0 \tag{2.27}$$

$$H^0\left(\mathbf{x}_0\right) \leq 0 \tag{2.28}$$

$$H^k\left(\mathbf{x}_0\right) \leq 0 \tag{2.29}$$

The TSC-OPF problem, reformulated in (2.26)-(2.29), has only ($\mathbf{x}_0$) as variables, with finite dimensions. Equations (2.26)-(2.29) can be viewed as the search problem of the optimal initial value of the variables ($\mathbf{x}_0$) for the specified disturbances; this problem can be solved by using standard optimization techniques. In [17], the Jacobian matrices of the transient stability constraints are also obtained, and two calculation algorithms are given, performed *ad-hoc* and based on the relaxation scheme, by exploiting the intrinsic properties of transient stability analysis of power systems. In [18], the Jacobian and Hessian matrices of the transient stability constraints are obtained, implementing a nonlinear direct method of Primal-Dual Interior Point with quadratic convergence. Furthermore, potential energy boundary surface method is adopted to detect angle instability [19].

A different approach is utilised by the authors of [20] and [21], in which the efforts are not aimed to reduce the size of the optimization problem, but to represent and integrate the dynamic equations of the system into the TSC-OPF model. Thus, in the transient stability model of the power system (2.11)-(2.19), the differential and algebraic equations are transformed into a set of numerically equivalent algebraic equations, using appropriate rules. This set of algebraic equations is then introduced into the OPF as transient stability constraints, resulting in a problem of large dimension.

In this new approach, the authors of [20] performed a discretization of the time domain simulations integrating them by using trapezoidal rule. Moreover, the linearization of all OPF constraints (including stability constraints) and the objective function is used. The authors developed the model algorithm based on the successive linear programming method, whose solution must satisfy the Karush-Tucker optimality condition associated with the original nonlinear problem.

In [22] and [23], the authors applied the same discretization model of trapezoidal rule, without linearization of equations. In [22], the study was performed taking into account multiple contingencies in the system and, as result, more expensive generators were dispatched to ensure stability. In the

solution, the economic dispatch cost is increased with respect to the consideration of a single contingency. In their work, the authors achieved a significant reduction in the equality constraints, and therefore in the CPU time, by using the concept of reduced admittance matrix, which only considers the internal nodes of the generators during the transient period. Furthermore, to solve the problem of TSC-OPF with multi contingencies an interior point method created ad-hoc is implemented. In [23] the same concept to reduce the size of the problem to be optimized is used.

In order to improve the computational efficiency of the discretized TSC-OPF, in [24]-[27] the authors propose mathematical manipulations resulting in improved numerical discretization methods. In [24] and [25], the keys to the proposed improvements are, firstly, to consider the relatively small number of degrees of freedom of the TSC-OPF, which makes it suitable for the solution using a technique of Reduced-Space Interior-Point method (RIPM). Secondly, to consider the truncation error of the numerical integration algorithm, representing the differential equations as inequality constraints rather than as equality constraints. The latter consideration decreases by nearly 50 % the size of the primal-dual linear system and improves the computational efficiency of the TSC-OPF algorithm, based on the interior point method.

In [26], a RIPM parallel algorithm with high computational efficiency for multiple contingencies TSC-OPF problems is presented. A two-level parallelism has been developed to maximize the computing power of a Beowulf cluster, equipped with multi-core CPUs [28], [29]. First, several compute intensive steps of the TSC-OPF algorithm are decomposed for contingencies, with using mathematical equivalent transformations. Corresponding computing tasks are assigned, stored and processed on different nodes. Second, the task of distributed computing is accelerated by elemental decomposition on Jacobian matrices, and high performance math libraries are used to maximize the multi-core processors in each node.

In [27], the authors present a model of unit commitment with transient stability constraints achieving the objective of maintaining the transient stability

and economic operation of the system facing contingences. In the proposed model, transient stability constraints are incorporated within the unit commitment. In order to solve efficiently the problem, augmented Lagrangian relaxation, variable duplication techniques and auxiliary-problem principle are used. The original problem is decomposed into two sub-problems: the first one is the traditional unit commitment, and the second one is a TSC-OPF. The first sub-problem is solved by dynamic programming, while the second is solved using a RIPM. An iterative process continues until the duality gap is sufficiently small.

As can be seen, the here called traditional method incorporates directly the limitations of transient stability into the OPF and solves the problem of TSC-OPF as a whole. In this case, the mathematical model of transient stability and the steady-state restrictions of the power system are fully preserved. The main inconvenient of these methods is still the heavy computational burden when working with large systems and more than one contingency. However, as mentioned, this problem is sometimes minimized using parallel processing techniques or faster CPU processors [30].

2.3.2 Direct methods

In [31]-[33], an approach based on sensitivity analysis of the trajectories is proposed, studying the variations on the system variables with respect to small variations of the initial conditions and control parameters. In particular, it is studied the sensitivity of the rotors angle trajectory and/or the angular velocity deviation, due to variations in the dispatched active power. Thus, for each contingency these trajectories are computed together with the dynamic state of the system. In each contingency, the most vulnerable machines, from the stability point of view, are identified and the generation is displaced toward the less vulnerable generator, following the sensitivity of the trajectories already calculated. The former studies choose between moving the most vulnerable generation either to a single machine or to a group of them.

In [34], a great simplification is done, reducing the multi-machine initial model to a two machines model, using the concept of "Single Machine Equivalent" (SIME) and thus decreasing the dimension of the system to be optimized. In this case, the stability of a one-machine infinite bus (OMIB) system is analyzed. In the paper, the analysis based on OMIB is used to estimate the power to change from critical machines to non-critical ones.

Direct methods require less computational resources than traditional methods, because the original set of differential and algebraic equations is drastically reduced. In the direct methods, the main burden of calculation is due to determine the required change of generation. The reduction in the number of generators and equations makes it possible to consider multi-contingencies and more detailed models of the system elements. Also, direct methods can provide more explicit control mechanisms, which can be taken as a reference for system operators and participants in the energy market. However, the direct methods only provide suboptimal and approximate result, since the change of generation is determined by the values obtained by the sensitiveness of trajectories or OMIB calculations, that is, without a complete optimization [30], [35].

Following the concept of model reduction present in [34], in [36] and [37] the OMIB is used to determine the maximum angular deviation. This information is included into the conventional OPF problem to dispatch or re-dispatch generators, and so to find a global approximate optimum by using the SIME method. In this way, a single transient stability constraint is included in the formulation of the conventional OPF to represent the limits of the multi-machine dynamic system. Thus, the original problem is reduced to an optimization problem with very similar dimension to the conventional OPF.

The authors of [38] propose to transforms the rotor angle trajectories of a multi-machine system to the angle space of a single rotor angle trajectory of OMIB equivalent whose stability properties, inferred from the equal area criterion, define the transient stability properties of the multi-machine system. Therefore, the transient stability of the multi-machine system can be controlled

by constraining the OMIB's rotor angle maximum excursion to a value that ensures system transient stability.

In [39] and [40], the SIME model is added to other substantial simplification of the original TSC-OPF problem, using independent dynamic simulations. In this approach, dynamic constraints are removed from the optimization formulation and are implemented in an external simulation algorithm. Based on the simulation results, a unique transient stability constraint is obtained. This constraint is then handled by the optimization algorithm to calculate the optimal steady-state operation point. Since the two algorithms are independently solved, the detail in the machine model and the integration step of the simulation does not affect the size of the optimization model. This approximation significantly reduces the TSC-OPF computational cost and, as a result, makes it possible to implement detailed models of the generators, [40].

2.3.3 Methods based on evolutionary algorithms

In this section, the analysed methods focus their efforts on how to solve the TSC-OPF problem, modelled in some of the above described forms, using modern optimization techniques, genetic algorithms [41], particle swarm optimization [42], differential evolution [43] and others.

Evolutionary algorithms solve the TSC-OPF problem by adopting mechanisms of modern heuristic search. Stability constraints are satisfied by a transient stability assessment in the system modelling, and multiple contingencies can be considered. Due to the characteristic of global search, theoretically it is possible to find the TSC-OPF global optimum. However, they usually require a considerable number of iterations to obtain a sufficiently good solution [30].

Articles [30] and [44] present a recent and more extensive review of methods used to solve the TSC-OPF, including heuristic and conventional ones.

2.4 Conclusions

In recent years an increasing interest about TSC-OPF problems can be observed. Different approaches have proposed, aiming to solve different issues emerging from the inclusion of transient stability constraints into the conventional OPF.

Firstly, research has focused on how to include such restrictions within the OPF model. Solutions as discretizing the differential-algebraic equations representing the model of transient stability in the time-domain, by means of the trapezoidal rule, are used in many cases. To reduce the computational burden, many approximations have been proposed, including reductions in the power system, SIME method, separation between steady-state and dynamic studies, sensitivity analyses, etc. In other cases, energy functions were used to model the transient stability problem.

Secondly, the researchers have focused on how to solve the optimization problem, once transient stability constraints are included. Two great sets of solutions arise: one, based on traditional methods such as linear programming, gradient or interior point methods; other, using modern techniques based on evolutionary algorithms, such as genetic algorithms, particle swarm, etc. Moreover, several researchers have focused on efficiency and computational power, with improvements in the solution algorithms such as the RIPM, parallel processing techniques, costumed-tailored interior point methods, etc.

The TSC-OPF problem proposed on this thesis is based, partially, on the formulation developed by the so-called traditional methods, because they allow a better representation and control of the dynamic behaviour of machines and systems. However, it includes also improvements in the representation of realistic systems, including more detailed generation machines, a model of a HVDC-LCC link, etc. The proposed models include power flow equations before the disturbance; technical limits of generators, lines and buses; oscillation equations for all generators in the system; and stability limit equations given by the angular or speed deviation between each generator and the reference.

Moreover, other problems not yet considered in TSC-OPF formulations have been explored, such as determination of the maximum loadability, economic effect of fault clearing times, and stability and economic effects related to recovering power injection in a HVDC link after a fault.

Regarding the solution method, an effort was made in this thesis to use conventional and easily available solvers. Therefore, the algorithms were implemented in MATLAB and GAMS. The data of same cases were prepared in PSS/E and interfaces written in Python were used. Evolutionary methods were not necessary to obtain the TSC-OPF solutions. In the following four chapters, some applications and results obtained from the proposed TSC-OPF formulations are presented.

2.5 References

[1] P. Kundur, J. Paserba, V. Ajjarapu, G. Andersson, A. Bose, C. Canizares, N. Hatziargyriou, D. Hill, A. Stankovic, C. Taylor, T. Van Cutsem and V. Vittal, "Definition and classification of power system stability IEEE/CIGRE joint task force on stability terms and definitions", IEEE Transactions on Power Systems, vol. 19, no. 3, pp. 1387–1401, 2004.

[2] P. Kundur, Power System Stability and Control. McGraw-Hill Professional, 1994.

[3] P. Ledesma Larrea, "Estabilidad transitoria". Universidad Carlos III de Madrid, 22-Sep-2008.

[4] L. L. Grigsby, Power system stability and control. CRC Press, 2007.

[5] J. Grainger and W. D. Stevenson Jr., Power System Analysis, 1 edition. New York: McGraw-Hill Science/Engineering/Math, 1994.

[6] J. Kiusalaas, Numerical Methods in Engineering with MATLAB ®, 2nd ed. Cambridge University Press, 2009.

[7] W. Y. Yang, W. Cao, T.-S. Chung and J. Morris, Applied Numerical Methods Using MATLAB, 1st ed. Wiley-Interscience, 2005.

[8] H. W. Dommel and N. Sato, "Fast Transient Stability Solutions", IEEE Transactions on Power Apparatus and Systems, vol. PAS-91, no. 4, pp. 1643–1650, 1972.

[9] J. Carpentier, "Contribution á l' étude du dispatching économique", Bulletin de la Société Française des Électricie, vol. 3, pp. 431–447, 1962.

[10] H. W. Dommel and W. F. Tinney, "Optimal Power Flow Solutions", IEEE Transactions on Power Apparatus and Systems, vol. PAS-87, no. 10, pp. 1866–1876, 1968.

[11] A. Gomez-Exposito, A. J. Conejo and C. Canizares, Electric Energy Systems: Analysis and Operation. CRC Press, 2008.

[12] M. Huneault and F. D. Galiana, "A survey of the optimal power flow literature", IEEE Transactions on Power Systems, vol. 6, no. 2, pp. 762–770, 1991.

[13] C. F. Moyano and E. Castronuovo, "Non-Linear Mathematical Programming Applied to Electric Power Systems Stability", in Optimization advances in electric power systems, Nova Science Publishers, Inc, 2009.

[14] F. Milano, Power System Modelling and Scripting, 1st Edition. Springer, 2010.

[15] O. Alsac and B. Stott, "Optimal Load Flow with Steady-State Security", IEEE Transactions on Power Apparatus and Systems, vol. PAS-93, no. 3, pp. 745–751, 1974.

[16] J. A. Momoh, R. J. Koessler, M. S. Bond, B. Stott, D. Sun, A. Papalexopoulos and P. Ristanovic, "Challenges to optimal power flow", IEEE Transactions on Power Systems, vol. 12, no. 1, pp. 444–455, 1997.

[17] L. Chen, Y. Taka, H. Okamoto, R. Tanabe and A. Ono, "Optimal operation solutions of power systems with transient stability constraints", IEEE Transactions on Circuits and Systems I: Fundamental Theory and Applications, vol. 48, no. 3, pp. 327–339, 2001.

[18] Y. Xia, K. W. Chan and M. Liu, "Direct nonlinear primal-dual interior-point method for transient stability constrained optimal power flow", IEE Proceedings-Generation, Transmission and Distribution, vol. 152, no. 1, pp. 11–16, 2005.

[19] Y. Sun, Y. Xinlin and H. F. Wang, "Approach for optimal power flow with transient stability constraints", IEE Proceedings-Generation, Transmission and Distribution, vol. 151, no. 1, pp. 8–18, 2004.

[20] D. Gan, R. J. Thomas and R. D. Zimmerman, "Stability-constrained optimal power flow", IEEE Transactions on Power Systems, vol. 15, no. 2, pp. 535–540, 2000.

[21] M. La Scala, M. Trovato and C. Antonelli, "On-line dynamic preventive control: an algorithm for transient security dispatch", IEEE Transactions on Power Systems, vol. 13, no. 2, pp. 601–610, 1998.

[22] Yue Yuan, J. Kubokawa and H. Sasaki, "A solution of optimal power flow with multicontingency transient stability constraints", IEEE Transactions on Power Systems, vol. 18, no. 3, pp. 1094–1102, 2003.

[23] D. Layden and B. Jeyasurya, “Integrating security constraints in optimal power flow studies”, in IEEE Power Engineering Society General Meeting, 2004., 2004, pp. 125–129 Vol.1.

[24] Q. Jiang and G. Geng, “A Reduced-Space Interior Point Method for Transient Stability Constrained Optimal Power Flow”, IEEE Transactions on Power Systems, vol. 25, no. 3, pp. 1232–1240, 2010.

[25] Quanyuan Jiang and Zhiguang Huang, “An Enhanced Numerical Discretization Method for Transient Stability Constrained Optimal Power Flow”, IEEE Transactions on Power Systems, vol. 25, no. 4, pp. 1790–1797, 2010.

[26] G. Geng and Q. Jiang, “A Two-Level Parallel Decomposition Approach for Transient Stability Constrained Optimal Power Flow”, IEEE Transactions on Power Systems, vol. 27, no. 4, pp. 2063–2073, 2012.

[27] Q. Jiang, B. Zhou and M. Zhang, “Parallel Augment Lagrangian Relaxation Method for Transient Stability Constrained Unit Commitment”, IEEE Transactions on Power Systems, vol. 28, no. 2, pp. 1140–1148, 2013.

[28] “Beowulf cluster - Wikipedia, the free encyclopedia”. Available: http://en.wikipedia.org/wiki/Beowulf_cluster.

[29] “Beowulf: a parallel workstation for scientific computation”. Available: http://www.phy.duke.edu/~rgb/brahma/Resources/beowulf/papers/ICPP95/icpp95.html.

[30] Y. Xu, Z. Y. Dong, Z. Xu, R. Zhang and K. P. Wong, “Power system transient stability-constrained optimal power flow: A comprehensive review”, in 2012 IEEE Power and Energy Society General Meeting, 2012, pp. 1–7.

[31] T. B. Nguyen and M. A. Pai, “Dynamic security-constrained rescheduling of power systems using trajectory sensitivities”, IEEE Transactions on Power Systems, vol. 18, no. 2, pp. 848–854, 2003.

[32] L. Tang and J. D. McCalley, “An efficient transient stability constrained optimal power flow using trajectory sensitivity”, in North American Power Symposium (NAPS), 2012, 2012, pp. 1–6.

[33] Y. H. Li, W. P. Yuan, K. W. Chan and M. B. Liu, “Coordinated preventive control of transient stability with multi-contingency in power systems using trajectory sensitivities”, International Journal of Electrical Power & Energy Systems, vol. 33, no. 1, pp. 147–153, Jan. 2011.

[34] D. Ruiz-Vega and M. Pavella, “A comprehensive approach to transient stability control. I. Near optimal preventive control”, IEEE Transactions on Power Systems, vol. 18, no. 4, pp. 1446–1453, 2003.

[35] Rafael Zarate Miñano, “Optimal Power Flow with Stability Constraints”, Tesis Doctoral, Universidad de Castilla-La Mancha, Ciudad Real, 2010.

[36] R. Zarate-Minano, T. Van Cutsem, F. Milano and A. J. Conejo, "Securing Transient Stability Using Time-Domain Simulations Within an Optimal Power Flow", IEEE Transactions on Power Systems, vol. 25, no. 1, pp. 243–253, 2010.

[37] A. Pizano-Martianez, C. R. Fuerte-Esquivel and D. Ruiz-Vega, "Global Transient Stability-Constrained Optimal Power Flow Using an OMIB Reference Trajectory", IEEE Transactions on Power Systems, vol. 25, no. 1, pp. 392–403, 2010.

[38] A. Pizano-Martinez, C. R. Fuerte-Esquivel and D. Ruiz-Vega, "A New Practical Approach to Transient Stability-Constrained Optimal Power Flow", IEEE Transactions on Power Systems, vol. PP, no. 99, p. 1, 2011.

[39] X. Tu, L.-A. Dessaint and H. Nguyen-Duc, "Transient stability constrained optimal power flow using independent dynamic simulation", IET Generation, Transmission Distribution, vol. 7, no. 3, pp. 244–253, 2013.

[40] X. Tu, L. Dessaint and I. Kamwa, "A global approach to transient stability constrained optimal power flow using a machine detailed model", Canadian Journal of Electrical and Computer Engineering, vol. 36, no. 1, pp. 32–41, 2013.

[41] K. Y. Chan, S. H. Ling, K. W. Chan, H. H. C. Iu and G. T. Y. Pong, "Solving multi-contingency transient stability constrained optimal power flow problems with an improved GA", in IEEE Congress on Evolutionary Computation, 2007. CEC 2007, 2007, pp. 2901 –2908.

[42] N. Mo, Z. Y. Zou, K. W. Chan and T. Y. G. Pong, "Transient stability constrained optimal power flow using particle swarm optimisation", IET Generation, Transmission Distribution, vol. 1, no. 3, pp. 476 –483, May 2007.

[43] H. R. Cai, C. Y. Chung and K. P. Wong, "Application of Differential Evolution Algorithm for Transient Stability Constrained Optimal Power Flow", IEEE Transactions on Power Systems, vol. 23, no. 2, pp. 719–728, 2008.

[44] F. Capitanescu, J. L. Martinez Ramos, P. Panciatici, D. Kirschen, A. Marano Marcolini, L. Platbrood and L. Wehenkel, "State-of-the-art, challenges, and future trends in security constrained optimal power flow", Electric Power Systems Research, vol. 81, no. 8, pp. 1731–1741, Aug. 2011.

Chapter 3.

Optimal Re-Dispatch of an Isolated System Considering Transient Stability Constraints

Abstract— In this paper, an algorithm for calculating the optimal operation of a system with different load states and fault clearing times is proposed. The algorithm simultaneously considers both economic and stability constraints. The proposed formulation is evaluated on the Majorca and Minorca islands power system, which is a small, isolated system with low inertia. A conventional optimisation tool is used to solve the optimisation problem. The results show the efficiency of the proposed approach and the advantages of including stability restrictions in the optimisation analysis. The application of the algorithm to different operation points is used to evaluate the cost of assuring the transient stability after a severe fault in the transmission grid. The analysis of different fault clearing times is used to estimate the economic savings of implementing a faster protection system.

Contents

3.1 Introduction

Optimal power flow (OPF) is an important tool for power system operation and planning. The main purpose of an OPF program is calculating the optimal operating point of a power system and setting the variables for the economic and secure operation of the system.

Transient stability studies test the optimal solution obtained from the OPF under credible disturbances to ensure the stability of the system. If the system is transiently unstable under one of the disturbances, the OPF solution must be modified. Heuristic trial-and-error methods, based on engineering experience, are typically used to re-dispatch the system to guarantee the stability of the operation [1], [2]. The conventional sequential procedures of dynamical simulation require the same number of equations and variables. Therefore, when the number of variables is greater than the number of equations, the best solution of the system is obtained by successive behaviour simulations to find a reasonable answer [3], [4].

Until recently, the dynamic of a power system could not be incorporated into a mathematical OPF formulation through a transient stability model.

However, the advance of computing resources and consolidation of optimisation methods for the solution of large-scale problems allow the temporal representation of the dynamical system in the optimisation problems. The main advantage of representing differential equations in optimisation problems is the possibility of giving a preferential direction to the solution of the dynamic equations when the number of variables exceeds the number of equations. In this manner, it is possible to minimise or maximise performance indexes, calculate optimal parameters and make the system more stable or economical. Of course, this integration of static and dynamic studies implies an increase in the dimension of the optimisation problem [5].

The transient stability-constrained OPF (TSC-OPF) aims to integrate economic objectives and both steady-state and stability constraints in one unique formulation. Previous studies on TSC-OPF show different ways to approach this complex problem. In [6] and [7], the infinite-dimensional TSC-OPF problem is converted to a solvable finite-dimensional programming problem using functional transformation techniques. The transformed problem has the same variables as those in the pure OPF problem. In this approach, the temporal behaviour of the dynamic variables cannot be observed. Alternatively, in [8], dynamic equations are transformed into numerically equivalent algebraic equations using the trapezoidal rule and then included in the conventional OPF formulation. For the algorithm to be solved, the OPF constraints, stability equations and objective function must be linearised. The authors of [9] and [10] propose the resolution of a multi-contingency TSC-OPF problem, including the temporal representation of the dynamical equations in the optimisation problem. To obtain the solution, a specifically modified algorithm of the Primal-Dual Interior-Point method is used. This algorithm can accommodate nonlinear equations, but a reduction method is necessary to efficiently handle the inequality constraints. Nonlinear equations are also represented in [11], which considers the algebraic equations (both equality and inequality constraints) that describe the steady-state situation of the power system during both the pre-fault and steady-state post-fault periods. In [12], the authors propose a similar

approach, reducing the multi-machine model to a scheme of two machines using the "single-machine equivalent" concept.

This study proposes an algorithm that includes all of the simulation period in one formulation: the pre-fault, fault and post-fault stages. The differential equations of the classical model of the generators for dynamical studies are explicitly included in the optimisation problem as nonlinear constraints using the trapezoidal rule. Two different simulation steps, during and after the fault, are used to reduce the computational burden. Using this approach, the most changing stage of the simulation can be represented in more detail.

The algorithm is applied to the interconnected system network of the islands of Majorca and Minorca, consisting of 15 buses and 3 generation machines in isolated operation. The optimal generation dispatch, considering economic parameters and assuring the stability of the system at different load states and after one of the most severe faults, is obtained. The generators must preserve a maximum angle deviation from the grid's centre of inertia (COI). The dynamic behaviours of the three generators are simultaneously calculated in the optimisation solution. At the end of the paper, two fault clearing times are considered to analyse the effect of using faster protections from an economic point of view.

The results show that the proposed algorithm can adequately calculate the optimal behaviour of the system for different load states and fault clearing times in an efficient manner. An initial calculation of the costs associated with the stability constraints for different operation states is performed. In the present system, the reduction of the clearing time of some protections (from 300 to 250 ms) can decrease the operational cost by 8.84 % for medium load conditions.

3.2 Transient stability model

Analysing the transient stability of power systems involves the computation of their nonlinear dynamic response to large disturbances, typically

a fault in the transmission network followed by the isolation of the faulted element by protective relaying. In this section, a mathematical model of the power system dynamics suitable for the TSC-OPF and a criterion for determining whether a case is acceptable with respect to rotor angle stability are proposed.

In this paper, the synchronous generators are represented by the classical generator model [13], which consists of a voltage source E'_i of fixed magnitude behind a transient reactance x'_{di}, as shown in Fig. 3.1. In the classical model, the swing equation provides the two differential equations for each generator as follows:

$$d\delta_i / dt = \omega_0 \Delta\omega_i \tag{3.1}$$

$$d\Delta\omega_i / dt = (1/2H_i)(P_{mi} - P_{ei} - D_i \Delta\omega_i) \tag{3.2}$$

where δ_i is the angular position of the rotor with respect to a synchronously rotating reference, $\Delta\omega_i$ is the rotor speed deviation, ω_0 is the reference frequency, H_i is the inertia constant, P_{mi} and P_{ei} are the input and output powers, respectively, D_i is the damping constant and d / dt is the derivate of the function with the time.

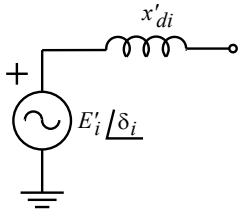

Fig. 3.1. Equivalent circuit of the synchronous generator.

The mechanical power input is considered to be constant throughout the study period, and the magnetic saturation is not represented. The three more usual static load models in transient stability studies are: constant impedance, constant current and constant power [14]. In this study, the loads are modelled as constant impedances and included in the system's admittance matrix. This representation allows the reduction of the admittance matrix during the transient

period, only representing the internal nodes of the synchronous generators. The representation of all loads as passive impedances is one of the common simplifications applied in TSC-OPF [5], [9], [10], [12], because it significantly reduces the number of equations. The output power of the i^{th} generator can then be expressed as:

$$P_{ei} = E_i' \sum_{j=1}^{N_g} E_j' Y_{red,ij} \cos\left(\delta_i - \delta_j - \theta_{red,ij}\right) \tag{3.3}$$

where N_g is the number of generators and the complex number, $Y_{red,ij}\angle\theta_{red,ij}$ is the element in position (i, j) of the reduced admittance matrix.

The classical generator model is commonly used in the state of the art TSC-OPF [8]-[12]. This model is a compromise between adequate dynamic representation and computational burden. In this study, conservative limits for the determination of the transient stability constraints are adopted, due to the difficulties associated with improving the representation of the generators by including additional differential equations.

The state of the system is considered acceptable for a given disturbance if the maximum rotor angle deviation during the electromechanical oscillations does not exceed a certain value. Here, instead of the maximum deviation between the angles of two machines [12], [15]-[17], the maximum deviation with respect to the COI is constrained [18]. The COI has the advantage of providing a reference that includes the component of the angle deviation due to the acceleration of the system and allowing to identify the component with the larger individual rotor oscillations. The angle of the COI is defined as

$$\delta_{COI} = \sum_{i=1}^{N_g} H_i \delta_i \Big/ \sum_{i=1}^{N_g} H_i \tag{3.4}$$

Differential equations (3.1) and (3.2) are solved using the trapezoidal rule, which is an L-stable implicit integration method [19]. The stability of the trapezoidal rule is important because it allows the computational time to be reduced by using larger time steps.

When applied to equations (3.1) and (3.2), the trapezoidal rule yields

$$\delta_i^{t+1} = \delta_i^t + \left(\Delta t/2\right)\omega_0\left(\Delta\omega_i^{t+1} + \Delta\omega_i^t\right) \tag{3.5}$$

$$\Delta\omega_i^{t+1} = \Delta\omega_i^t + \left(\Delta t/4H_i\right)\left(2P_{mi} - P_{ei}^{t+1} - P_{ei}^t - D_i\left(\Delta\omega_i^{t+1} + \Delta\omega_i^t\right)\right) \tag{3.6}$$

where t is the iteration step and Δt is the time step. The fact that the trapezoidal rule is an implicit method is not a problem in this study because the optimisation algorithm solves all of the equations simultaneously, obtaining the dynamic positions in all of the simulation periods and the optimal initial conditions at the same time.

3.3 Formulation of the TSC-OPF problem

The objective of this study is to obtain the optimal operational conditions of the system when the system is affected by a symmetrical three-phase fault to ground with different load levels. The fault is applied for a short period of time, and after that period, the protection systems disconnect the faulted part of the network. Therefore, the problem presents the following three network conditions:

- The pre-fault stage, with all of the circuits in service, that is used to calculate the initial conditions of the system;
- The fault stage, in which the voltage at the point of failure is zero;
- The post-fault stage, in which the fault has been cleared by the protection systems, and the voltage is restored.

To calculate the best system response using both economic and stability criteria, these three stages must be simultaneously represented in an optimisation problem. The optimisation formulation aims to minimise the generation cost of operating the system considering the bids of the producers. The variables of the problem are the active and reactive power productions, the internal voltage of the generators, the voltage in the buses, the current through the lines during the pre-fault stage, and the angle and speed of the generators at each discretisation

point of the temporal dynamic representation. The solution of the optimisation problem calculates the optimal value of the dispatched powers while maintaining the stability of the operation.

The proposed optimisation problem with transient stability constraints is represented by the following equations.

$$\text{Min.} \quad f(P_{gi}) = \sum_{i=1}^{N_g} p_i P_{gi} \tag{3.7}$$

subject to

$$P_{g,bus_n} - P_{d,bus_n} - V_n \sum_{m=1}^{N_b} V_m Y_{nm} \cos\left(\phi_n - \phi_m - \theta_{nm}\right) = 0 \tag{3.8}$$

$$Q_{g,bus_n} - Q_{d,bus_n} - V_n \sum_{m=1}^{N_b} V_m Y_{nm} \sin\left(\phi_n - \phi_m - \theta_{nm}\right) = 0 \tag{3.9}$$

$$I_{nm} - \left[\left(V_n \cos\phi_n - V_m \cos\phi_m\right)^2 + \left(V_n \sin\phi_n - V_m \sin\phi_m\right)^2\right]^{1/2} Y_{Branch_{nm}} = 0 \tag{3.10}$$

$$P_{gi} x'_{di} - E'_i V_{gi} \sin\left(\delta_i^0 - \phi_{gi}\right) = 0 \tag{3.11}$$

$$Q_{gi} x'_{di} + V_{gi}^2 - E'_i V_{gi} \cos\left(\delta_i^0 - \phi_{gi}\right) = 0 \tag{3.12}$$

$$\Delta\omega_i^0 = 0 \tag{3.13}$$

$$\delta_i^{t+1} - \delta_i^t - \left(\Delta t/2\right)\omega_0 \left(\Delta\omega_i^{t+1} + \Delta\omega_i^t\right) = 0 \tag{3.14}$$

$$\begin{aligned} &\Delta\omega_i^{t+1}\left(1 + \left(\Delta t/4H_i\right) D_i\right) - \\ &\Delta\omega_i^t \left(1 - \left(\Delta t/4H_i\right) D_i\right) - \left(\Delta t/4H_i\right)\left(2P_{mi} - P_{ei}^{t+1} - P_{ei}^t\right) = 0 \end{aligned} \tag{3.15}$$

$$P_{ei}^t - E'_i \sum_{\substack{j=1 \\ j\neq i}}^{N_g} E'_j Y_{red,ij} \cos\left(\delta_i^t - \delta_j^t - \theta_{red,ij}\right) = 0 \tag{3.16}$$

$$\delta_{COI}^t - \sum_{i=1}^{N_g} H_i \delta_i^t \Big/ \sum_{i=1}^{N_g} H_i = 0 \tag{3.17}$$

$$\delta_{t\min} \le \delta_i^t - \delta_{COI}^t \le \delta_{t\max} \tag{3.18}$$

$$\Delta\omega_{\min} \le \Delta\omega_i^t \le \Delta\omega_{\max} \tag{3.19}$$

$$P_{\min} \le P_{gi} \le P_{\max} \tag{3.20}$$

$$Q_{\min} \le Q_{gi} \le Q_{\max} \tag{3.21}$$

$$E'_{\min} \le E'_i \le E'_{\max} \tag{3.22}$$

$$\delta_{\min} \le \delta_i^t \le \delta_{\max} \tag{3.23}$$

$$V_{\min} \le V_n \le V_{\max} \tag{3.24}$$

$$\phi_{\min} \le \phi_n \le \phi_{\max} \tag{3.25}$$

$$0 \le I_{nm} \le I_{\max} \tag{3.26}$$

$$\forall i, j = 1,...,N_g ; \forall m, n = 1,...,N_b ; \ \forall t = 1,...,N_t = t_{fc}/\Delta t_1 + (t_{\max} - t_{fc})/\Delta t_2$$

where P_{g,bus_n} and Q_{g,bus_n} are the active and reactive powers injected in the n^{th} bus, respectively; P_{gi} and Q_{gi} are the active and reactive power generations of the i^{th} producer, respectively; p_i is the price factor of the i^{th} generator; P_{d,bus_n} and Q_{d,bus_n} are the active and reactive powers of the n^{th} load, respectively; $V_n\angle\phi_n$ is the voltage at bus n; $Y_{nm}\angle\theta_{nm}$ is the element (n, m) of the admittance matrix; I_{nm} is the current between buses n and m; $Y_{Branch_{nm}}$ is the line admittance between buses n and m; $V_{g_i}\angle\phi_{g_i}$ is the voltage at generation bus i; $Y_{red,ij}\angle\theta_{red,ij}$ is the transfer admittance of the reduced admittance matrix; t is the index of the iteration step; t_{fc} is the duration of the fault; t_{max} is the maximum simulation period; Δt_1 is the integration step width during the fault; Δt_2 is the integration step width post-fault; $(\cdot)_{min}$ and $(\cdot)_{max}$ are the lower and upper limits of the variables and quantities, respectively; N_g is the number of generators; N_b is the number of buses; and N_t is the number of time steps.

Objective function (3.7) aims to calculate the optimal generation cost using linear price functions for a given generated active power. The

representation of the market can be easily improved in the formulation without affecting the algorithm. In the present case, a simple modelisation is preferred for clarity.

The equality constraints are as follows:

- Equations (3.8) and (3.9) represent the balances in the active and reactive power flows, respectively, in the pre-fault stage in all of the buses.
- Equation (3.10) calculates the current transmission into the lines in the pre-fault stage. In (3.8)-(3.10), matrix Y includes all of the buses in the system.
- The initial study state values of the rotor angle and constant voltage E_i' are calculated in (3.11) and (3.12). In the pre-fault stage, the system is in synchronism, so the initial rotor speed deviation is zero (3.13).
- Using the trapezoidal rule, equations (3.14) and (3.15) represent the dynamics of the machines in both the fault and post-fault stages.
- Equation (3.16) calculates the generated active power in both the fault and post-fault stages. In this equation, the matrix Y_{red} is a reduced matrix, including only the internal nodes of the generators. In the fault and post-fault periods, all the loads of the system are represented as passive impedances, allowing the use of the Kron reduction method [4], [9], [10], [12] and drastically reducing the number of equations. It must be stressed that the Kron reduction does not require any other approximation in the representation of the system.
- Equation (3.17) represents the equivalent angle of the system's COI in each integration step.

The inequality constraints are as follows:

- The stability limits are represented through (3.18) and (3.19) for the rotor angles and the rotor speed deviation, respectively. The angular stability limits are measured with respect to the equivalent angle of the system's COI in each integration step.
- The technical limits of the installed capacity are represented in (3.20) and (3.21), limiting the power production of the generators.
- In (3.22) and (3.23), the restrictions on the internal voltage of the generators are shown.
- The system operating limits are represented in (3.24) and (3.25) for the voltage modules and angles in the buses of the system, respectively; (3.26) represents the system operating limits for the currents in the transmission lines.

As mentioned in the Introduction, two integration steps are used in equations (3.14) and (3.15) to represent the fault and post-fault periods. Time step Δt_1 (used in the representation of the fault) is smaller than step Δt_2 (used in the post-fault period) to reduce the computational burden without losing accuracy in the representation of the fault period.

In this study, the problem is solved using MATLAB [20]. A conventional solver based on the Interior-Point method is utilised to obtain the solutions of the (3.7)-(3.26) without particular modifications. The tolerances in the convergence are adjusted to 10^{-6}.

3.4 Case of study

The proposed optimisation method (3.7)-(3.26) is applied to a reduced version of the power system of Majorca and Minorca, which are two islands in the western Mediterranean Sea located near the eastern coast of the Iberian Peninsula. Fig. 3.2 shows a simplified map of the power system, including the main power plants and the 220 and 132 kV grids. The study case contains three

power plants: G_1 is a 600 MW combined cycle power plant, G_2 is a 510 MW coal-fired power plant, and G_3 is a 275 MW gas turbine plant. The main load areas are located in the west of Majorca (close to buses 4, 5 and 6) in the north of Majorca (close to bus number 8) and east of Minorca.

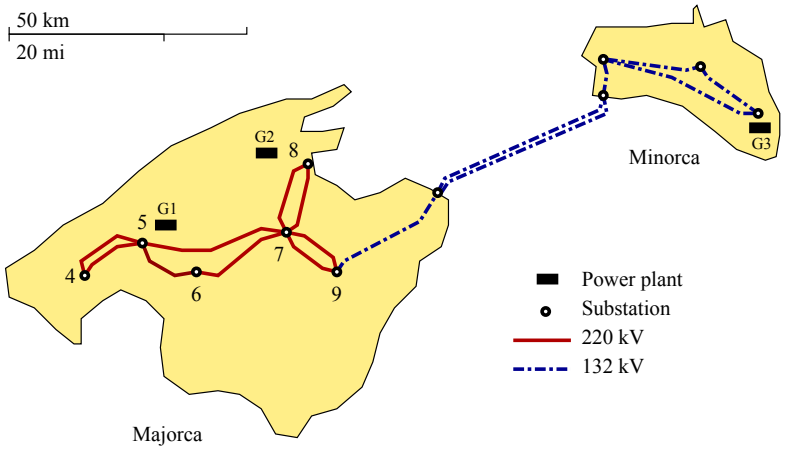

Fig. 3.2. Map of the power system of Majorca and Minorca.

Most previous studies on TSC-OPF have been applied to systems with one or two generators or large interconnected systems that were later reduced to two generators. In this case, the dynamic behaviours of the three generators are strictly preserved using separated models for each one. Furthermore, in this study, the dynamics of an isolated system facing disturbances is more difficult to control than those of interconnected grids, due to the relatively small inertia of the isolated system.

Fig. 3.3 shows the one-line diagram of the system. The transmission grid contains three voltage levels: 220, 132 and 66 kV. The 220 kV grid is the bulk of the power system. The 132 kV grid (which includes two 43 km long AC submarine cables between both islands) is represented by a single line because a more detailed representation does not affect the results. The 66 kV grid has been included in the model because it is a mesh network, and provides alternative routes between the 220 kV buses and thus affects the power flows during the electromechanical transients after the fault.

In the Appendix, the full dynamic generator data (Table 3.2), the prices for the active power generation (Table 3.3), the parameters of the lines and

transformers of the system (Table 3.4), the load data (Table 3.5) and the limits of the variables (Table 3.6) are provided. The prices for active power generation are obtained from historical data [21] representing typical values for January 2011 in Spain. In the pre fault stage, bus 1 is the slack bus, with fixed angle zero. During and after the fault, the maximum deviation of the rotor angles to the COI is 50°, which corresponds to a maximum deviation of 100° between individual generators.

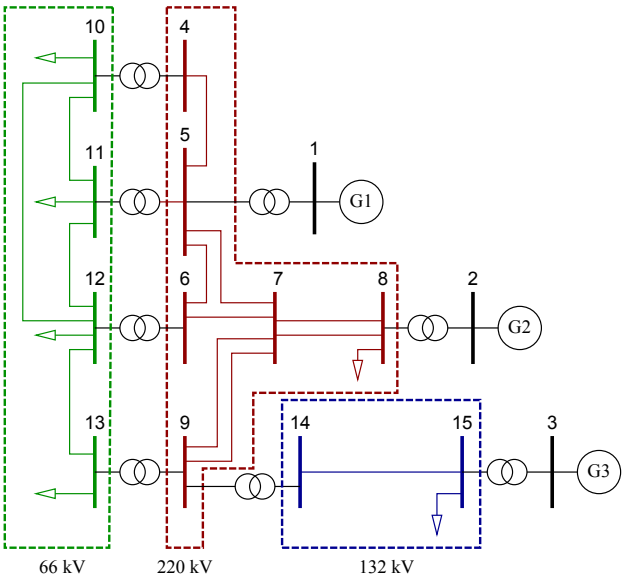

Fig. 3.3. One-line diagram of the case study.

In this study, the effect of a three-phase fault to ground in the line between buses 5 and 7, close to bus 5, is analysed. The fault is cleared by disconnecting the faulty line in ends 5 and 7. This fault is selected because it is dangerous from the point of view of the system's transient stability; the short circuit is close to generator G_1 (the largest of the three generators), and the disconnection of the line between buses 5 and 7 eliminates a mesh in the middle of the transmission grid. Simulations have shown that this is the most critical disturbance in the system for the present configuration.

The optimisation problem (3.7)-(3.26) requires a relatively large number of constraints and variables to represent the considered case study. For the analysed system, a simulation time of $t_{max} = 3$ s, a fault clearing time of 300 ms and discretisation periods of $\Delta t_1 = 0.02$ s and $\Delta t_2 = 0.05$ s, the numbers of

variables, equality and inequality constraints are 748, 886 and 1,358, respectively. The conventional solution algorithm used (based on the interior-point method) solves this optimisation problem in approximately one minute using a medium-cost laptop (Processor 1600 MHz, RAM 2GB).

3.5 Results

In this section, the validation of the optimisation program using the Runge-Kutta (R-K) method is shown, and the dispatch obtained in a conventional OPF is compared with the result of the TSC-OPF for a fault clearing time of t_{fc} = 300 ms and different levels of demand. The effects of using a faster protection in the TSC-OPF results are then presented. Finally, an initial quantification of the cost of considering transient stability constraints in the generation dispatch of the system is performed.

3.5.1 Validation of the optimisation algorithm

The optimisation algorithm has been validated with respect to the accuracy of the dynamic simulation, the satisfaction of the constraints and the convergence. All of the examples provided in this section correspond to the same case, in which the system operates at 75 % of the load rate and a fault clearing time of 300 ms, although the validation has been performed for different operational conditions.

To validate the solution of the dynamic equations provided by the optimisation algorithm, the results are compared with those obtained using a Runge-Kutta method. Both results are very similar, as shown in Fig. 3.4. The upper graph shows the speed deviation of the three generators as provided by the optimisation algorithm. The lower graph is obtained by applying the MATLAB solver ode45, which is based on an explicit Runge-Kutta (4,5) formula [20], to equations (3.1) and (3.2). The initial point used to apply the Runge-Kutta method is the optimal power dispatch provided by the optimisation algorithm so that both simulations begin at the same initial point. Because no substantial difference is observed between both graphics, the trapezoidal method and

integration step used by the optimisation algorithm are sufficiently accurate to represent the system dynamics.

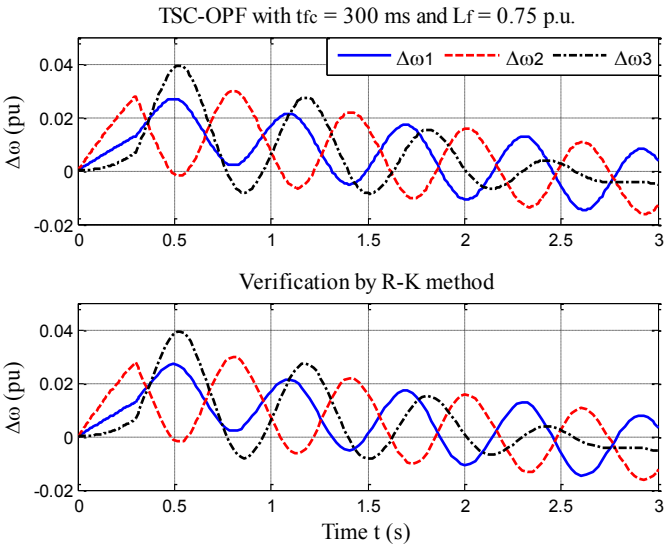

Fig. 3.4. Verification of the results obtained with the TSC-OPF using the Runge-Kutta method.

Fig. 3.5 shows the evolution of the rotor angles of the three generators and the COI. The upper and lower bounds are the stability margin of 50° maximum deviations from the COI. As shown in the figure, the larger deviations occur at the beginning of the simulation. The damping effect reduces the amplitude of the deviations in the post-fault stage.

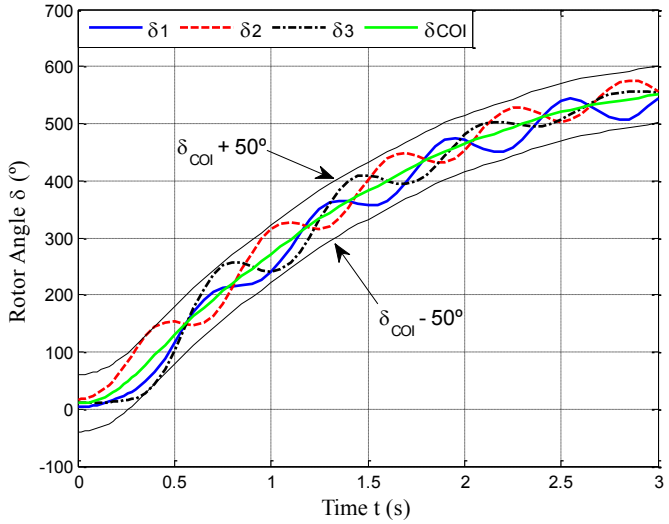

Fig. 3.5. Evolution of the rotor angles.

Fig. 3.6 and Fig. 3.7 show the evolution of the objective function and the first-order optimality, respectively, during the iterations of the conventional solution algorithm implemented in MATLAB. Fig. 3.6 shows that after 16 iterations, the objective function reaches a value similar to the final value, but the program requires an additional 14 iterations to determine the optimal value that meets the required tolerances.

The first-order optimality shown in Fig. 3.7 is a measure of the closeness between the solution point obtained at each iteration and the optimal point, as specified by the strict observance of the Karush-Kuhn-Tucker conditions [22]. The first-order optimality, among other criteria, must be less than the maximum tolerance for the algorithm to stop the iterative process.

Fig. 3.6 and Fig. 3.7 show a general trend in the studied cases: while the value of the objective function decreases, the first-order optimality remains almost constant. Once the objective function is near the minimum cost, the program continues iterating until the value of the first-order optimality is less than the defined tolerance.

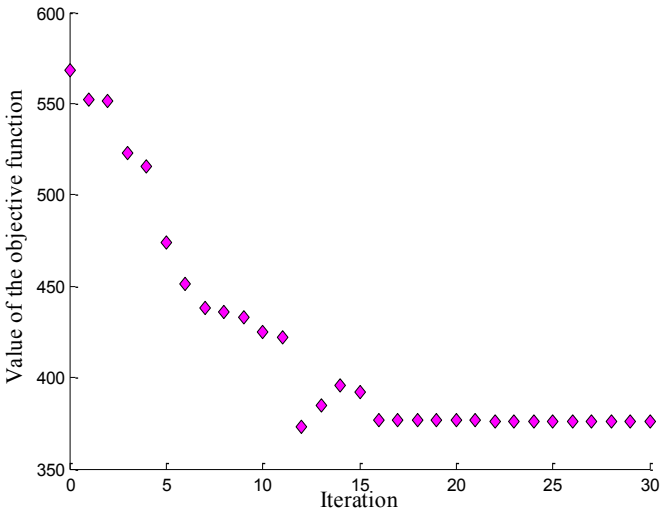

Fig. 3.6. Evolution of the objective function during the iterations.

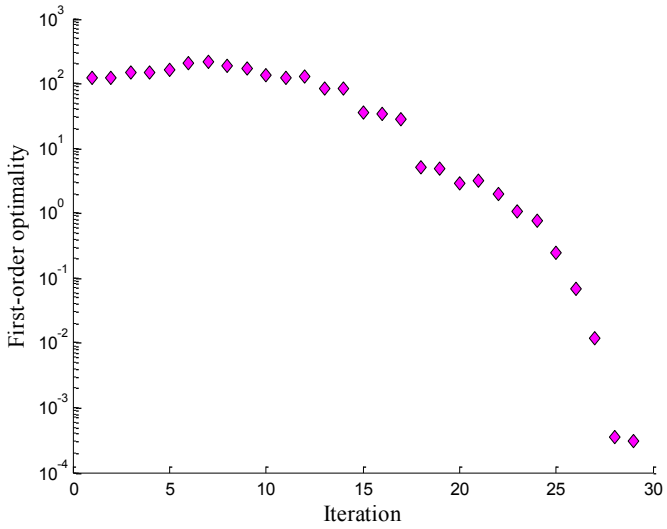

Fig. 3.7. Evolution of the first-order optimality during the iterations.

3.5.2 Comparison of the classical OPF and TSC-OPF for t_{fc} = 300 ms

The classical OPF and proposed TSC-OPF have been applied to a number of operation points to study the cost of satisfying the transient stability constrains. Each operation point corresponds to a different load level specified by a load factor L_f, i.e., $L_f = 1$ corresponds to the rated load and $L_f = 0.5$ corresponds to half the rated load. The load factor L_f affects to both the active and reactive powers in the same proportion. Therefore, equations (3.8) and (3.9) are substituted by

$$P_{g_n} - L_f P_{d_n} - V_n \sum_{m=1}^{N_b} V_m Y_{nm} \cos\left(\phi_n - \phi_m - \theta_{nm}\right) = 0 \tag{3.27}$$

$$Q_{g_n} - L_f Q_{d_n} - V_n \sum_{m=1}^{N_b} V_m Y_{nm} \sin\left(\phi_n - \phi_m - \theta_{nm}\right) = 0 \tag{3.28}$$

The conventional OPF is performed by solving an optimisation problem with equations (3.7)-(3.10), (3.20), (3.21) and (3.24)-(3.26) [23]. Fig. 3.8 shows the active power produced by the generators when L_f varies between 0.1 p.u. and 1.45 p.u. The obtained dispatch is purely economic, without consideration of the stability constraints.

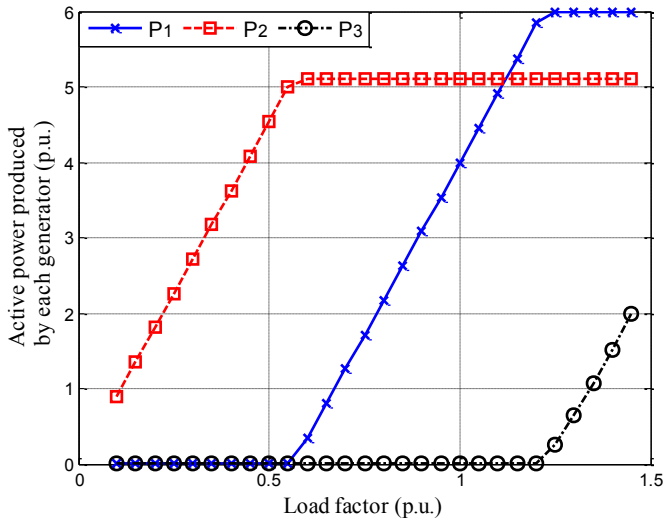

Fig. 3.8. Dispatch obtained with the OPF.

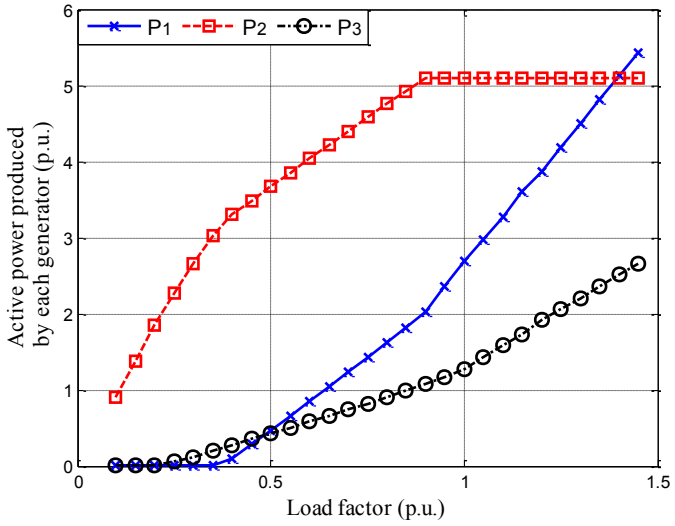

Fig. 3.9. Active power dispatch obtained with TSC-OPF for t_{fc} = 300 ms.

Fig. 3.9 shows the optimal values provided by the optimisation algorithm when the stability constraints are included and the fault clearing time is t_{fc} = 300 ms. The problem is defined by equations (3.7)-(3.26), substituting (3.8) and (3.9) with (3.27) and (3.28), respectively, to reflect the different operation points. The optimal values obtained using the TSC-OPF are different from those obtained with the classical OPF. The changes in the dispatch reflect the need to comply with the restrictions imposed to assure the stability of the system. From

L_f = 0.2 p.u. onwards, stability is only assured by forcing the dispatch of generators G_1 and G_3, which are more expensive than generator G_2.

3.5.3 Effect of a faster switch

The use of faster protection systems is one of the main resources available for transmission system operators to improve the transient stability of a system. However, the replacement of an existing switch by a faster switch has an economical cost, and the operator must evaluate whether it is justified or not.

To provide an economic assessment for the convenience of a faster switch, the proposed optimisation algorithm is applied to the base case and the fault clearing time is changed from 300 ms to 250 ms. Fig. 3.10 shows the obtained results. Comparing Fig. 3.8, Fig. 3.9 and Fig. 3.10 shows that the reduction of the fault clearing time displaces the solution of the TSF-OPF towards that of the OPF. The use of a faster switch improves the stability of the system and thus allows the power generated by the cheapest plants to increase.

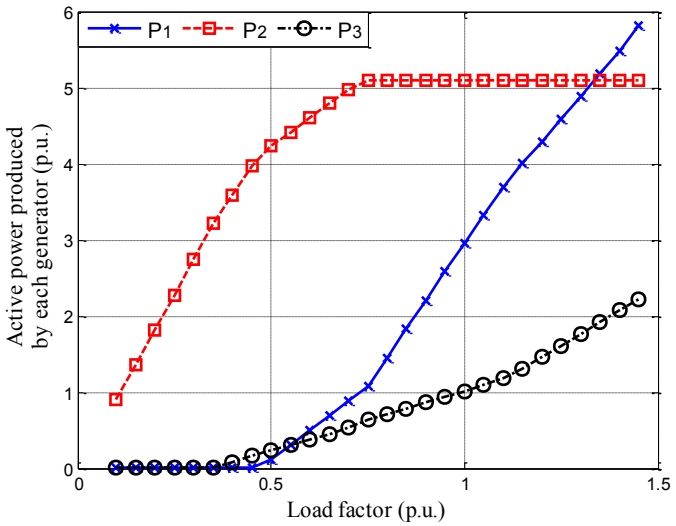

Fig. 3.10. Active power dispatch obtained with TSC-OPF for t_{fc} = 250 ms.

3.5.4 Transient stability cost assessment

The previous analysis allows the cost of assuring the stability of the system to be initially quantified. Fig. 3.11 shows the increase in the generation

cost of the TSC-OPF with respect to the classical OPF. The dashed line corresponds to the initial fault clearing time of 300 ms; this line can be interpreted as the increment of the cost due to ensuring the transient stability of the system for the selected fault with different load levels.

The continuous line corresponds to the difference in generation costs for the fault clearing time of 250 ms. The difference between both lines in Fig. 3.11 represents the economic savings of installing a protection system that clears the selected fault in 250 ms.

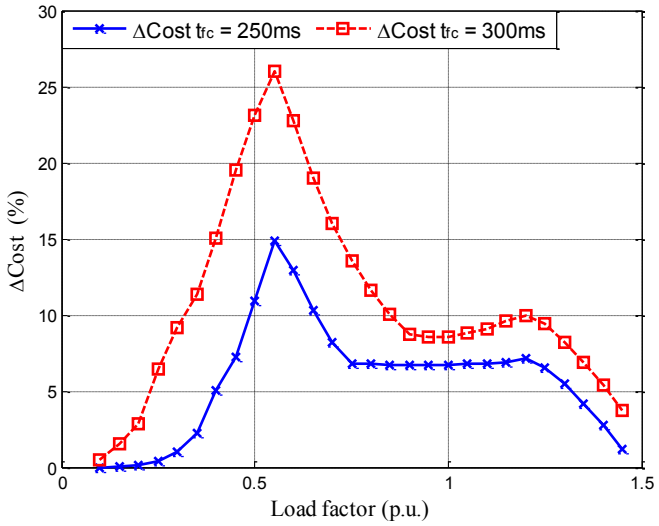

Fig. 3.11. Cost increase to meet the transient stability constraints.

The cost increase due to the transient stability constraints ranges between 3 % and 26 % when $t_{fc} = 300$ ms and between 0 and 13 % when $t_{fc} = 250$ ms. The figure has two clearly defined areas, which are described below.

For a load factor between 0.1 p.u. and 0.55 p.u., the generation cost increases considerably when stability constraints are considered because the more expensive generators G_1 and G_3 must be dispatched to guarantee the stability of the system, a fact that does not occur in the classical OPF.

When $L_f > 0.55$ p.u., the difference between the costs of the OPF and TSC-OPF is reduced because the generator G_2 is fully dispatched in the classical OPF (see Fig. 3.8), and thus, the generator G_1 (more expensive) begins to

produce. From L_f = 1.2 p.u. onwards, the difference between the OPF and TSC-OPF decreases further because G_3 is also dispatched in the classical OPF.

In Table 3.1, the last line (Average Value) was calculated with the values of ΔCost obtained for all of the load factors in Fig. 3.11.

TABLE 3.1: COST COMPARISON.

Load Factor	OPF	TSC-OPF					
		t_{fc} = 300 ms		t_{fc} = 250 ms		Difference between the 300 ms and 250 ms cases	
	Cost (a)	Cost (b)	ΔCost = ((b-a)/a)*100	Cost (c)	ΔCost = ((c-a)/a)*100	ΔCost = (b-c)	ΔCost = ((b-c)/b)*100
[p.u.]	[€]	[€]	[%]	[€]	[%]	[€]	[%]
0.10	37.07	37.24	0.46	37.07	0.00	0.17	0.46
0.55	205.57	259.03	26.01	236.13	14.87	22.90	8.84
1.20	623.84	685.93	9.95	668.27	7.12	17.66	2.58
1.45	844.84	876.58	3.76	854.88	1.19	21.68	2.47
Average Value	-	-	10.91	-	5.77	-	4.49

The advantages of changing the protective system depend on the most frequent load level in the operation of the system. Table 3.1, which complements Fig. 3.8, shows the total costs of the OPF and TSC-OPF at several operating points. At a load factor of L_f = 0.55 p.u., for example, the satisfaction of the transient stability constraints increases the cost of the electrical energy from 205.57 to 259.03 € (26.01 % increase) for the present clearing time (300 ms). At the same operation point, the reduction of the fault clearing time from 300 to 250 ms would reduce the cost of the energy from 259.03 to 236.13 € (14.87 % increase with respect to the conventional OPF and 8.84 % less than that with a clearing time of 300 ms). The TSC-OPF, in addition to providing the optimal operation of the system satisfying the stability constraints, is an interesting cost assessment tool with respect to investments in faster protection systems.

3.6 Conclusions

The proposed optimisation problem integrates economic objectives and stability constraints without numerical approximations. When applied to the

studied system, the computational burden of the algorithm does not pose a problem, with each case solved in approximately one minute on average using a medium-cost laptop. The results show that the proposed optimisation algorithm adequately calculates the optimal dispatch of the system for different load levels in an efficient manner. The application of the proposed algorithm to several operation points and fault clearance times serves as an assessment tool for the transmission system operator with respect to estimating the cost of assuring the transient stability of the system. Furthermore, the model can be used to analyse the economic savings provided by a faster protection system. In this case, the reduction of the clearance time of some protections (from 300 to 250 ms) reduces the operational cost of the system (at medium load) by 8.84 %.

In the proposed algorithm, the representation of the market and power plant dynamic models can be modified and improved without modifying the accuracy or efficiency of the method.

3.7 Appendix

TABLE 3.2: DYNAMIC PARAMETERS OF THE GENERATORS.

Generator	X'_d [p.u.]	S_b [MVA]	H [s]	D [p.u.]
G_1	0.3	600	3.0	2
G_2	0.3	510	3.2	2
G_3	0.25	275	2.0	2

TABLE 3.3: ECONOMIC DATA.

Generator	*P* [€/MWh]
G_1	70.90
G_2	41.11
G_3	105.57

All of the parameters in the following tables refer to a common 100 MVA base and corresponding voltage rating.

TABLE 3.4: PARAMETERS OF THE LINES AND TRANSFORMERS.

Branch	R [p.u.]	X [p.u.]	B [p.u.]
1-5	0	0.0117	0
2-8	0	0.0137	0
3-15	0	0.0255	0
4-5	0.0022	0.0145	0.0253
5-6	0.0019	0.0121	0.0211
5-7	0.0051	0.0330	0.0576
6-7	0.0042	0.0274	0.0477
7-8 (1)	0.0025	0.0161	0.0281
7-8 (2)	0.0025	0.0161	0.0281
7-9 (1)	0.0024	0.0153	0.0267
7-9 (2)	0.0024	0.0153	0.0267
14-15	0.0804	0.1205	0.0451
10-11	0.0202	0.0421	0.0132
10-12	0.0826	0.1722	0.0060
11-12	0.0184	0.0383	0.0120
12-13	0.0730	0.1521	0.0212
4-10	0	0.0267	0
5-11	0	0.0267	0
6-12	0	0.0267	0
9-13	0	0.0356	0
9-14	0	0.0267	0

TABLE 3.5: LOAD DATA.

Bus	P [p.u.]	Q [p.u.]
8	2.5	0.42
10	1.5	0.25
11	1.5	0.25
12	1.5	0.25
13	1.0	0.17
15	1.0	0.17

TABLE 3.6: LIMITS OF THE VARIABLES.

Variable	Lower bound	Upper bound
δ_i - δ_{COI}	-50°	50°
$\Delta\omega_i$	-0.1 p.u.	0.1 p.u.
P_{g1}	0 p.u.	6.00 p.u.
P_{g2}	0 p.u.	5.10 p.u.
P_{g3}	0 p.u.	2.75 p.u.
Q_{g1}	-3.2 p.u.	3.2 p.u.
Q_{g2}	-2.7 p.u.	2.7 p.u.
Q_{g3}	-1.5 p.u.	1.5 p.u.
E_i	0.8 p.u.	1.2 p.u.
δ_i	-9999°	9999°
V_n	0.95 p.u.	1.05 p.u.
ϕ_n	-180°	180°

3.8 References

[1] D. Chattopadhyay and D. Gan, "Market dispatch incorporating stability constraints," International Journal of Electrical Power & Energy Systems, vol. 23, no. 6, pp. 459–469, Aug. 2001.

[2] H. R. Cai, C. Y. Chung and K. P. Wong, "Application of Differential Evolution Algorithm for Transient Stability Constrained Optimal Power Flow," IEEE Transactions on Power Systems, vol. 23, no. 2, pp. 719–728, 2008.

[3] P. Kundur, Power System Stability and Control. McGraw-Hill Professional, 1994.

[4] J. J. Grainger and W. D. Stevenson Jr., Power System Analysis, 1 edition. New York: McGraw-Hill Science/Engineering/Math, 1994.

[5] C. F. Moyano and E. Castronuovo, "Non-Linear Mathematical Programming Applied to Electric Power Systems Stability," in Optimization advances in electric power systems, Nova Science Publishers, Inc, 2009.

[6] L. Chen, Y. Taka, H. Okamoto, R. Tanabe and A. Ono, "Optimal operation solutions of power systems with transient stability constraints," IEEE

Transactions on Circuits and Systems I: Fundamental Theory and Applications, vol. 48, no. 3, pp. 327–339, 2001.

[7] X. Tong, C. Ling and L. Qi, “A semi-infinite programming algorithm for solving optimal power flow with transient stability constraints,” Journal of Computational and Applied Mathematics, vol. 217, no. 2, pp. 432–447, Aug. 2008.

[8] D. Gan, R. J. Thomas and R. D. Zimmerman, “Stability-constrained optimal power flow,” IEEE Transactions on Power Systems, vol. 15, no. 2, pp. 535–540, 2000.

[9] Y. Yuan, J. Kubokawa and H. Sasaki, “Optimal power flow solution with multi-contingency transient stability constraints,” in PowerCon 2002. International Conference on Power System Technology, 2002. Proceedings., 2002, vol. 4, pp. 2009–2013 vol.4.

[10] Yue Yuan, J. Kubokawa and H. Sasaki, “A solution of optimal power flow with multicontingency transient stability constraints,” IEEE Transactions on Power Systems, vol. 18, no. 3, pp. 1094–1102, 2003.

[11] D. Layden and B. Jeyasurya, “Integrating security constraints in optimal power flow studies,” in IEEE Power Engineering Society General Meeting, 2004., 2004, pp. 125–129 Vol.1.

[12] R. Zarate-Minano, T. Van Cutsem, F. Milano and A. J. Conejo, “Securing Transient Stability Using Time-Domain Simulations Within an Optimal Power Flow,” IEEE Transactions on Power Systems, vol. 25, no. 1, pp. 243–253, 2010.

[13] P. M. Anderson and A. A. Fouad, Power System Control and Stability, 2nd ed. Wiley-IEEE Press, 2002.

[14] Siemens Power Technologies International, “PSSE 32.0 “Program Application Guide”.”2009.

[15] D. Ruiz-Vega and M. Pavella, “A comprehensive approach to transient stability control. I. Near optimal preventive control,” IEEE Transactions on Power Systems, vol. 18, no. 4, pp. 1446–1453, 2003.

[16] M. Pavella, D. Ernst and D. Ruiz-Vega, Transient Stability of Power Systems: A Unified Approach to Assessment and Control, 1st ed. Springer, 2000.

[17] I. A. Calle and E. D. Castronuovo, "Optimal Power Flow with Transient Stability Constraints," in MIXGENERA 2011 Options for the future, University Carlos III de Madrid, Leganés, Madrid, Spain., 2011.

[18] Y. H. Li, W. P. Yuan, K. W. Chan and M. B. Liu, "Coordinated preventive control of transient stability with multi-contingency in power systems using trajectory sensitivities," International Journal of Electrical Power & Energy Systems, vol. 33, no. 1, pp. 147–153, Jan. 2011.

[19] K. Atkinson, W. Han and D. E. Stewart, Numerical Solution of Ordinary Differential Equations, 1st ed. Wiley, 2009.

[20] MathWorks, Inc., MATLAB, The Languages of Technical Computing. Version 7.10.0.499 (R2010a). 2010.

[21] "OMIE - Operador del Mercado Ibérico de España." Available: http://www.omie.es.

[22] M. S. Bazaraa, H. D. Sherali and C. M. Shetty, Nonlinear Programming: Theory and Algorithms, 3rd ed. Wiley-Interscience, 2006.

[23] E. D. Castronuovo, J. M. Campagnolo and R. Salgado, "On the application of high performance computation techniques to nonlinear interior point methods," IEEE Transactions on Power Systems, vol. 16, no. 3, pp. 325–331, Aug. 2001.

Chapter 4.

Maximum Loadability of an Isolated System Considering Steady-State and Dynamic Constraints

Abstract— An optimization model to calculate the maximum loadability of a system when subjected to a severe fault is proposed. The model simultaneously considers steady-state and dynamic constraints, with the dynamics of the generators explicitly included in the formulation. The armature current and the field current heating limits of the synchronous generators are also taken into account. The model is solved using a conventional solver based on the primal-dual interior point algorithm, and tested in a realistic system with three generators. The results show that the dynamic constraints can significantly affect the maximum loadability of the system. The effect on the solution of the maximum allowed rotor angle deviation is studied over a wide range of angle limits. Finally, the effect on the loadability of increasing the generation capability of certain plants is studied.

Contents

4.1 Introduction

The continuous increase in the demand and the difficulty of constructing new lines, together with the liberalization of energy markets, has increased significantly the stress in power systems. As a result, the determination of the maximum possible loadability has become an important issue, and studies using optimization algorithms are often executed to determine the maximum loading point of a system.

Frequently the loadability is calculated considering only steady-state restrictions such as voltage limits at buses, current limits at lines and transformers, and generation limits at power plants [1]-[10]. The strong relationship that sometimes arises between voltage stability and loadability is also studied in some of these works [3]-[10]. The limits found in these cases can be associated with static bifurcation points, such as saddle-node bifurcations (in which the state Jacobian matrix of the equilibrium equations becomes singular) or with the generation reactive power limits [2], [12]-[14]. In some cases, the loading limit can be described as the limit of the voltage stability of the system

[4], [15]. In [5]-[8], the maximum loadability limit is calculated using genetic and other innovative algorithms, developed to update power flow variables considering the power mismatches. In [11] a Chaotic Local Search (CLS) is included in the genetic algorithm to overcome possible local optima and reach the global optimum.

Alternatively, the Transient Stability Constrained-Optimal Power Flow (TSC-OPF) is an optimization tool that explicitly includes both steady-state and dynamic constraints in the formulation, and that has received increasing attention over the last years [16]. The TSC-OPF usually includes large numbers of equations and variables, resulting from the addition to the conventional steady-state equations of the dynamic equations representing the electromechanical oscillations at all the discretization points of the time domain simulation. Synchronous generators are usually represented in TSC-OPF by the classical generator model [17]-[22], consisting of a voltage source of constant magnitude behind a transient reactance [23]. Although this model offers a limited accuracy in the representation of the electromechanical transients, it is frequently used to reduce the computational burden of the model. Some approaches handle the size and complexity of the problem by the reduction of the multimachine system to a scheme of two machines (a "single-machine equivalent" strategy) [17], [24], or the modification of the discretization method [25]. Multicontingency cases are also addressed in [18] and [22].

In [26] and [27], an optimization problem considering the effects of both steady-state and dynamic security constraints in the loadability of a system is proposed. In this case, the problem is solved using a mathematical programming method comprising an iterative scheme of two kernels. The first kernel evaluates the security of the operation, and the second one adjusts the generation dispatch. The algorithm requires iterative loops to achieve the optimal values. These works and the work presented in this paper are similar in that they calculate the maximum load considering dynamic constraints, but differ in some important aspects. In the present work: a) the solution is obtained using a single application of a conventional solver, b) reactive power constraints are applied,

and c) the dynamic equations are solved using the trapezoidal rule, which has better stability properties than explicit integration methods.

The restrictions that ensure that the solution is transiently stable usually assume the form of a limitation in the rotor angle deviations. A wide range of rotor angle limits have been used in previous works [18], [20]-[22], [28]-[31]. However, an assessment on the effect of the rotor angle limit on the results, which can help the operator to select a suitable value, has not been found in the literature.

The aim of this study is to extend the later developments of the TSC-OPF tools to the problem of the maximum loadability. This is done by establishing the following objectives:

To propose an optimization model to calculate the maximum loadability of a small system (15 buses, 3 generators) that allows it to retain transient stability after a severe fault. For a given fault, the solution must be obtained by the single solution of the optimization model, without any further iteration.

To analyze the effect of the rotor angle deviation limit on the solution of the maximum loadability of a system.

The first objective is accomplished through an optimization model that includes the static and the dynamic constraints in a unique formulation, and an objective function that accounts for the load. The second objective is studied by means of a systematic solution of the optimization model using different rotor angle limits, and the discussion of the results. The model is applied to a network of 15 buses and 3 generators that represents the power system of two islands in the western Mediterranean Sea. The feasibility of the model is shown by the variety of the situations analyzed, the good convergence obtained in all the cases using a conventional solver and the consistence of the solutions.

4.2 Formulation

4.2.1 Maximum loadability in the optimization model

The model is based on the following assumptions:

- After a severe fault, the transient stability of the system can be ensured if the rotor angle deviation of each generator with respect to the Center of Inertia (COI) does not exceed a certain limit.
- The dynamics of the synchronous generators are represented using the classical model.
- During the electromechanical oscillations the loads are modeled as constant admittances.
- In the search for the maximum load, all loads increase proportionally and the power factor remains constant in each of the loads.

The model imposes restrictions on the bus voltages, the branch currents, the field current, output current and output power of the generators and on the rotor angle deviation with respect to the COI during the electromechanical oscillations. The dynamic equations are integrated using the trapezoidal rule, and the resulting equations are included in the optimization model as equality restrictions.

The objective of the model is to maximize the load scale factor λ. When λ is one, the load at each bus *i* is the load at the base case, P_{Di}, Q_{Di}; as λ increases, the active and reactive load at each bus increases to λP_{Di} , λQ_{Di}. The load is supposed to increase proportionally at every node of the system, although this formulation can be easily modified to scale the load only at some selected buses.

The complete formulation of the model is as follows; the explanation of the equations is presented below.

$$\text{Max.} \quad f(\lambda) = \lambda \tag{4.1}$$

subject to the equality constraints:

$$P_{Gi} - \lambda\, P_{Di} = V_i \sum_{n=1}^{N_b} V_n Y_{in} \cos\left(\phi_i - \phi_n - \theta_{in}\right) \tag{4.2}$$

$$-\lambda\, P_{Dl} = V_l \sum_{n=1}^{N_b} V_n Y_{ln} \cos\left(\phi_l - \phi_n - \theta_{ln}\right) \tag{4.3}$$

$$Q_{Gi} - \lambda\, Q_{Di} = V_i \sum_{n=1}^{N_b} V_n Y_{in} \sin\left(\phi_i - \phi_n - \theta_{in}\right) \tag{4.4}$$

$$-\lambda\, Q_{Dl} = V_l \sum_{n=1}^{N_b} V_n Y_{ln} \sin\left(\phi_l - \phi_n - \theta_{ln}\right) \tag{4.5}$$

$$\begin{aligned} I_{mn} = \Big[&\left(V_m \cos\phi_m - V_n \cos\phi_n\right)^2 + \\ &\left(V_m \sin\phi_m - V_n \sin\phi_n\right)^2 \Big]^{1/2} Y_{Bmn} \end{aligned} \tag{4.6}$$

$$I_{Gi} = \left[\left(E_i' \cos\delta_i^0 - V_i \cos\phi_i\right)^2 + \left(E_i' \sin\delta_i^0 - V_i \sin\phi_i\right)^2 \right]^{1/2} / x_{Di}' \tag{4.7}$$

$$P_{Gi} = E_i' V_i \sin\left(\delta_i^0 - \phi_i\right) / x_{Di}' \tag{4.8}$$

$$Q_{Gi} = -V_i^2 / x_{Di}' + E_i' V_i \cos\left(\delta_i^0 - \phi_i\right) / x_{Di}' \tag{4.9}$$

$$\Delta\omega_i^0 = 0 \tag{4.10}$$

$$\delta_i^{t+1} - \delta_i^t - \omega_0 \Delta t \left(\Delta\omega_i^{t+1} + \Delta\omega_i^t\right) / 2 = 0 \tag{4.11}$$

$$\begin{aligned} &\Delta\omega_i^{t+1}\left(1 + D_i \Delta t / \left(4H_i\right)\right) - \\ &\Delta\omega_i^t \left(1 - D_i \Delta t / \left(4H_i\right)\right) - \Delta t \left(2P_{Gi} - P_{Ei}^{t+1} - P_{Ei}^t\right) / \left(4H_i\right) = 0 \end{aligned} \tag{4.12}$$

$$P_{Ei}^t = E_i' \sum_j E_j' Y_{REDij}(\lambda) \cos\left(\delta_i^t - \delta_j^t - \theta_{REDij}\right) \tag{4.13}$$

$$\delta_{COI}^t = \sum_i H_i \delta_i^t \Big/ \sum_i H_i \tag{4.14}$$

and subject to the inequality constraints:

$$V_{MIN} \le V_m \le V_{MAX} \tag{4.15}$$

$$0 \le I_{mn} \le I_{MAX} \tag{4.16}$$

$$P_{Gi}^2 + \left(Q_{Gi} + V_{Gi}^2 / x'_{Di}\right)^2 \le \left(E_{\mathrm{MAXi}} V_{Gi} / x'_{Di}\right)^2 \tag{4.17}$$

$$P_{MIN} \le P_{Gi} \le P_{MAX} \tag{4.18}$$

$$0 \le I_{Gi} \le I_{GMAX} \tag{4.19}$$

$$-\delta_{MAX} \le \delta_i^t - \delta_{COI}^t \le \delta_{MAX} \tag{4.20}$$

$$\delta_{ABSMIN} \le \delta_i^t \le \delta_{ABSMAX} \tag{4.21}$$

$$\Delta\omega_{MIN} \le \Delta\omega_i^t \le \Delta\omega_{MAX} \tag{4.22}$$

$$E'_{MIN} \le E'_i \le E'_{MAX} \tag{4.23}$$

$$\phi_{MIN} \le \phi_m \le \phi_{MAX} \tag{4.24}$$

$$\lambda_{MIN} \le \lambda \le \lambda_{MAX} \tag{4.25}$$

$\forall i, j \in \{generators\}; \forall l \in \{loads\}; \forall m, n \in \{buses\}; \forall t \in \{iterations\}$

The meaning of the equality constraints is:

- Equations (4.2) to (4.5) represent the balance between input and output power in the generation and non-generation buses. The load in these equations is directly affected by the load scale factor.
- Equation (4.6) calculates the current in the branches of the power system (lines and transformers).
- Equation (4.7) calculates the output current of the generators.
- Equations (4.8) and (4.9) obtain the initial output active and reactive power of the generators as a function of the internal voltage, the terminal voltage and the transient reactance.

- Equation (4.10) sets the initial value of the speed deviation of the generators, which is zero.
- Equations (4.11) and (4.12) represent the application of the trapezoidal rule to the swing equation of the generators at each time step. Two different time steps have been used in order to reduce the number of constraints: $\Delta t = 0.02$ s during the fault and $\Delta t = 0.05$ s after the fault.
- Equation (4.13) calculates the active power output of the generators at each time step. This value is computed as a function of the internal voltages of the machines and the reduced admittance matrix Y_{RED}. The matrix Y_{RED} is calculated by applying the Kron reduction to the bus admittance matrix Y, retaining only the internal nodes of the generators [17]-[19].
- Equation (4.14) calculates the angle of the COI at each iteration step.

The meaning of the inequality constraints is:

- Equations (4.15) and (4.16) represent the limits on the voltages at the buses and on the currents through the branches, respectively.
- Equation (4.17) represents the limit on the field current of the generators. The maximum loadability of the system usually corresponds to a situation in which the reactive production of the power plants is close to the limit. Therefore it is important to model the reactive power capability of the generators. Fig. 4.1 shows the power plant capability curves [34] used in the optimization model. Equation (4.17) corresponds to the field current heating limit in this figure.
- Equations (4.18) and (4.19) represent the bounds due to the active power limit and the armature current heating limit in Fig. 4.1.
- Equation (4.20) represents the maximum allowed rotor angle deviation with respect to the COI during the electromechanical

oscillations following the disturbance. The COI has been used in previous TSC-OPF works [22], [25], [32], [33], and has the advantage of providing a central reference that makes it possible to separate the rotor angle deviations due to the electromechanical oscillations from the deviation due to the acceleration of the system.

- Equations (4.21)-(4.25) specify the range of the rest of the variables.

When the applied fault is a short circuit, the dynamic representation includes: a) The pre-fault stage, with all the circuits in service, determining the initial conditions of the system; b) The fault stage, in which the voltage at the point of the short circuit is zero; and c) The post-fault stage, in which the fault has been cleared by the protection systems and the voltage is restored. Equations (4.2)-(4.10), (4.15)-(4.19) and (4.23)-(4.25) refer to the pre-fault stage, while equations (4.11)-(4.14) and (4.20)-(4.22) refer to the fault and post-fault stages.

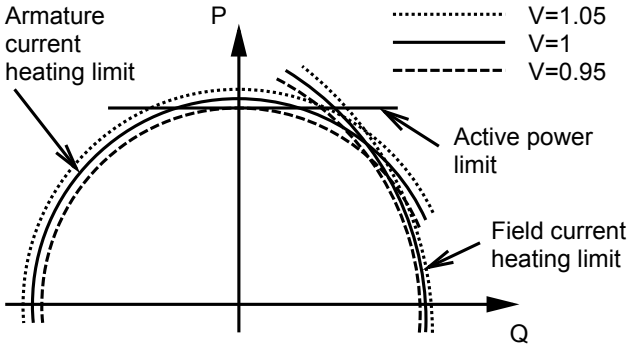

Fig. 4.1. Capability limits of the generators.

4.2.2 Maximum rotor angle deviation

A special consideration must be given to the selection of the rotor angle limits in the optimization model. The state of the system is considered acceptable for a given disturbance if the maximum rotor angle deviation during the electromechanical oscillations with respect to the COI does not exceed a certain value. The selection of the maximum rotor angle deviation results from a compromise between accuracy and reliability. On one hand, using a large angle (for example, close to 180°) makes it possible to maximize the loadability, according to the dynamic model used in the study. On the other hand, reducing

the maximum angle deviation has the advantage of introducing a security margin, which is very convenient because the complexity of the dynamics of the system cannot be modeled in detail due to computational constraints.

As mentioned in Section 4.1, previous works have used different rotor angle limits over a wide range although, to the knowledge of the authors, neither the effect of the angle limits on the numerical stability nor on the solution has been previously addressed. An estimation of the effect of the rotor angle limit on the solution can provide valuable information for the selection of this limit. The effect is difficult to estimate *a priori* because, due to the non-linear nature of the electromechanical oscillations in power systems, a slight modification of the initial operating point can result in major differences in the rotor angle oscillations.

The effect of the rotor angle limits on the solution of the optimization problem has been studied in this work by the systematic application of different limits over a wide range, from 20º to 180°. The sensibility of the loadability to the rotor angle limits can then be inferred from the results.

4.3 Results and discussion

4.3.1 Case of study

The proposed optimization model is applied to a model of the power system of Majorca and Minorca, two islands in the western Mediterranean Sea. Fig. 4.2 shows the one-line diagram of the system, consisting of 15 buses and 3 generators rated 660 MVA, 560 MVA and 300 MVA. The line between buses 14 and 15 is a submarine AC cable that connects both islands. The relevant data of the case, such as the parameters of the dynamic generators (Table 4.1), the parameters of the lines and transformers (Table 4.2), the load data (Table 4.3) and the limits of the variables (Table 4.4) can be found in the Appendix. The total load is 900 MW in the base case.

The proposed optimization model requires a relatively large number of constraints to represent this case. For a total simulation time of $t_{max} = 3$ s and

discretization periods of $\Delta t = 0.02$ s and $\Delta t = 0.05$ s (for the fault and post-fault periods, respectively) the numbers of variables, equality and inequality constraints are 749, 886 and 1,360, respectively. The model is solved on MATLAB using a conventional solver based on the primal-dual interior point method [35]. The tolerances in the convergence are adjusted to 10^{-5}. The solutions are reached in approximately one minute using a medium-cost laptop (Processor 1600 MHz, RAM 2GB).

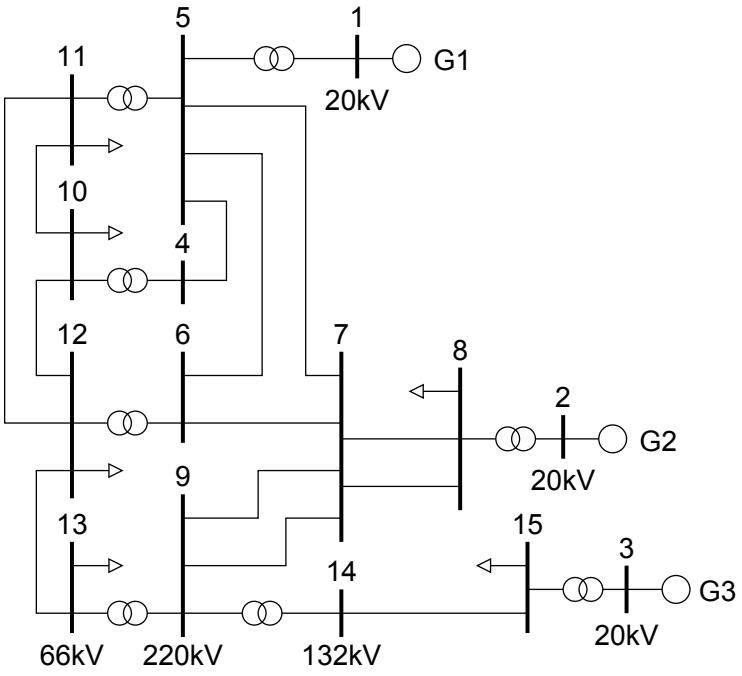

Fig. 4.2. One-line diagram of the case of study.

4.3.2 Maximum loadability without transient stability constraints

For comparison purposes, a classical optimization problem without transient stability constraints is solved. This is done by eliminating equations (10)-(14) and (20)-(22) from the optimization model. A maximum load scale factor $\lambda_{sta.} = 1.48$ is obtained, which means that it is theoretically possible to assume a linearly distributed increase in the load from 900 MW to 1,335 MW considering only steady-state constraints.

Fig. 4.3 shows the current loading at each generator, line and transformer of the system at the maximum load operating point without transient stability

constraints. As can be seen, the capability of generators G_1 and G_2 and the submarine line 14-15 are imposing the limit on the loadability. G_1 and G_2 plants reach their maximum capability, while G_3 generates only 232 MW because the line 14-15 reaches its current limit.

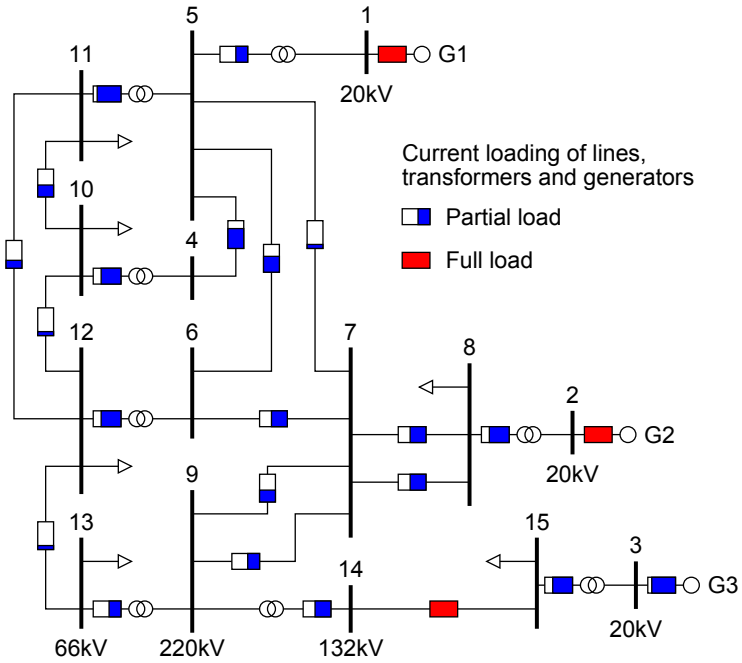

Fig. 4.3. Current load at the point of maximum loadability without transient stability constraints.

4.3.3 Maximum loadability considering transient stability constraints

In this section the dynamic constraints are applied, using the complete formulation proposed in Section 4.2.1. The maximum allowed rotor angle deviation during the electromechanical oscillations imposes an additional limit on the maximum generation. Three different faults are analyzed: a three-phase short circuit close to the main generators (at line 5-7, close to bus 5), a three-phase short circuit far from the main generators (at transformer 9-13, close to bus 13), and the loss of generator G_3.

4.3.3.1 *Three-phase fault close to main generators with maximum rotor angle deviation of 50º*

A three-phase fault is applied in the transmission line between buses 5 and 7, close to bus 5. The fault is cleared by disconnecting the faulty line at both ends after 300 ms. From previous studies this is known to be a very severe fault in the system, due to its proximity to a major generator and to the weakening of the synchronization torque between generators G_1 and G_2 after the loss of this line.

This section shows in detail the solution obtained with a maximum rotor angle deviation of 50° with respect to the COI, which is in the range typically used in TSC-OPF. Parameter δ_{MAX} is set to the value of 50º in equation (4.20). The solution of the complete optimization problem results in a maximum load scale factor $\lambda_{dyn.} = 1.20$, corresponding to a demand of 1,080 MW. This implies a reduction in the maximum loadability of 255 MW, or 19 %, with respect to the solution when no dynamic constraints are considered. The maximum possible generation of G_1 and G_3 is reduced to 381 MW and 200 MW respectively.

In this case, 20 iterations are required by the solver to achieve the convergence, with a CPU time of approximately 60 s. The solution of the optimization problem makes it possible to represent the trajectories of the rotor angles of the three generators in all the discretization points, which are shown in Fig. 4.4. It can be seen that the rotor angle of generator G_3 reaches the limit COI ± 50º during the first oscillation and that the electromechanical oscillations are progressively damped. The accuracy of the numerical integration using the trapezoidal rule and the proposed time steps has been validated by comparison with a conventional 4^{th} order Runge-Kutta algorithm, and it has been verified that both methods provide the same results.

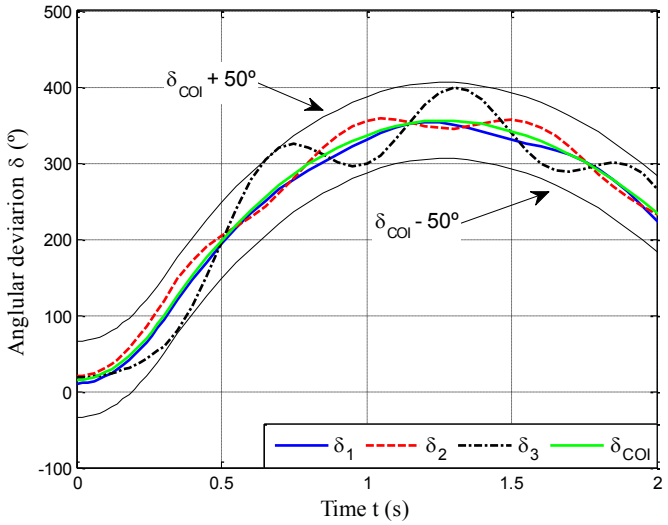

Fig. 4.4. Rotor angle oscillations and limits.

4.3.3.2 *Three-phase fault close to main generators: effect of the rotor angle limit*

Fig. 4.5 a) shows the results obtained when repeating this process with different rotor angle deviation limits δ_{MAX} from 40° to 80°. The dashed line represents the maximum load (1,335 MW) obtained using only steady-state constraints, as explained in Section 4.3.2. The triangle-marked line represents the maximum load obtained using the complete model, for different maximum rotor angular deviations in equation (4.20). In each case, the maximum load in MW is obtained by multiplying the load factor by the initial demand P_d = 900 MW.

The results show that the loadability of the system is considerably reduced when considering the dynamic constraints. The reduction in the loadability is a function of the maximum allowed rotor angle deviation. For example, with a maximum allowed deviation of 40° the reduction in the loadability is 29 %, and with 60° it is 11 %. When the rotor angle limit is above 75° the static restrictions, instead of the dynamic ones, impose the maximum load. The solver provides good convergence in all the studied range.

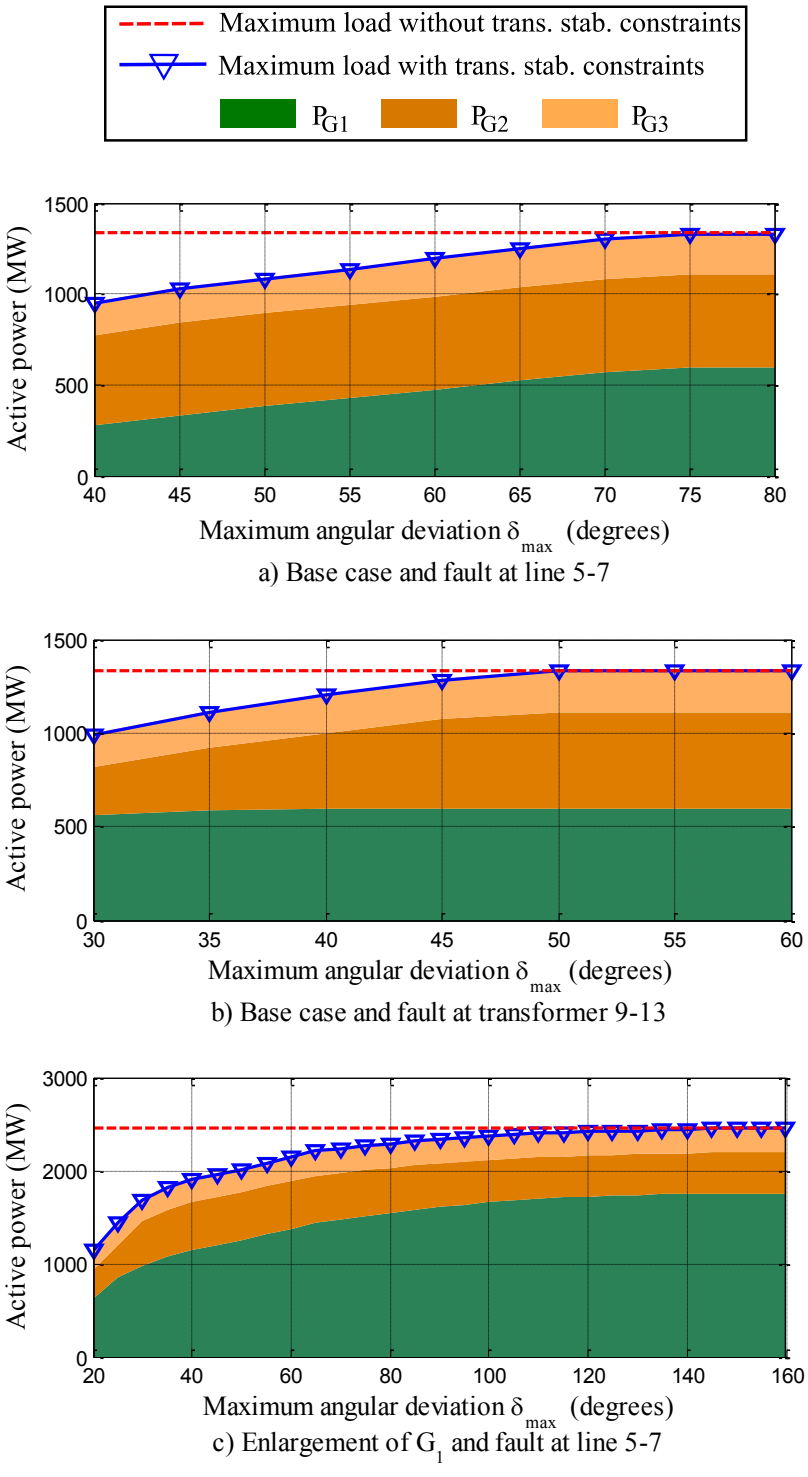

a) Base case and fault at line 5-7

b) Base case and fault at transformer 9-13

c) Enlargement of G_1 and fault at line 5-7

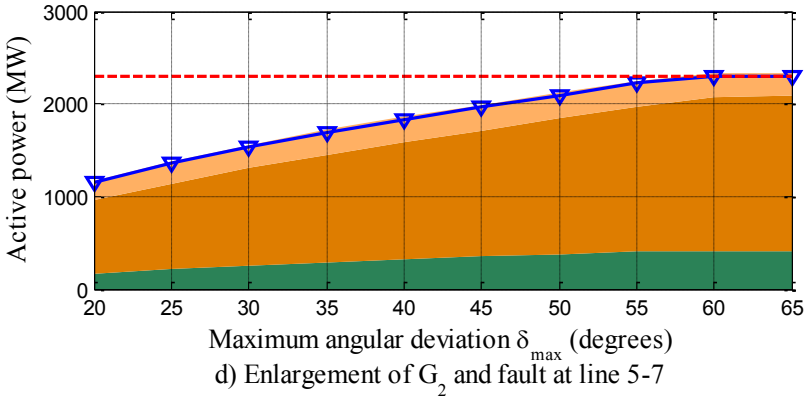

Fig. 4.5. Maximum load and generation dispatch as a function of the rotor angle limit.

The decrease in the maximum load when the rotor angle limit is reduced can be seen as the price that the operator must pay, in terms of maximum acceptable load, to obtain a larger security margin. This decrease is approximately linear in the studied range, up to a rotor angle limit of 75°.

Fig. 4.5 a) shows also the generation profile for different angle limits. It can be seen that generator G_1 (lower area) significantly reduces its output power for small maximum rotor angle deviations. This can be explained because the fault is applied close to generator G_1, and therefore reducing the output power in this generator is the most effective way to reduce the electromechanical oscillations.

Fig. 4.6 a) shows the voltages at the generation and load buses. It can be seen that, to enlarge the loadability of the system when the maximum allowed rotor angle deviation is larger than 55º, the voltages are increased in all the buses. This allows a reduction in the losses, and therefore a maximum use of the capability of the power plants. When the maximum allowed rotor angle deviation is larger than 80º, all the voltages in the generation buses reach the maximum operational limit, 1.05 p.u.

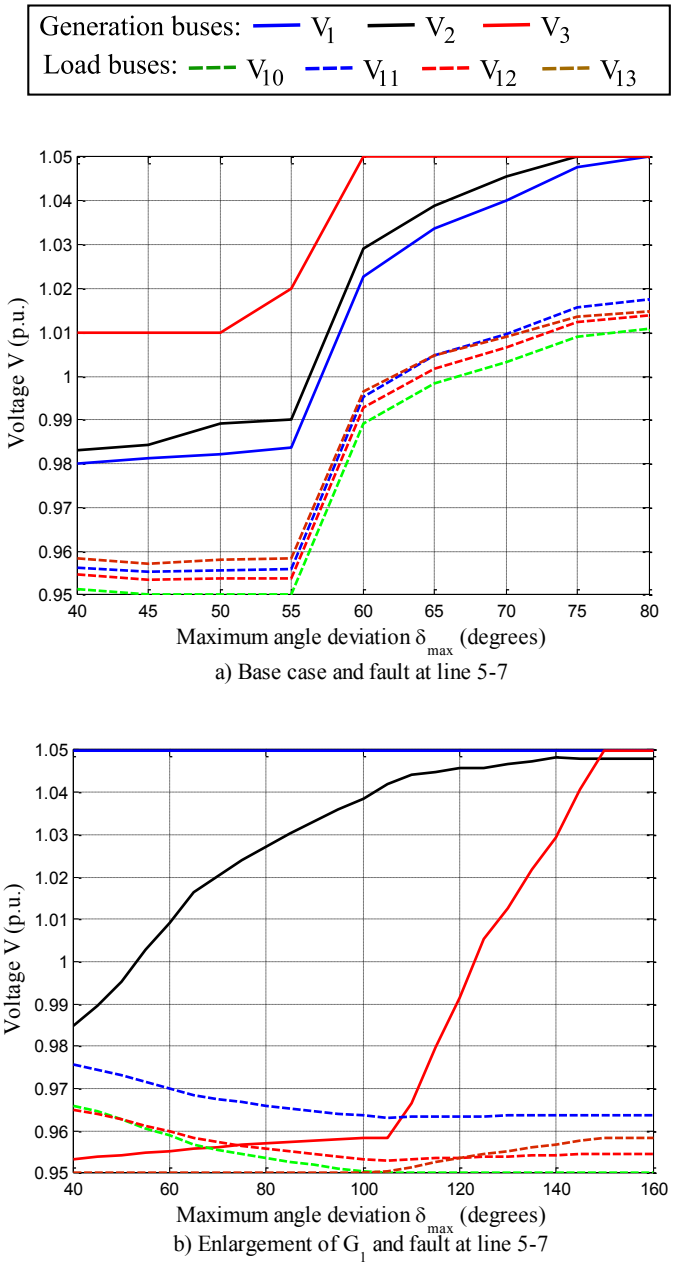

Fig. 4.6. Voltages as a function of the rotor angle limit.

4.3.3.3 *Three-phase fault at a transformer located far from main generators*

A second fault, applied far from the main generators, is analyzed. This fault consists on a three-phase short circuit at bus 9, cleared after 300 ms by the disconnection of the transformer 9-13. Fig. 4.5 b) shows the relationship between the angular deviation limit during the electromechanical transients and the maximum loadability. The comparison of Fig. 4.5 a) and Fig. 4.5 b) shows

that this fault is less restrictive, which can be explained because it is located far from the generators and results in smaller rotor angle oscillations.

Fig. 4.5 b) shows that in this case it is generator G_2 that reduces its output power for small rotor angle deviations. The reason is that generator G_2 is closer to the fault, and therefore reducing its power is the most effective way to reduce electromechanical oscillations.

4.3.3.4 *Loss of generation*

In order to validate the performance of the model a third fault is evaluated, consisting of the loss of generator G_3. While the solver provides a satisfactory solution, it has been observed that the transient stability constraints do not impose any further restriction on the solution. The reason is that the loss of generator G_3 does not result in large electromechanical oscillations between the remaining generators G_1 and G_2.

4.3.4 Effect of installing new generation

In this section, the rated power of the generating plants G_1 and G_2 is enlarged to calculate the effect of installing new generation on the maximum load. This study can help to determine the most effective bus to increase the generation, taking into account both steady-state and dynamic constraints. When increasing each generator, the parameters of the generator model and the corresponding evacuation transformers and lines are scaled according to the increase in the rated power. The enlargement of the plant G_3 is not studied here, because the submarine cable linking buses 14 and 15 does not allow a significant increase in the production of G_3. The applied fault is a short circuit at bus 5 cleared after 300 ms, as in Section 4.3.3.2, because it is the most severe fault here studied.

4.3.4.1 *Enlargement of generator G_1*

As in the Section 4.3.2, the maximum loadability without transient stability constraints is calculated for comparison purposes. When increasing the

rated power of G_1 to 1,980 MVA and 1,800 MW, the maximum static loadability is $\lambda_{sta.} = 2.73$ (2,457 MW). In this case, G_1 is producing 1,756 MW, below the new maximum capacity. Fig. 4.7 shows the distribution of the voltage at the grid at the point of maximum static loadability in this case, while Fig. 4.8 shows the voltage profile. It can be seen from these figures that the loadability of the system is limited by the voltage constraints: the voltage at generation buses 1, 2 and 3 are at the maximum level (1.05 p.u.) while the voltage at bus 10 is at the minimum (0.95 p.u.).

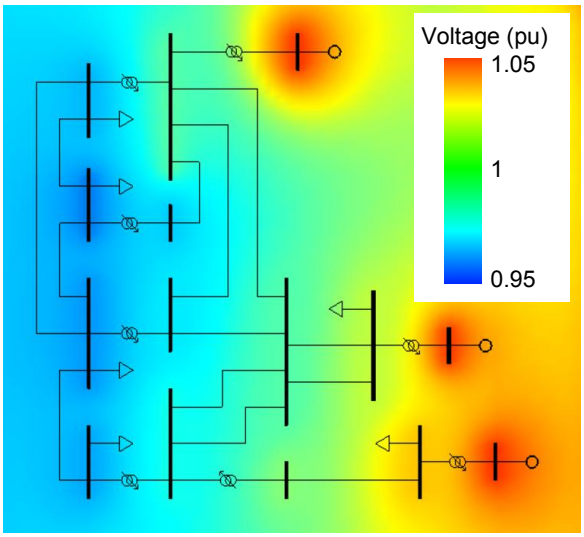

Fig. 4.7. Voltage distribution with extra generation at G_1 and without dynamic constraints.

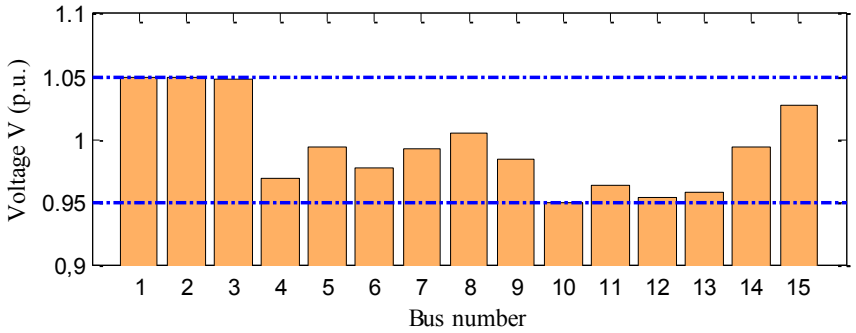

Fig. 4.8. Voltage profile with extra generation at G_1 and without dynamic constraints.

When the dynamic constraints are considered, the maximum load of the system is reduced depending on the value of the maximum rotor angle deviation, as shown in Fig. 4.5 c). Due to the electrical proximity of generator G_1 to the

fault, the dynamic constraints limit the maximum loadability up to a rotor angle limit of 140°.

In this case a strong non linearity appears in the relationship between the rotor angle limit and the loadability. The loadability curve in Fig. 4.5 c) can be explained as follows: a decrease in the rotor angle limit from 160° to 75° results in a larger security margin without a major loss in system loadability; a further decrease below 75° increases the security margin but at the cost of a major reduction in loadability; below 40º the decrease in the loadability is even steeper.

Fig. 4.6 b) shows the voltages at the generation and load buses. To increase the loadability, the solution of the optimization model maintains the voltage at bus 1 at its upper limit. When the rotor angle limit is lower than 100º, the voltages V_2 and V_3 at the generation buses remain inside the allowed area. When the rotor angle limit is larger than 100º, the voltages rapidly go to the limits. This result confirms that when large rotor variations are allowed (reducing the security margin), the system reaches the maximum loadability due to steady-state constraints.

4.3.4.2 *Enlargement of generator G_2*

The maximum static loadability provided by the optimization algorithm when enlarging G_2 capacity to 2,040 MW and 2,244 MVA is $\lambda_{sta.} = 2.56$ (2,304 MW). The voltage restrictions are responsible again for the maximum loadability, and the maximum generation of G_2 in this situation is 1,679 MW.

Fig. 4.5 d) shows the maximum loadability when the dynamic constraints are considered. It can be seen that the effect of the dynamic constraints is not as important as in the previous case, because the generator G_2 is not so close to the fault. Only for rotor angle deviation limits smaller than 60°, the transient stability requirements impose a limitation on the loadability. However, it must be noted that this value is larger than the rotor angle limit used in many dynamic studies.

4.4 Conclusions

A method to obtain the maximum loadability of a system, taking into account both steady-state and transient stability constraints, is proposed. The optimization problem is formulated as a compact set of equations that include the steady-state and dynamic analyses of the fault, and the solution is obtained using a conventional solver. The method is applied to a system with 15 buses and 3 generators. The viability of the model is proved by the variety of the cases to which it is applied and the variety of the restrictions that impose a limit on the solution. Throughout the study, and depending on the case, the most constraining limits are:

- The capability of the generators, as shown in generators G_1 and G_2 in Fig. 4.3.
- The maximum current through a line, as shown in line 14-15 in Fig. 4.3.
- The voltage limits, as shown in Fig. 4.6 b), Fig. 4.7 and Fig. 4.8.
- The transient stability constraints, as shown in Fig. 4.4.

Good convergence is obtained in all the cases.

The effect of the transient stability constraints on the maximum loadability is quantified by comparing the results with those calculated with a classical optimization problem with only steady-state constraints. Fig. 4.5 shows that in many cases the transient stability constraints significantly reduce the loadability margins. This proves that it is necessary to include the dynamic constraints in the optimization model to achieve transiently stable solutions.

The effect of the rotor angle deviation limit on the maximum loadability is evaluated by performing the analysis over a wide range of angle limits, as shown in Fig. 4.5. This analysis provides a useful resource to assist in the selection of the maximum angle limit for the operation. While the studied cases do not allow the inferring of a general principle, a strong non-linearity has been found in the range between 20° and 120°. Fig. 4.5 c) suggests that a security

margin can be obtained by decreasing the rotor angle deviation limit from 120° to 75°, without affecting largely to the loadability. However, further decreases in the rotor angle limit result in large reductions in the admissible load.

The small size of the studied system allows to retain the dynamics of the different plants without resorting to the aggregation of generators. Although the computational burden of the TSC-OPF remains always a limitation in its full development, from a strictly mathematical point of view the proposed formulation can be extended to larger power systems. The relatively short time taken by the optimization algorithm and the good convergence in all the cases, suggest that the model could probably be applied to larger systems.

4.5 Nomenclature

Name	Variable	Units
E'_i	Internal voltage of the i^{th} generator	p.u.
I_{mn}	Current between buses *m* and *n*	p.u.
I_{Gi}	Output current of the i^{th} generator	p.u.
P^t_{Ei}	Active power output of the i^{th} generator at time step *t*	p.u.
P_{Gi}	Active power generation at bus *i*	p.u.
Q_{Gi}	Reactive power generation at bus *i*	p.u.
V_i	Voltage magnitude at bus *i*	p.u.
δ^t_i	Angular deviation of the i^{th} generator at time step *t*	rad.
δ^t_{COI}	Angle of the center of inertia at time step *t*	rad.
ϕ_i	Voltage angle at bus *i*	rad.
λ	Load scale factor	-
$\Delta\omega^t_i$	Frequency deviation of the i^{th} generator at time step *t*	p.u.

Name	Parameter	Units
D_i	Damping coefficient of the i^{th} generator	p.u.
H_i	Inertia constant of the i^{th} generator	s
P_{Di}	Active power demand at bus *i*	p.u.
Q_{Di}	Reactive power demand at bus *i*	p.u.
Δt	Time step	s
x'_{Di}	Transient reactance of the i^{th} generator	p.u.
Y_{Bmn}	Branch admittance between buses *m* and *n*	p.u.

Y_{in}	Magnitude of the element (i,n) of the bus admittance matrix	p.u.
Y_{REDij}	Magnitude of the element (i,j) of the reduced admittance matrix	p.u.
θ_{in}	Phase of the element (i,n) of the bus admittance matrix	rad.
θ_{REDij}	Phase of the element (i,j) of the reduced admittance matrix	rad.
ω_0	Frequency reference	rad./s

4.6 Appendix

TABLE 4.1: DYNAMIC PARAMETERS OF THE GENERATORS.

Generator	X'd [p.u.]	Sb [MVA]	H [s]	D [p.u.]	Technology
G_1	0.3	660	3.0	2	Combined cycle
G_2	0.3	560	3.2	2	Coal
G_3	0.25	300	2.0	2	Gas

All parameters in the following tables are referred to a common 100 MVA base and to the corresponding voltage rating.

TABLE 4.2: PARAMETERS OF LINES AND TRANSFORMERS.

Branch	R [p.u.]	X [p.u.]	B [p.u.]	Imax [p.u.]
1-5	0	0.0117	0	10.0
2-8	0	0.0137	0	10.0
3-15	0	0.0255	0	5.0
4-5	0.0022	0.0145	0.0253	2.5
5-6	0.0019	0.0121	0.0211	2.5
5-7	0.0051	0.0330	0.0576	1.0
6-7	0.0042	0.0274	0.0477	1.0
7-8 (1)	0.0025	0.0161	0.0281	1.0
7-8 (2)	0.0025	0.0161	0.0281	1.0
7-9 (1)	0.0024	0.0153	0.0267	1.0
7-9 (2)	0.0024	0.0153	0.0267	1.0
14-15	0.0804	0.1205	0.0451	0.8
10-11	0.0202	0.0421	0.0132	0.5
10-12	0.0826	0.1722	0.0060	0.5
11-12	0.0184	0.0383	0.0120	0.5
12-13	0.0730	0.1521	0.0212	0.5
4-10	0	0.0267	0	3
5-11	0	0.0267	0	3
6-12	0	0.0267	0	3
9-13	0	0.0356	0	3
9-14	0	0.0267	0	1.5

TABLE 4.3: LOAD DATA.

Bus	P [p.u.]	Q [p.u.]
8	2.5	0.42

10	1.5	0.25
11	1.5	0.25
12	1.5	0.25
13	1.0	0.17
15	1.0	0.17

TABLE 4.4: LIMITS OF VARIABLES.

Variable	Lower bunder	Upper bunder
$\Delta\omega_i$	-0.1 p.u.	0.1 p.u.
P_{G1}	0	6.00 p.u.
P_{G2}	0	5.10 p.u.
P_{G2}	0	2.75 p.u.
I_{G1}	- 6.6 p.u.	6.6 p.u.
I_{G2}	- 5.6 p.u.	5.6 p.u.
I_{G3}	- 3.0 p.u.	3.0 p.u.
E_i	0.8 p.u.	1.2 p.u.
δ_i^0	$-\pi$ rad.	π rad.
δ_i^t	-999 rad.	999 rad.
V_n	0.95 p.u.	1.05 p.u.
$\phi_n; n \neq 1$	$-\pi$ rad.	π rad.
ϕ_1	0	0

4.7 References

[1] L. V. Barboza and L. A. Heckttheuer, “Identifying Critical Limits for the Maximum Loadability of Electric Power Systems”, in Large Engineering Systems Conference on Power Engineering, 2007, 2007, pp. 148 -153.

[2] C. F. Moyano, R. Salgado and L. V. Barboza, “Calculating participation factors in the maximum loadability”, in Power Tech Conference Proceedings, 2003 IEEE Bologna, 2003, vol. 2, p. 6 pp. Vol.2.

[3] N. P. Patidar and J. Sharma, “Loadability margin estimation of power system using model trees”, in 2006 IEEE Power India Conference, 2006, p. 6 pp.

[4] C. D. Vournas, M. Karystianos and N. G. Maratos, “Bifurcation points and loadability limits as solutions of constrained optimization problems”, in Power

Engineering Society Summer Meeting, 2000. IEEE, 2000, vol. 3, pp. 1883 - 1888 vol. 3.

[5] P. Acharjee, “Identification of Maximum Loadability Limit under security constraints using Genetic Algorithm”, in 2011 International Conference on System Science and Engineering (ICSSE), 2011, pp. 234 -238.

[6] P. Acharjee and S. K. Goswami, “Power flow analysis under critical conditions by the linear perturbation-based simple algorithm”, Electrical Engineering, vol. 94, n.o 4, pp. 187-196, dic. 2011.

[7] P. Acharjee, “Identification of maximum loadability limit and weak buses using security constraint genetic algorithm”, International Journal of Electrical Power & Energy Systems, vol. 36, n.o 1, pp. 40-50, mar. 2012.

[8] P. Acharjee, “Identification of voltage collapse points and weak buses under security constraints using hybrid particle swarm optimization technique”, International Transactions on Electrical Energy Systems, vol. 23, n.o 2, pp. 230–248, 2013.

[9] P. W. Sauer, B. C. Lesieutre and M. A. Pai, “Maximum loadability and voltage stability in power systems”, International Journal of Electrical Power & Energy Systems, vol. 15, n.o 3, pp. 145-153, jun. 1993.

[10] G. D. Irisarri, X. Wang, J. Tong and S. Mokhtari, “Maximum loadability of power systems using interior point nonlinear optimization method”, IEEE Transactions on Power Systems, vol. 12, n.o 1, pp. 162 -172, feb. 1997.

[11] P. Acharjee, S. Mallick, S. S. Thakur and S. P. Ghoshal, “Detection of maximum loadability limits and weak buses using Chaotic PSO considering security constraints”, Chaos, Solitons & Fractals, vol. 44, n.o 8, pp. 600-612, ago. 2011.

[12] B. Tamimi, C. A. Canizares and S. Vaez-Zadeh, “Effect of Reactive Power Limit Modeling on Maximum System Loading and Active and Reactive Power Markets”, IEEE Transactions on Power Systems, vol. 25, n.o 2, pp. 1106 -1116, may 2010.

[13] T. Van Cutsem, "A method to compute reactive power margins with respect to voltage collapse", IEEE Transactions on Power Systems, vol. 6, n.o 1, pp. 145 -156, feb. 1991.

[14] I. Dobson and L. Lu, "Voltage collapse precipitated by the immediate change in stability when generator reactive power limits are encountered", IEEE Transactions on Circuits and Systems I: Fundamental Theory and Applications, vol. 39, n.o 9, pp. 762 -766, sep. 1992.

[15] L. L. Grigsby, Power system stability and control. CRC Press, 2007.

[16] C. F. Moyano and E. Castronuovo, "Non-Linear Mathematical Programming Applied to Electric Power Systems Stability", in Optimization advances in electric power systems, Nova Science Publishers, Inc, 2009.

[17] R. Zarate-Minano, T. Van Cutsem, F. Milano and A. J. Conejo, "Securing Transient Stability Using Time-Domain Simulations Within an Optimal Power Flow", IEEE Transactions on Power Systems, vol. 25, n.o 1, pp. 243-253, 2010.

[18] Yue Yuan, J. Kubokawa and H. Sasaki, "A solution of optimal power flow with multicontingency transient stability constraints", IEEE Transactions on Power Systems, vol. 18, n.o 3, pp. 1094-1102, 2003.

[19] Y. Yuan, J. Kubokawa and H. Sasaki, "Optimal power flow solution with multi-contingency transient stability constraints", in PowerCon 2002. International Conference on Power System Technology, 2002. Proceedings., 2002, vol. 4, pp. 2009-2013 vol.4.

[20] D. Gan, R. J. Thomas and R. D. Zimmerman, "Stability-constrained optimal power flow", IEEE Transactions on Power Systems, vol. 15, n.o 2, pp. 535-540, 2000.

[21] D. Layden and B. Jeyasurya, "Integrating security constraints in optimal power flow studies", in IEEE Power Engineering Society General Meeting, 2004., 2004, pp. 125-129 Vol.1.

[22] L. Hakim, J. Kubokawa, Y. Yuan, T. Mitani, Y. Zoka, N. Yorino, Y. Niwa, K. Shimomura and A. Takeuchi, "A Study on the Effect of Generation

Shedding to Total Transfer Capability by Means of Transient Stability Constrained Optimal Power Flow", IEEE Transactions on Power Systems, vol. 24, n.o 1, pp. 347 -355, feb. 2009.

[23] P. M. Anderson and A. A. Fouad, Power System Control and Stability, 2.a ed. Wiley-IEEE Press, 2002.

[24] A. Pizano-Martianez, C. R. Fuerte-Esquivel and D. Ruiz-Vega, "Global Transient Stability-Constrained Optimal Power Flow Using an OMIB Reference Trajectory", IEEE Transactions on Power Systems, vol. 25, n.o 1, pp. 392-403, 2010.

[25] Quanyuan Jiang and Zhiguang Huang, "An Enhanced Numerical Discretization Method for Transient Stability Constrained Optimal Power Flow", IEEE Transactions on Power Systems, vol. 25, n.o 4, pp. 1790-1797, 2010.

[26] D. Gan, Z. Qu, H. Cai and X. Wang, "Loadability of generation/transmission systems with unified steady-state and dynamic security constraints", in 1996 IEEE Transmission and Distribution Conference, 1996. Proceedings, 1996, pp. 537 -542.

[27] D. Gan, Z. Qu and X. Wu, "Loadability of power systems with steady-state and dynamic security constraints", International Journal of Electrical Power & Energy Systems, vol. 25, n.o 2, pp. 91-96, feb. 2003.

[28] Y. Xia, K. W. Chan and M. Liu, "Direct nonlinear primal-dual interior-point method for transient stability constrained optimal power flow", IEE Proceedings-Generation, Transmission and Distribution, vol. 152, n.o 1, pp. 11-16, 2005.

[29] L. Chen, Y. Taka, H. Okamoto, R. Tanabe and A. Ono, "Optimal operation solutions of power systems with transient stability constraints", IEEE Transactions on Circuits and Systems I: Fundamental Theory and Applications, vol. 48, n.o 3, pp. 327-339, 2001.

[30] D. Z. Fang, Y. Xiaodong, S. Jingqiang, Y. Shiqiang and Z. Yao, "An Optimal Generation Rescheduling Approach for Transient Stability Enhancement", IEEE Transactions on Power Systems, vol. 22, n.o 1, pp. 386-394, 2007.

[31] T. B. Nguyen and M. A. Pai, "Dynamic security-constrained rescheduling of power systems using trajectory sensitivities", IEEE Transactions on Power Systems, vol. 18, n.o 2, pp. 848-854, 2003.

[32] Y. H. Li, W. P. Yuan, K. W. Chan and M. B. Liu, "Coordinated preventive control of transient stability with multi-contingency in power systems using trajectory sensitivities", International Journal of Electrical Power & Energy Systems, vol. 33, n.o 1, pp. 147-153, ene. 2011.

[33] I. A. Calle, E. D. Castronuovo and P. Ledesma, "Optimal re-dispatch of an isolated system considering transient stability constraints", International Journal of Electrical Power & Energy Systems, vol. 44, n.o 1, pp. 728-735, Jan.. 2013.

[34] P. Kundur, Power System Stability and Control. McGraw-Hill Professional, 1994.

[35] MathWorks, Inc., MATLAB, The Languages of Technical Computing. Version 7.10.0.499 (R2010a). 2010.

Chapter 5.

Advanced Application of Transient Stability Constrained-Optimal Power Flow to a Transmission System Including an HVDC-LCC Link

Abstract— In this paper, a Transient Stability Constrained-Optimal Power Flow (TSC-OPF) model is proposed and applied to a realistic case in the currently interconnected Balearic Islands-Iberian Peninsula system. The TSC-OPF retains the dynamics of all generators in the islands with 4th degree transient synchronous generator models and includes a representation of a High Voltage Direct Current (HVDC) link on the inverter side. The proposed model is used to assess the economic impact of the HVDC on the Balearic Islands generation cost under different circumstances, using TSC-OPF and traditional OPF on the dispatch. Different recovery patterns of the HVDC link after a severe fault in the transmission grid are evaluated from the viewpoint of the cost and stability of power generation.

Contents

5.1 Introduction

Transient Stability Constrained-Optimal Power Flow (TSC-OPF) techniques include an economic objective and static and dynamic constraints in the same optimization problem [1]-[3]. Therefore, TSC-OPF is an adequate tool for creating a transparent mechanism for calculating optimal economic operation when the system is restricted by steady-state and stability constraints.

During the past decade, TSC-OPF techniques have received increasing attention, with clearly differentiated approaches for representing and assessing the problem of transient stability [1], [4]. In the traditional TSC-OPF methods, transient stability constraints are formulated as rotor angle swing equations [1], [5]-[12]. The differential equations used in the dynamic models of synchronous machines are converted to algebraic form, using implicit numerical integration methods, such as the trapezoidal rule, and are included in the optimization model [5]. This technique increases the dimensions of the problem because it introduces large numbers of variables and equations that grow with the number of integration steps. Previously, most studies have focused on reducing the size

of the problem and improving the computational efficiency. For example, the authors of [6] proposed a method based on functional transformation techniques and converted an infinite-dimensional into a finite-dimensional optimization problem. In [7] and [8], a modified formulation using the reduced admittance matrix to represent the electric power in the swing equation was used, which considerably reduced the equality constraints. These studies allowed [7] to implement multi-contingencies studies. In [9], steady-state and dynamic behaviors were separately analyzed using different solvers. In [10], the authors propose a penalty-based approach in which the adjoint equation method is applied to evaluate the gradient of the penalty term associated with the stability constraints, improving the method proposed in [6]. In [11], a method for calculating the Jacobian and Hessian matrices is introduced to reduce the massive calculation of these matrices when functional transformation techniques are used. In [12], considering the truncation error of specific numerical integration algorithms, the differential equations are discretized as inequality constraints rather than equality constraints, to improve the computational efficiency. All previous studies use the classical dynamic model to represent the generators because it only requires two differential equations for each power plant. This approach reduces the computational burden of the problem at the cost of neglecting electromagnetic transients in the rotor that have an impact on transient stability [13].

Other approaches are based on direct methods (Lyapunov functions; equal area criterion, etc.), as in [2], [14]-[18]. In these studies, generators are classified as critical or non-critical machines and the Single-Machine Equivalent (SIME) method is generally used to obtain the most simplified equivalent system. The angle trajectory on a one-machine vs. infinity-bus equivalent (OMIB) is used to obtain information about the transient stability margins. Direct methods require less computational effort but can introduce non-negligible errors due to the highly nonlinear nature of the problem [1].

This paper follows a traditional approach, in which the dynamics of all power plants in the system are retained and the TSC-OPF model is solved as a

whole. The proposed TSC-OPF model is applied to the Balearic Islands power system in Spain. This system covers three islands that are interconnected by submarine AC cables and was recently (2013) connected to the mainland by a High-Voltage Direct Current link with Line-Commutated Converters (HVDC-LCC). This link has an important impact on the economic dispatch, because the cost of energy is lower on the mainland than on the islands. In addition, this link affects other critical technical aspects, such as transient stability. Particularly, the strategy for recovering the HVDC link after a severe fault in the islands transmission grid significantly affects the stability of the system. The TSC-OPF model proposed in this paper is used to analyze several alternatives to recover the HVDC link after a fault based on the viewpoint of economic dispatch and transient stability.

Section 5.2 describes two novel features of the proposed TSC-OPF model. First, an HVDC-LCC link is included, modeled as a power injection and that can represent different recovery strategies after a fault. Second, the implementation of the transient synchronous two-axes generator model improves the accuracy of the simulation by representing the electromagnetic transients in the stator. Section 5.3 details the mathematical formulation of the proposed TSC-OPF, Section 5.4 describes the Balearic power system and Section 5.5 shows the results obtained from the solution of the proposed model. Finally, the conclusions are presented in Section 5.6.

5.2 System representation

The TSC-OPF model contains two different parts [1]. The first part corresponds with pre-fault steady-state conditions and includes all conventional OPF constraints, including power flow equations, the capability limits of generators and voltage, current limits throughout the grid, and equality constraints for determining the initial conditions of the dynamic variables. The second part corresponds with the transient stage and includes equality constraints (to represent the dynamic equations of the generators at the fault and post-fault stages) and inequality constraints (to represent the stability condition).

Transient equations are formulated by using a reduced admittance matrix, which is obtained by applying the Kron reduction to the original nodal admittance matrix [19]. The reduced admittance matrix usually only retains the internal nodes of the generators. In addition to the generator buses, the Point of Common Coupling (PCC) of the HVDC is also retained in the present formulation. Next subsections explain two novel features included in the proposed TSC-OPF model, the HVDC link and the synchronous generator two-axes transient model.

5.2.1 HVDC-LCC model for TSC-OPF

HVDC transmission can be based on two alternative technologies: Line Commutated Converter (LCC) that uses thyristors, and Voltage Source Converter (VSC) that uses Insulated Gate Bipolar Transistors (IGBT). VSCs do not require an external voltage source for its operation and its reactive power control is independent of the active power control. Generally, HVDC-LCC is used for high power applications of up to 6300 MW. This technology requires an external source to provide commutation voltage and to allow the converters to work properly [20]. The HVDC link between the continent and the Balearic Islands is a 2x200 MW double link with ± 250 kV transmission cables based on LCC technology. Its length is 244 km with a maximum depth of 1,485 m below sea level, and it is operated under normal conditions at a maximum power of 310 MW. During normal operations, the rectifier side of the HVDC functions in current control mode and the inverter side functions in voltage control mode, resulting in constant power injection at the HVDC output bus [13]. For example, if the voltage decreases slightly in the output bus, the current from the HVDC increases to maintain a constant power. However, the current increase cannot exceed 10 to 20 % of the rated current [13], [21].

When a three-phase fault occurs near the inverter side in the AC system, the voltage decreases more or less depending on the location and the severity of the disturbance. The Voltage Dependent Current Order Limit (VDCOL) function plays an important role during voltage dips because it imposes a limit on the maximum current when the AC voltage drops below a predetermined

value. Fig. 5.1 (a) shows a typical VDCOL function, such as the one implemented in the studied case [13]. The minimum voltage, V_{min}, is the limit under which the HVDC disconnects, and the maximum voltage, V_{max}, is the limit above which the HVDC can operate without restrictions on the current.

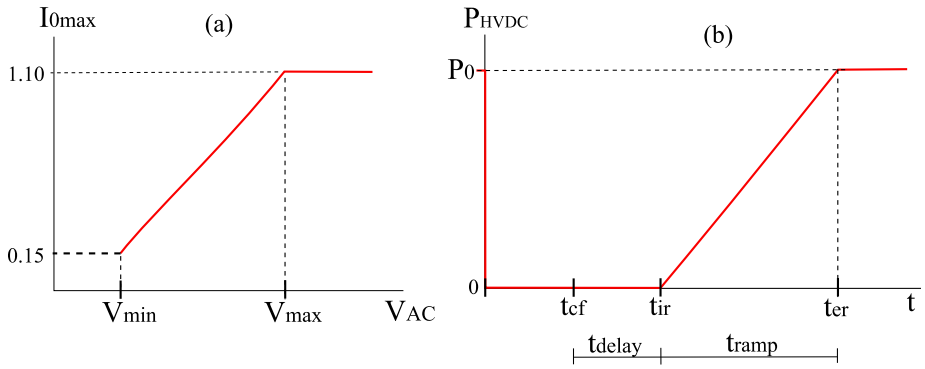

Fig. 5.1. Dynamic behaviour of the HVDC facing disturbances.

Transient stability studies consider worst-case scenarios in which the most severe disturbances are analyzed. Preliminary simulations of the relatively small power system considered in this paper and described in Section 5.4, indicated that a 3-phase short circuit at the transmission level near the HVDC inverter side always results in a voltage dip under V_{min} that triggers the disconnection of the HVDC. In addition, once the fault is cleared, the voltage at the PCC of the HVDC recovers to a level greater than V_{max}. Fig. 5.2 shows an example of the voltage at the PCC of the HVDC during and after a short-circuit in the transmission network.

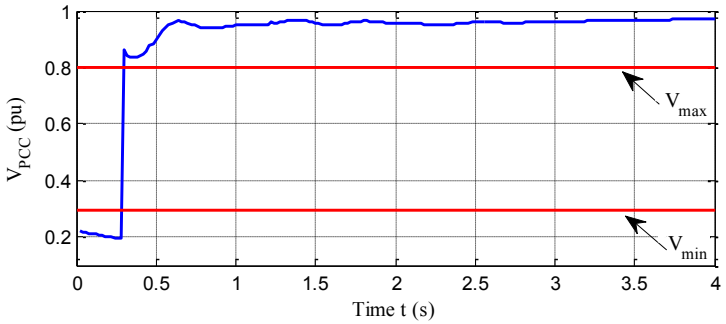

Fig. 5.2. Voltage profile in the connection bus of the HVDC link.

Fig. 5.1 (b) shows a typical curve of the active power provided by the HVDC link during and after a severe voltage drop at the PCC. When the fault

occurs at time $t = 0$, the voltage decreases to below V_{min} and the output power from the HVDC is decreased to zero. After the fault is cleared at $t = t_{cf}$, a delay time of t_{delay} is applied to allow the voltage to stabilize. At $t = t_{ir} = t_{cf} + t_{delay}$, the HVDC begins operating again and the power control gradually increases the power set point during a time t_{ramp}, until the pre-fault value is reached at $t = t_{er}$. Mathematically, this model is written as follows:

$$P_{HVDC_h}^{t} = \begin{cases} P_{HVDC_h}^{0} & \text{at} \quad t = 0 \\ 0 & \text{at} \quad 0 < t \le t_{ir} \\ P_{HVDC_h}^{0}(t - t_{ir}) / t_{ramp} & \text{at} \quad t_{ir} < t \le t_{er} \\ P_{HVDC_h}^{0} & \text{at} \quad t_{er} < t \end{cases} \tag{5.1}$$

where the power at $t = 0$ is calculated using steady-state and dynamic initial equations in the pre-fault stage.

The HVDC-LCC link always demands reactive power during its operation. In the present case, the reactive power demanded by the HVDC-LCC is assumed to be 50 % of the injected active power. The values of t_{delay} and t_{ramp} are important because a fast recovery of the HVDC-LCC after a short-circuit can imply that a weak AC system (such as the one studied in this paper) could have problems in providing sufficient reactive power at the rate required by the HVDC. The time for a HVDC system to recover to 90 % of its pre-fault power is typically between 100 and 500 ms, depending on the DC and AC system characteristics and the control strategy used [22]. Different values of t_{delay} and t_{ramp}, including $t_{ramp} = 0$ (i.e., a step recovery), are evaluated in Section 5.5 to analyze their impact on operation costs.

The response of the control of an HVDC system to a fault in the AC network is very fast, compared with the time frame of electromechanical oscillations between synchronous generators. This difference in the speed of response makes it possible to neglect the dynamics of the controls of HVDC links in transient stability studies and to model the HVDC link as a power injection. Consequently, the following equations represent the active and

reactive power injected by a HVDC-LCC link connected at bus *h* during the transient stage:

$$\left.\begin{aligned} P_{HVDC} &= V_h \sum_{\forall v} V_v Y_{hv} \cos\theta_{hv} - \\ &\quad V_h \sum_{\forall j} Y_{hj} \left(E'_{dj} \sin(\delta_j + \theta_{hj} - \alpha_h) + E'_{qj} \cos(\delta_j + \theta_{hj} - \alpha_h) \right) \\ Q_{HVDC} &= V_h \sum_{\forall v} V_v Y_{hv} \sin\theta_{hv} - \\ &\quad V_h \sum_{\forall j} Y_{hj} \left(E'_{dj} \cos(\delta_j + \theta_{hj} - \alpha_h) + E'_{qj} \sin(\delta_j + \theta_{hj} - \alpha_h) \right) \end{aligned}\right\} \quad (5.2)$$

Where $V_v \angle \alpha_v$ is the voltage at the connection bus of the v^{th} HVDC link, and E'_{dj}, E'_{qj} and δ_j are the *d* and *q* components and the angle of the internal voltage of the j^{th} generator. $Y_{hj} \angle \theta_{hj}$ is the (*h, j*) element of the reduced admittance matrix that only retains the connection buses of the HVDC links and the internal nodes of the synchronous generators.

5.2.2 Transient model of the synchronous generator for TSC-OPF

Due to the heavy computational effort required to solve the TSC-OPF model, previous studies retained the dynamics of all power plants by using the classical model to represent synchronous generators [5], [7]. To improve the accuracy of this study, it is used the 4^{th} order synchronous generator transient model, which makes it possible to represent the electromagnetic transients in the generator rotor. These transients affect the electromagnetic torque of the machines, and the transient stability of the system. The well-known electrical equations of the transient model are [13], [19]:

$$dE'_{di}/dt = \left(-E'_{di} + \left(x_{qi} - x'_{qi} \right) I_{qi} \right) / T'_{q0i} \quad (5.3)$$

$$dE'_{qi}/dt = \left(-E'_{qi} - \left(x_{di} - x'_{di} \right) I_{di} + E_{fdi} \right) / T'_{d0i} \quad (5.4)$$

$$\left.\begin{aligned} E'_{di} &= V_{di} + r_{ai} I_{di} - x'_{qi} I_{qi} \\ E'_{qi} &= V_{qi} + r_{ai} I_{qi} + x'_{di} I_{di} \end{aligned}\right\} \quad (5.5)$$

where $V_{di} = V_i \sin(\delta_i - \alpha_i)$, $V_{qi} = V_i \cos(\delta_i - \alpha_i)$, $I_{di} = I_{Gi} \sin(\delta_i - \alpha_i + \varphi_i)$, $I_{qi} = I_{Gi} \cos(\delta_i - \alpha_i + \varphi_i)$.

The mechanical equations are:

$$d\Delta\omega_i / dt = \left(P_{mi} - P_{ei} - D_i \Delta\omega_i\right) / (2H_i) \tag{5.6}$$

$$d\delta_i / dt = \omega_0 \Delta\omega_i \tag{5.7}$$

$$P_{ei} = E'_{di} I_{di} + E'_{qi} I_{qi} \tag{5.8}$$

The trapezoidal rule is used to discretize differential equations (5.3)-(5.4) and (5.6)-(5.7) and the resulting equations are included in the optimization model (as shown in Section 5.3).

All machine electrical variables are referred to a *dq* reference frame fixed to the rotor of the generator. Because grid electrical variables are referred to in a common synchronous rotating *αβ* reference frame, an additional *dq*-*αβ* rotation is required at each machine to calculate the voltage or current within the grid. To reduce the number of constraints in the optimization model, electrical variables at the grid are eliminated and the current $I_{di} + jI_{qi}$, is calculated as a function of the internal voltages [19]:

$$\left.\begin{aligned} I_{di} &= \sum_{\forall j} Y_{ij} \left(E'_{dj} \cos\left(\delta_i - \delta_j - \theta_{ij}\right) + E'_{qj} \sin\left(\delta_i - \delta_j - \theta_{ij}\right)\right) \\ I_{qi} &= \sum_{\forall j} Y_{ij} \left(E'_{qj} \cos\left(\delta_i - \delta_j - \theta_{ij}\right) - E'_{dj} \sin\left(\delta_i - \delta_j - \theta_{ij}\right)\right) \end{aligned}\right\} \tag{5.9}$$

5.3 Mathematical formulation

This section provides the complete set of equations that constitute the proposed TSC-OPF model, to facilitate the replication of the results. The proposed model is programmed on GAMS [23] and solved using the CONOPT tool, which is a solver for large-scale nonlinear optimization [24]. Because the Balearic Power System is not currently operated as a liberalized market, the objective function includes the production costs of the power plants. In this application, the cost is computed as a linear function of power plants production.

The cost of the power injected from the HVDC link depends on the Iberian market. A linear representation of the prices in the Iberian day-ahead market is included in the simulations obtained from data provided by the Iberian Market Operator [25]. From the economic viewpoint, the HVDC injection is dispatched as any other conventional producer on the Islands. The complete mathematical formulation of the considered TSC-OPF model is:

$$\text{Min. } f(P_{Gi},P^{0}_{HVDC_h}) = \sum\left(a_i P_{Gi} + a_h P^{0}_{HVDC_h}\right) \tag{5.10}$$

subject to

$$\left.\begin{aligned} P_{Gi} - P_{Di} - V_i\sum_{\forall n} V_n Y^{Bus}_{in}\cos\left(\alpha_i-\alpha_n-\theta^{Bus}_{in}\right)=0\\ P^{0}_{HVDC_h} - P_{Dh} - V_h\sum_{\forall n} V_n Y^{Bus}_{hn}\cos\left(\alpha_h-\alpha_n-\theta^{Bus}_{hn}\right)=0\\ -P_{Dl} - V_l\sum_{\forall n} V_n Y^{Bus}_{ln}\cos\left(\alpha_l-\alpha_n-\theta^{Bus}_{ln}\right)=0 \end{aligned}\right\} \tag{5.11}$$

$$\left.\begin{aligned} Q_{Gi} - Q_{Di} - V_i\sum_{\forall n} V_n Y^{Bus}_{in}\sin\left(\alpha_i-\alpha_n-\theta^{Bus}_{in}\right)=0\\ Q^{0}_{HVDC_h} - Q_{Dh} - V_h\sum_{\forall n} V_n Y^{Bus}_{hn}\sin\left(\alpha_h-\alpha_n-\theta^{Bus}_{hn}\right)=0\\ -Q_{Dl} - V_l\sum_{\forall n} V_n Y^{Bus}_{ln}\sin\left(\alpha_l-\alpha_n-\theta^{Bus}_{ln}\right)=0 \end{aligned}\right\} \tag{5.12}$$

$$\left(I_{mn}\right)^2 - \left[\left(V_m\cos\alpha_m - V_n\cos\alpha_n\right)^2 + \left(V_m\sin\alpha_m - V_n\sin\alpha_n\right)^2\right]\left(Y^{Bus}_{mn}\right)^2 = 0 \tag{5.13}$$

$$\left.\begin{aligned} \left(V_i I_{Gi}\right)^2 - {P_{Gi}}^2 - {Q_{Gi}}^2 = 0\\ \sin\varphi_i - Q_{Gi}/V_i I_{Gi} = 0 \end{aligned}\right\} \tag{5.14}$$

$$\left.\begin{aligned} E'^{0}_{di} - \left(x_{qi}-x'_{qi}\right)I_{Gi}\cos\left(\delta^0_i-\alpha_i+\varphi_i\right)=0\\ E'^{0}_{qi} + \left(x_{di}-x'_{di}\right)I_{Gi}\sin\left(\delta^0_i-\alpha_i+\varphi_i\right) - E_{fdi}=0 \end{aligned}\right\} \tag{5.15}$$

$$\left.\begin{aligned} V_i \sin\left(\delta_i^0 - \alpha_i\right) - E_{di}'^0 + \left(r_{ai} \sin\left(\delta_i^0 - \alpha_i + \varphi_i\right) - \right. \\ \left. x_{qi}' \cos\left(\delta_i^0 - \alpha_i + \varphi_i\right)\right) I_{Gi} = 0 \\ V_i \cos\left(\delta_i^0 - \alpha_i\right) - E_{qi}'^0 + \left(r_{ai} \cos\left(\delta_i^0 - \alpha_i + \varphi_i\right) + \right. \\ \left. x_{di}' \sin\left(\delta_i^0 - \alpha_i + \varphi_i\right)\right) I_{Gi} = 0 \end{aligned}\right\} \tag{5.16}$$

$$\left.\begin{aligned} I_{di}^0 - I_{Gi} \sin\left(\delta_i^0 - \alpha_i + \varphi_i\right) = 0 \\ I_{qi}^0 - I_{Gi} \cos\left(\delta_i^0 - \alpha_i + \varphi_i\right) = 0 \end{aligned}\right\} \tag{5.17}$$

$$\left.\begin{aligned} P_{ei}^0 - P_{Gi} = 0 \\ \Delta\omega_i^0 = 0 \end{aligned}\right\} \tag{5.18}$$

$$\left.\begin{aligned} E_{di}'^{t+1}\left(1 + \Delta t/2T_{q0i}'\right) - \\ E_{di}'^{t}\left(1 - \Delta t/2T_{q0i}'\right) - \left(\Delta t/2T_{q0i}'\right)\left(x_{qi} - x_{qi}'\right)\left(I_{qi}^{t+1} + I_{qi}^{t}\right) = 0 \\ E_{qi}'^{t+1}\left(1 + \Delta t/2T_{d0i}'\right) - \\ E_{qi}'^{t}\left(1 - \Delta t/2T_{d0i}'\right) - \left(\Delta t/2T_{d0i}'\right)\left[2E_{fdi} - \left(x_{di} - x_{di}'\right)\left(I_{di}^{t+1} + I_{di}^{t}\right)\right] = 0 \end{aligned}\right\} \tag{5.19}$$

$$\left.\begin{aligned} \Delta\omega_i^{t+1}\left(1 + D_i\Delta t/4H_i\right) - \\ \Delta\omega_i^{t}\left(1 - D_i\Delta t/4H_i\right) - \left(\Delta t/4H_i\right)\left(2P_{mi} - P_{ei}^{t+1} - P_{ei}^{t}\right) = 0 \\ \delta_i^{t+1} - \delta_i^{t} - \left(\Delta t/2\right)\omega_0\left(\Delta\omega_i^{t+1} + \Delta\omega_i^{t}\right) = 0 \end{aligned}\right\} \tag{5.20}$$

$$P_{ei}^t - E_{di}'^t I_{di}^t - E_{qi}'^t I_{qi}^t = 0 \tag{5.21}$$

$$\left.\begin{aligned} P_{HVDC_h}^t - V_h^t \sum_{\forall v} V_v^t Y_{hv} \cos\theta_{hv} - \\ V_h^t \sum_{\forall j} Y_{hj}\left(E_{dj}'^t \sin(\delta_j^t + \theta_{hj} - \alpha_h^t) + E_{qj}'^t \cos(\delta_j^t + \theta_{hj} - \alpha_h^t)\right) = 0 \\ Q_{HVDC_h}^t - V_h^t \sum_{\forall v} V_v^t Y_{hv} \sin\theta_{hv} - \\ V_h^t \sum_{\forall j} Y_{hj}\left(E_{dj}'^t \cos(\delta_j^t + \theta_{hj} - \alpha_h^t) + E_{qj}'^t \sin(\delta_j^t + \theta_{hj} - \alpha_h^t)\right) = 0 \end{aligned}\right\} \tag{5.22}$$

$$Q_{HVDC_h}^t + P_{HVDC_h}^t / 2 = 0 \tag{5.23}$$

$$\left.\begin{array}{ll} P^{t}_{HVDC_h} = 0 & \text{at} \quad 0 < t \le t_{ir} \\ P^{t}_{HVDC_h} - P^{0}_{HVDC_h}(t - t_{ir})/t_{ramp} = 0 & \text{at} \quad t_{ir} < t \le t_{er} \\ P^{t}_{HVDC_h} - P^{0}_{HVDC_h} = 0 & \text{at} \quad t_{er} < t \end{array}\right\} \tag{5.24}$$

$$\left.\begin{array}{l} I^{t}_{d_i} - \sum\limits_{\forall j} Y_{ij}\left(E''^{t}_{d_j}\cos\left(\delta^{t}_{i} - \delta^{t}_{j} - \theta_{ij}\right) + E''^{t}_{q_j}\sin\left(\delta^{t}_{i} - \delta^{t}_{j} - \theta_{ij}\right)\right) - \\ \quad \sum\limits_{\forall h} Y_{ih}V^{t}_{h}\sin\left(\delta^{t}_{i} - \alpha^{t}_{h} - \theta_{ih}\right) = 0 \\ I^{t}_{q_i} - \sum\limits_{\forall j} Y_{ij}\left(E''^{t}_{q_j}\cos\left(\delta^{t}_{i} - \delta^{t}_{j} - \theta_{ij}\right) - E''^{t}_{d_j}\sin\left(\delta^{t}_{i} - \delta^{t}_{j} - \theta_{ij}\right)\right) - \\ \quad \sum\limits_{\forall h} Y_{ih}V^{t}_{h}\cos\left(\delta^{t}_{i} - \alpha^{t}_{h} - \theta_{ih}\right) = 0 \end{array}\right\} \tag{5.25}$$

$$\delta^{t}_{COI} - \sum_{i} H_i\delta^{t}_{i} \Big/ \sum_{i} H_i = 0 \tag{5.26}$$

$$-\delta^{MAX.}_{Stab.} \le \delta^{t}_{i} - \delta^{t}_{COI} \le \delta^{MAX.}_{Stab.} \tag{5.27}$$

$$V^{MIN.}_{m} \le V_m \le V^{MAX.}_{m};\ \alpha^{MIN.}_{m} \le \alpha_m \le \alpha^{MAX.}_{m};\ 0 \le I_{mn} \le I^{MAX.}_{mn} \tag{5.28}$$

$$\begin{array}{c} P^{MIN.}_{Gi} \le P_{Gi} \le P^{MAX.}_{Gi};\ 0 \le I_{Gi} \le I^{MAX.}_{Gi}; \\ P^{2}_{Gi} + \left(Q_{Gi} + V^{2}_{Gi}/x'_{Di}\right)^{2} \le \left(E_{\mathrm{MAXi}}V_{Gi}/x'_{Di}\right)^{2} \end{array} \tag{5.29}$$

$$\Delta\omega^{MIN.} \le \Delta\omega^{t}_{i} \le \Delta\omega^{MAX.};\ \delta^{MIN.} \le \delta^{t}_{i} \le \delta^{MAX.} \tag{5.30}$$

$$\begin{array}{c} E'^{MIN.}_{di} \le E''^{t}_{di} \le E'^{MAX.}_{di};\ E'^{MIN.}_{qi} \le E''^{t}_{qi} \le E'^{MAX.}_{qi};\ E^{MIN.}_{fdi} \le E_{fdi} \le E^{MAX.}_{fdi}; \\ I^{MIN.}_{di} \le I^{t}_{di} \le I^{MAX.}_{di};\ I^{MIN.}_{qi} \le I^{t}_{qi} \le I^{MAX.}_{qi} \end{array} \tag{5.31}$$

$\forall h, v \in \{\mathcal{HVDC}\}; \forall i, j \in \{\mathcal{G}\}; \forall l \in \{\mathcal{L}\}; \forall m, n \in \{\mathcal{N}\}; \forall t \in \{\mathcal{T}\}$.

The meaning of the constraints is described below.

- Equations (5.11) and (5.12) represent the active and reactive power balances in the generation, non-generation and HVDC buses. Bus 1 is the slack bus, with a fixed angle of $\alpha_1 = 0$.
- Equations (5.13) and (5.14) are used to calculate the currents through the branches of the system and in the generators, respectively.

- Equations (5.15) to (5.18) initialize the transient-state variables of the generators $(E'^{0}_{di}, E'^{0}_{qi}, \delta^{0}_{i}, \Delta\omega^{0}_{i}, P^{0}_{ei}, I^{0}_{di}, I^{0}_{qi})$.

- Equations (5.19) and (5.20) result from the application of the trapezoidal rule to the transient stability model of the generators at each time step. The time step used during the fault and post-fault periods is $\Delta t = 0.02$ s.

- Equation (5.21) calculates the active power output of each generator at each time step as a function of the current and internal voltage.

- Equations (5.22) to (5.24) represent the HVDC link during the transient stage. Equations (5.22) are used to calculate the power inputs/outputs from the HVDC. In (5.23), the reactive power absorption of the HVDC-LCC link is 50 % of the active power injection. The active power injection is calculated in (5.24), according to (5.1).

- Equations (5.25) are used to calculate the synchronous generator output currents. These equations are a generalization of (5.9) and include the HVDC link. The values of these currents are computed as a function of the internal voltages of the machines, the voltage at the PCC of the HVDC link and the reduced admittance matrix.

- Equation (5.26) is used to calculate the angle of the Centre of Inertia (COI) at each time step and Equation (5.27) represents the transient stability criterion [8], [12], [26], [27]. The COI provides a reference, making it possible to separate the rotor angle deviations due to the electromechanical oscillations from the deviations that result from the acceleration of the system. Therefore, the system is considered fully stable when the separations between any one of the generator angles and the COI remain enclosed in a range.

- Equations (5.28) represent the limits of the bus voltages and branch currents.

- Equations (5.29)-(5.31) represent the limits imposed on the variables.

Equations (5.29) represents the capability limits of the generators, Equations (5.30) represents the limits on speed deviations and rotor angles and Equation (5.31) represents the range of variation of the remaining variables of the generators.

5.4 Studied case

The optimization problem is applied to the power system of Balearic Islands, in the western Mediterranean Sea near the eastern coast of the Iberian Peninsula. Fig. 5.3 shows a simplified map of the power system, including the main power plants, the 220 and 132 kV grids, the HVDC submarine cable linking the Iberian Peninsula and Majorca, and the AC submarine cables between the islands. A new AC submarine cable is being constructed between Majorca and Ibiza Islands and is scheduled to being operating in 2015. In the present case, this cable is also represented using design specifications.

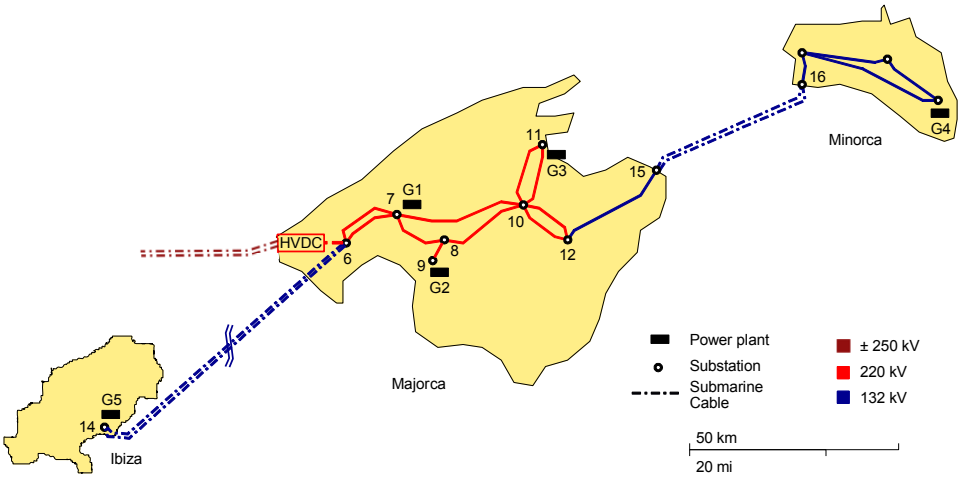

Fig. 5.3. Map of the power system of Balearic Islands.

Fig. 5.4 shows the one-line diagram of the system, which contains five power plants. Here G_1 and G_2 are combined cycle power plants with 660 MVA (600 MW) and 520 MVA (470 MW) respectively, G_3 is a 560 MVA (510 MW) coal-fired power plant, and G_4 and G_5 are 300 MVA (275 MW) and 385 MVA (350 MW) gas turbine plants, respectively. Bus 6 is the PCC of the submarine HVDC-LCC link connecting the Peninsular and the Balearic power systems.

This bipolar link has a rated power of 400 MW with an operating power of 310 MW.

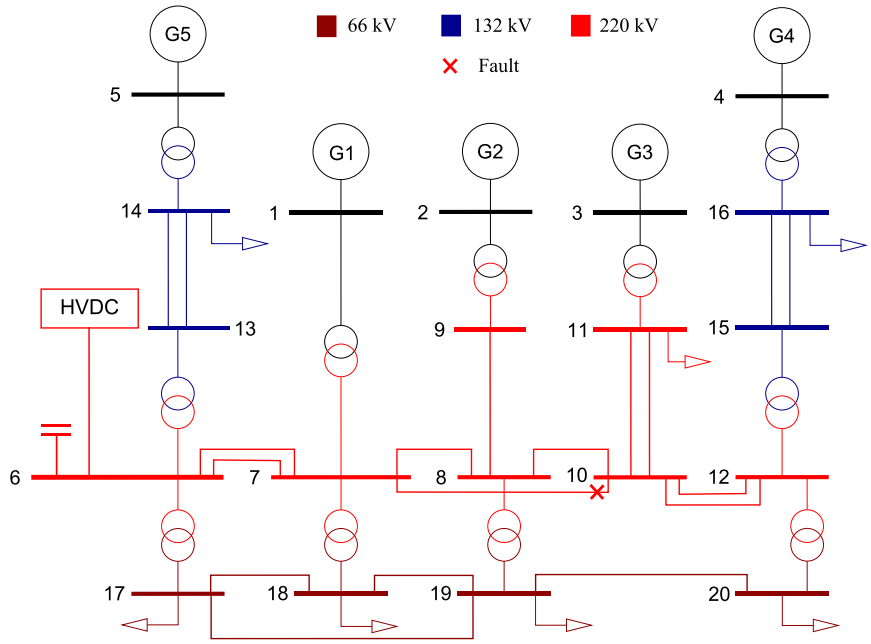

Fig. 5.4. One-line diagram of the studied case.

The AC transmission grid contains three voltage levels: 220, 132 and 66 kV. The HVDC-LCC link is connected to the AC 220 kV level at bus 6. The 66 kV grid has been included in the model because it is a meshed network that provides alternative routes between the 220 kV buses and affects the power flows during the electromechanical transients after the fault.

The Appendix provides detailed data regarding the dynamic parameters of the generators (Table 5.4), the generation prices (Table 5.5), the parameters of the lines and transformers (Table 5.6), the loads (Table 5.7) and the limits of operation (Table 5.8).

The effect of a three-phase fault to ground in the line between buses 7 and 10 and near to bus 10 is analyzed. The fault is cleared after $t_{cf} = 300$ ms by disconnecting the faulty line at both ends. Previous simulations show that this is the most critical disturbance regarding transient stability because it is located near to generator G_3. Generator G_3 is one of the largest generators in the system

and is generally highly dispatched because it is less expensive than other generators.

5.5 Results and discussion

For comparison purposes, Table 5.1 shows the generation costs for the studied case from a conventional OPF (only equations (5.10)-(5.14) and (5.28)-(5.29) of the model) and from the TSC-OPF (equations (5.10)-(5.31)) when the HVDC link is in operation and when it is not in operation ($P_{HVDC} = Q_{HVDC} = 0$). The off-peak load is assumed to be 50 % of the peak load. As shown in the first two columns, when the transient stability is not accounted for, the inclusion of the HVDC link reduces the cost for the peak and off-peak cases by 7.14 % and 12.72 %, respectively. The savings provided by the interconnection are higher at peak load (626.40 – 581.70 = 44.70 M.U.) than at off-peak load (233.85 – 204.10 = 29.75 M.U.), because at peak load the insular generation displaced by the continental market through the HVDC link is more expensive.

TABLE 5.1: COMPARISON OF GENERATION COST WITH AND WITHOUT HVDC, IN MONETARY UNITS [M.U.].

	OPF - no HVDC [M.U.]	OPF with HVDC [M.U.]	Increase [%]	TSC-OPF - no HVDC [M.U.]	Increase [%]
Peak	626.40	581.70	-7.14	716.30	14.35
Off-Peak	233.85	204.10	-12.72	360.28	54.06

By comparing the first and fourth columns in Table 5.1, it can be observed that including the transient stability constraints results in generation costs increases of 14.35 % and 54.06 % for peak and off-peak load scenarios, respectively. The greater cost for providing a stable dispatch results from transferring the power generation from G_3 to more expensive power plants within the insular system.

5.5.1 TSC-OPF with the HVDC link in operation

When the HVDC link is in operation, the stability of the system is affected by its recovery strategy after the fault. In order to provide examples of the solution of the TSC-OPF, this section shows the results with two extreme cases

(as shown un Fig. 5.1 (b)) a fast recovery (t_{delay} = 0 ms, t_{ramp} = 0 s) and a slow recovery (t_{delay} = 300 ms, t_{ramp} = 1.5 s). In all of the cases studied in this paper, it is used a simulation time of $t_{max.}$ = 4.0 s, a time step of Δt = 0.02 s and the maximum deviation of the rotor angles with respect to the COI is set at 60°. Each solution is obtained within approximately 110 seconds, by using a conventional computer with a 3.4 GHz processor and 4 GB RAM.

Fig. 5.5 shows the rotor angles of the generators provided by the optimal TSC-OPF solution when the system is at peak load and with a fast reconnection of the HVDC link after the fault (t_{delay} = 0 ms, t_{ramp} = 0 s). The upper and lower limits represent the stability margin of 60° with respect to the COI. The largest deviation occurs at approximately t = 400 ms, when generator G_3 reaches the angle limit.

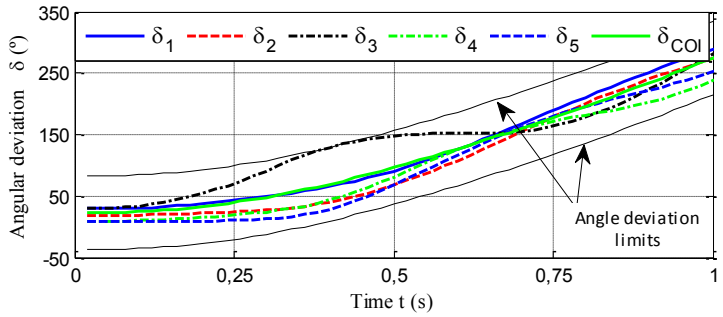

Fig. 5.5. Rotor angular deviation with a fast recovery strategy on the HVDC link.

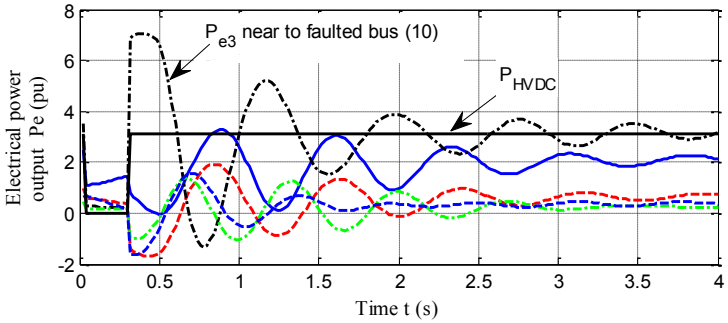

Fig. 5.6. Active power output with a fast recovery strategy on the HVDC link.

Fig. 5.6 shows the active power output from the generators and the HVDC link in the same case and shows that the maximum oscillation corresponds to

G_3. The damping effect of the electromagnetic transients in the rotor progressively reduces the amplitudes of the deviations in the post-fault stage.

Fig. 5.7 and Fig. 5.8 show the same variables when a slow reconnection of the HVDC link is applied (t_{delay} = 300 ms, t_{ramp} = 1.5 s). Again, the optimal solution occurs when generator G_3 reaches the angle limit at approximately t = 400 ms. The speed gained by the system after the fault is lower due to the slow recovery of the HVDC link, which is observed when comparing the final values of the COI in Fig. 5.5 and Fig. 5.7. The recovery pattern of the HVDC following a ramp is shown in Fig. 5.8 , and can be compared to the fast recovery of the HVDC shown in Fig. 5.6.

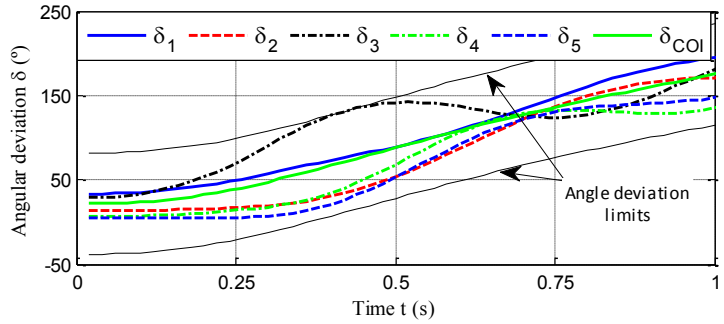

Fig. 5.7. Rotor angular deviation with a slow recovery strategy on the HVDC link.

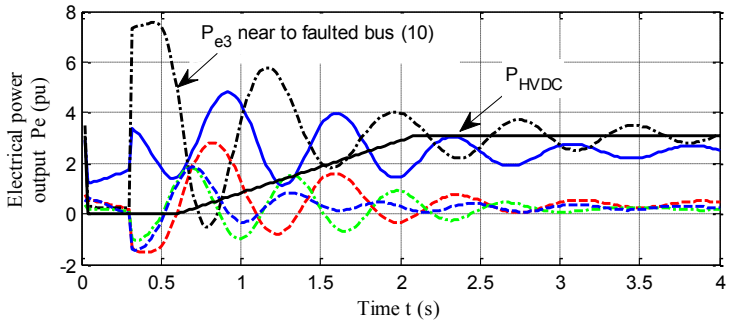

Fig. 5.8. Active power output with a slow recovery strategy on the HVDC link.

5.5.2 Effect of the strategy of recovery of the HVDC on the cost of generation

To determine the most economic option, the proposed TSC-OPF was systematically applied to different power recovery patterns of the HVDC link.

Several values were assigned to parameters t_{delay} and t_{ramp} in the peak and off-peak load scenarios.

Table 5.2 shows the results obtained at peak load for the following extreme values: $t_{delay} = 0$ or 300 ms and $t_{ramp} = 0$ or 1.5 s. Columns P_{G1} to P_{G5} show the generation assigned to each power plant, column P_{HVDC} shows the optimal power transmission assigned to the HVDC link, and the *Cost* column shows the total generation cost in Monetary Units. The last column shows the increasing cost of the corresponding TSC-OPF over the cost of the traditional OPF, which can be considered as the cost of ensuring transient stability when the HVDC link is in operation.

TABLE 5.2: COMPARISON OF GENERATION DISPATCHES AT PEAK LOAD.

	t_{delay} [ms]	t_{ramp} [s]	P_{G1} [MW]	P_{G2} [MW]	P_{G3} [MW]	P_{G4} [MW]	P_{G5} [MW]	P_{HVDC} [MW]	Cost [M.U.]	Increase [%]
OPF	---	---	296	0	510	0	0	310	581.70	---
TSC-OPF	0	0	248	96	350	45	61	310	679.24	16.77
	300	0	291	74	347	40	48	310	669.97	15.17
	0	1.5	289	76	348	39	49	310	670.04	15.19
	300	1.5	292	74	348	38	48	310	669.42	15.08

Table 5.2 shows that the HVDC link is injecting power at its maximum capacity of 310 MW in all five cases. However, to ensure transient stability, generation is transferred from G_1 and G_3 to G_2, G_4 and G_5, which are more expensive power plants. Considering the most economical solution in Table 5.2, (last row, which is a cost of 669.42 M.U.) and comparing it with the values in Table 5.1, it can be seen that the cost of ensuring transient stability without HVDC (716.30 – 626.40 = 89.90 M.U.) is very similar to the case with HVDC (669.42 – 581.70 = 87.72 M.U.). This can be interpreted by saying that the HVDC link only very slightly enhances transient stability in the peak scenario.

Fig. 5.9 shows the increment in cost of the TSC-OPF relative to the OPF at peak load for several t_{delay} and t_{ramp} values, including intermediate values relative to those shown in Table 5.2. In this case, the cost increases when the HVDC link recovers its pre-fault operation point soon after fault clearance.

Fig. 5.9 shows that transient stability can be ensured at a lower cost if the recovery strategy for the HVDC link combines a certain delay and/or a progressive increase in the active power set point. However, this effect also involves a saturation point, where further cost reductions cannot be obtained even if the delay increases or the power injection ramp slows.

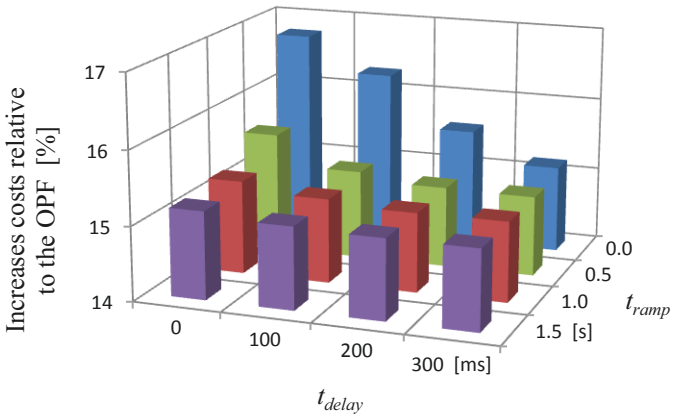

Fig. 5.9. Increases in the TSC-OPF costs relative to the OPF at peak load.

Table 5.3 and Fig. 5.10 show the same study conducted on the off-peak scenario. The first row in Table 5.3 shows that a conventional OPF dispatches the full power from the continental market through the HVDC link, and generator G_3 to cover the demand. The rows corresponding to the TSC-OPF show that the most economical solution also dispatches the HVDC link to its maximum capacity when transient stability constraints are included.

TABLE 5.3: COMPARISON OF GENERATION DISPATCHES AT OFF-PEAK LOAD.

	t_{delay} [ms]	t_{ramp} [s]	P_{G1} [MW]	P_{G2} [MW]	P_{G3} [MW]	P_{G4} [MW]	P_{G5} [MW]	P_{HVDC} [MW]	Cost [M.U.]	Increase [%]
OPF	---	---	0	0	239	0	0	310	204.10	---
TSC-OPF	0	0	44	27	133	14	23	310	254.92	24.90
	300	0	29	21	165	10	14	310	238.54	16.87
	0	1.5	21	16	181	7	15	310	233.11	14.21
	300	1.5	18	14	186	7	15	310	231.09	13.22

Again Fig. 5.10 shows that it is possible to reduce the generation costs while ensuring transient stability if the recovery of the power injected by the HVDC link is delayed after the fault clearance. This characteristic is similar to that obtained in a peak load scenario, and more acute in terms of relative

increments. In this case, the difference between fast (254.92 M.U.) and slow (231.09 M.U.) recovery strategies is 9.35 %.

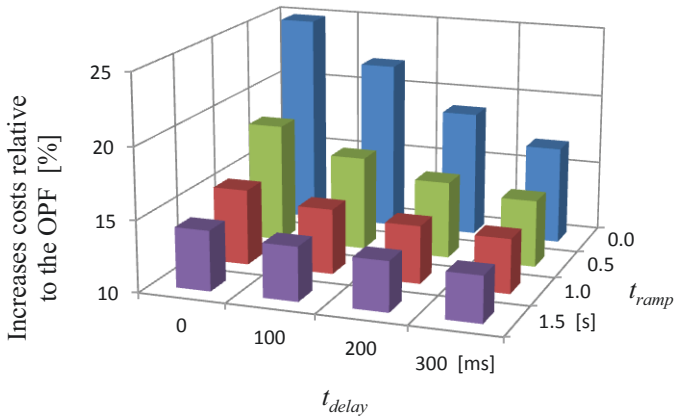

Fig. 5.10. Increases in the TSC-OPF costs relative to the OPF at off-peak load.

It is interesting to note that without the HVDC link, the cost for ensuring transient stability is (360.28 – 233.85 = 126.43 M.U., Table 5.1). When the HVDC link is in operation, the cost for ensuring transient stability is (231.09 – 204.10 = 26.99 M.U., Table 5.3). Therefore, during off-peak operation, the HVDC link has a positive economic impact not only because it has a lower cost compared to the power plants within the island, but because it reduces the cost to stabilize the power system.

Fig. 5.9 and Fig. 5.10 can be used to select the recovery strategy of the HVDC link after a short-circuit in the grid. Given that from the point of view of the frequency stability it is interesting to recover the generation as soon as possible, parameters t_{delay} = 200 ms and t_{ramp} = 1.0 s are a sensible option that results in a significant reduction of costs with respect to a fast reconnection, for both peak and off-peak periods.

5.6 Conclusions

An improved TSC-OPF model is proposed, including an HVDC-LCC link model with a control of power injection and a transient 4^{th} order synchronous generator model on the *dq*-axes to represent the synchronous machines. The dynamics of all synchronous generators are explicitly retained. The proposed model is applied to a realistic test case and solved using GAMS. No

convergence problems have been observed in the solution of the proposed model.

A practical application of the proposed model is analyzed through the study, showing the economic implications of connecting the HVDC-LCC link to an isolated cost-dispatched system. The proposed TSC-OPF model makes it possible to include transient stability constraints in the economic dispatch. It is shown that the stability constraints can increase the generation cost in the studied system up to 25 %, which justifies the use of TSC-OPF over traditional OPF.

The proposed TSC-OPF model allows the analysis of different HVDC link recovery patterns after a severe fault regarding generation cost. This approach largely simplifies a study that involves generation costs, static and dynamic constraints and power control. It is found that a fast reconnection of the HVDC link after a fault in the transmission network results in higher costs, while a short delay in the reconnection can save up to 9.35 % of the generation cost.

5.7 Nomenclature

Name	Variable	Units
$E_d'^t$, $E_q'^t$	Generator internal transient voltage components	p.u.
E_{fd}	Field voltage	p.u.
I_d^t, I_q^t	Generator output current components	p.u.
I_G	Magnitude of the generator output current	p.u.
I_{mn}	Current between buses *m* and *n*	p.u.
P_e^t	Generator active power output	p.u.
P_G, Q_G	Generator active and reactive power output	p.u.
P_{HVDC}^t, Q_{HVDC}^t	HVDC link active and reactive power output	p.u.
V	Bus voltage magnitude	p.u.
V_h^t	Voltage at the HVDC connection bus	p.u.
α	Bus voltage phase	rad.
α_h^t	Voltage phase at the HVDC connection bus	rad.
δ^t	Generator angular deviation	rad.
δ_{COI}^t	Center of inertia angle deviation	rad.
$\Delta\omega^t$	Generator speed deviation	p.u.

φ	Bus angle between current and voltage	rad.

Name	Parameter	Units
a	Generation price	M.U/MW
D	Damping coefficient	p.u.
H	Inertia constant	s
r_a	Armature resistance	p.u.
P_D, Q_D	Active and reactive power demand	p.u.
T'_{d0}, T'_{q0}	Generator transient time constants	s
x_d, x_q	dq axes synchronous reactance	p.u.
x'_d, x'_q	dq axes transient reactance	p.u.
$\mathbf{Y}$	Reduced admittance matrix	p.u.
$\mathbf{Y}^{bus}$	Bus admittance matrix	p.u.
Y_{ij}	Magnitude of the element (i,j) of $\mathbf{Y}$	p.u.
Y_{mn}^{Bus}	Magnitude of the element (m,n) of $\mathbf{Y}^{bus}$	p.u.
Δt	Time step	s
θ_{ij}	Phase of the element (i,j) of $\mathbf{Y}$	rad.
θ_{mn}^{Bus}	Phase of the element (m,n) of $\mathbf{Y}^{bus}$	rad.
ω_0	Frequency reference	rad./s

$()^{MAX}$ $()^{MIN}$ upper and lower limits of the variables.

Sets: $\mathcal{G}$, generators; $\mathcal{HVDC}$, HVDC buses; $\mathcal{L}$, non-generator buses; $\mathcal{N}$, buses; $\mathcal{T}$, time steps.

5.8 Appendix

TABLE 5.4: DYNAMIC PARAMETERS OF THE GENERATORS (MAGNITUDES IN P.U. REFERRED TO BASE POWER 100 MVA).

Generator	S_b [MVA]	R_a [p.u.]	X_d [p.u.]	X'_d [p.u.]	X_q [p.u.]	X'_q [p.u.]	H [s]	D [p.u.]	T'_d [s]	T'_q [s]
G_1	660	0.00	0.227	0.046	0.227	0.046	21.12	13.20	39.60	6.60
G_2	520	0.00	0.290	0.058	0.290	0.058	15.51	10.34	31.02	5.17
G_3	560	0.00	0.267	0.054	0.267	0.054	16.38	11.22	33.66	5.61
G_4	300	0.00	0.496	0.099	0.496	0.099	6.050	6.05	18.15	3.03
G_5	385	0.00	0.390	0.078	0.390	0.078	7.700	7.70	23.10	3.85

TABLE 5.5: ECONOMIC DATA.

Generator	*a* [M.U./MW]
G_1	70.00
G_2	80.00
G_3	40.00
G_4	100.00
G_5	120.00
HVDC	55.00 (Peak) 35.00 (Off-Peak)

All of the parameters in the following tables have a common 100 MVA base and corresponding voltage rating.

TABLE 5.6: PARAMETERS OF THE LINES AND TRANSFORMERS.

Branch	R [p.u.]	X [p.u.]	B [p.u.]
1-7	0	0.0117	0
2-9	0	0.0137	0
3-11	0	0.0137	0
4-16	0	0.0255	0
5-14	0	0.0255	0
6-7 (1)	0.0022	0.0145	0.0253
6-7 (2)	0.0022	0.0145	0.0253
7-8	0.0019	0.0121	0.0211
7-10	0.0051	0.0330	0.0576
8-9	0.0042	0.0274	0.0477
8-10	0.0042	0.0274	0.0477
10-11 (1)	0.0025	0.0161	0.0281
10-11 (2)	0.0025	0.0161	0.0281
10-12 (1)	0.0024	0.0153	0.0267
10-12 (2)	0.0024	0.0153	0.0267
13-14 (1)	0.0080	0.0121	0.0450
13-14 (2)	0.0080	0.0121	0.0450
15-16 (1)	0.0025	0.0377	0.0141
15-16 (2)	0.0025	0.0377	0.0141
17-18	0.0202	0.0421	0.0132
17-19	0.0826	0.1722	0.0060
18-19	0.0184	0.0383	0.0120
19-20	0.0730	0.1521	0.0212

6-13	0	0.0267	0
6-17	0	0.0267	0
7-18	0	0.0267	0
8-19	0	0.0267	0
12-15	0	0.0267	0
12-20	0	0.0356	0

TABLE 5.7: RATED LOADS.

Bus	P [p.u.]	Q [p.u.]
11	2.50	0.42
14	2.10	0.35
16	1.20	0.20
17	1.50	0.25
18	1.50	0.25
19	1.50	0.25
20	1.75	0.29

TABLE 5.8: LIMITS OF THE VARIABLES.

Variable	Lower bound	Upper bound
δ_i - δ_{COI}	-60°	60°
$\Delta\omega_i$	-0.10 p.u.	0.10 p.u.
P_{G1}	0.00 p.u.	6.00 p.u.
P_{G2}	0.00 p.u.	4.70 p.u.
P_{G3}	0.00 p.u.	5.10 p.u.
P_{G4}	0.00 p.u.	2.75 p.u.
P_{G5}	0.00 p.u.	3.50 p.u.
P_{HVDC}	0.00 p.u.	3.10 p.u.
Q_{G1}	-3.00 p.u.	3.00 p.u.
Q_{G2}	-2.35 p.u.	2.35 p.u.
Q_{G3}	-2.55 p.u.	2.55 p.u.
Q_{G4}	-1.35 p.u.	1.35 p.u.
Q_{G5}	-1.75 p.u.	1.75 p.u.
Q_{HVDC}	-1.55 p.u.	0.00 p.u.
E_i	0.8 p.u.	1.2 p.u.
δ_i	-9,999°	9,999°
V_n	0.95 p.u.	1.05 p.u.
ϕ_n	-180°	180°

5.9 References

[1] Y. Xu, Z. Y. Dong, Z. Xu, R. Zhang and K. P. Wong, "Power system transient stability-constrained optimal power flow: A comprehensive review", in 2012 IEEE Power and Energy Society General Meeting, 2012, pp. 1–7.

[2] X. Tu, L.-A. Dessaint and H. Nguyen-Duc, "Transient stability constrained optimal power flow using independent dynamic simulation", IET Generation, Transmission Distribution, vol. 7, no. 3, pp. 244–253, 2013.

[3] K. Verma and K. R. Niazi, "A coherency based generator rescheduling for preventive control of transient stability in power systems", International Journal of Electrical Power & Energy Systems, vol. 45, no. 1, pp. 10–18, Feb. 2013.

[4] F. Capitanescu, J. L. Martinez Ramos, P. Panciatici, D. Kirschen, A. Marano Marcolini, L. Platbrood and L. Wehenkel, "State-of-the-art, challenges and future trends in security constrained optimal power flow", Electric Power Systems Research, vol. 81, no. 8, pp. 1731–1741, Aug. 2011.

[5] D. Gan, R. J. Thomas and R. D. Zimmerman, "Stability-constrained optimal power flow", IEEE Transactions on Power Systems, vol. 15, no. 2, pp. 535–540, 2000.

[6] L. Chen, Y. Taka, H. Okamoto, R. Tanabe and A. Ono, "Optimal operation solutions of power systems with transient stability constraints", IEEE Transactions on Circuits and Systems I: Fundamental Theory and Applications, vol. 48, no. 3, pp. 327–339, 2001.

[7] Yue Yuan, J. Kubokawa and H. Sasaki, "A solution of optimal power flow with multicontingency transient stability constraints", IEEE Transactions on Power Systems, vol. 18, no. 3, pp. 1094–1102, 2003.

[8] I. A. Calle, E. D. Castronuovo and P. Ledesma, "Optimal re-dispatch of an isolated system considering transient stability constraints", International Journal of Electrical Power & Energy Systems, vol. 44, no. 1, pp. 728–735, Jan. 2013.

[9] D. Layden and B. Jeyasurya, "Integrating security constraints in optimal power flow studies", in IEEE Power Engineering Society General Meeting,

2004., 2004, pp. 125–129 Vol.1.

[10] Y. Sun, Y. Xinlin and H. F. Wang, "Approach for optimal power flow with transient stability constraints", IEE Proceedings-Generation, Transmission and Distribution, vol. 151, no. 1, pp. 8–18, 2004.

[11] Y. Xia, K. W. Chan and M. Liu, "Direct nonlinear primal-dual interior-point method for transient stability constrained optimal power flow", IEE Proceedings-Generation, Transmission and Distribution, vol. 152, no. 1, pp. 11–16, 2005.

[12] Quanyuan Jiang and Zhiguang Huang, "An Enhanced Numerical Discretization Method for Transient Stability Constrained Optimal Power Flow", IEEE Transactions on Power Systems, vol. 25, no. 4, pp. 1790–1797, 2010.

[13] P. Kundur, Power System Stability and Control. McGraw-Hill Professional, 1994.

[14] A. Pizano-Martinez, C. R. Fuerte-Esquivel and D. Ruiz-Vega, "A New Practical Approach to Transient Stability-Constrained Optimal Power Flow", IEEE Transactions on Power Systems, vol. PP, no. 99, p. 1, 2011.

[15] D. Ruiz-Vega and M. Pavella, "A comprehensive approach to transient stability control. I. Near optimal preventive control", IEEE Transactions on Power Systems, vol. 18, no. 4, pp. 1446–1453, 2003.

[16] R. Zarate-Minano, T. Van Cutsem, F. Milano and A. J. Conejo, "Securing Transient Stability Using Time-Domain Simulations Within an Optimal Power Flow", IEEE Transactions on Power Systems, vol. 25, no. 1, pp. 243–253, 2010.

[17] H. Ahmadi, H. Ghasemi, A. M. Haddadi and H. Lesani, "Two approaches to transient stability-constrained optimal power flow", International Journal of Electrical Power & Energy Systems, vol. 47, pp. 181–192, May 2013.

[18] X. Tu, L. Dessaint and I. Kamwa, "A global approach to transient stability constrained optimal power flow using a machine detailed model", Canadian Journal of Electrical and Computer Engineering, vol. 36, no. 1, pp. 32–41, 2013.

[19] P. M. Anderson and A. A. Fouad, Power System Control and Stability, 2 edition. Piscataway, N.J.: Wiley-IEEE Press, 2002.

[20] M. Montilla-DJesus, D. Santos-Martin, S. Arnaltes and E. D. Castronuovo, "Optimal reactive power allocation in an offshore wind farms with LCC-HVdc link connection", Renewable Energy, vol. 40, no. 1, pp. 157–166, Apr. 2012.

[21] C.E. Grund, M.P. Bahrman, N. Balu, L. Bergstrom, W.F. Long, R.J. Newell, D. Osborne and R.V. Pohl, "Dynamic Performance Characteristics of North American HVDC Systems for Transient and Dynamic Stability Evaluations", IEEE Transactions on Power Apparatus and Systems, vol. PAS-100, no. 7, pp. 3356–3364, Jul. 1981.

[22] "IEEE Guide for Planning DC Links Terminating at AC Locations Having Low Short-Circuit Capacities", IEEE Std 1204-1997, p. i–, 1997.

[23] "GAMS. GAMS Development Corporation 1217 Potomac Street, NW Washington, DC 20007, USA." Available: http://www.gams.com/.

[24] "CONOPT. ARKI Consulting & Development, Bagsvaerd, Denmark." Available: http://www.conopt.com/.

[25] "OMIE - Operador del Mercado Ibérico de España". Available: http://www.omie.es.

[26] L. Hakim, J. Kubokawa, Y. Yuan, T. Mitani, Y. Zoka, N. Yorino, Y. Niwa, K. Shimomura and A. Takeuchi, "A Study on the Effect of Generation Shedding to Total Transfer Capability by Means of Transient Stability Constrained Optimal Power Flow", IEEE Transactions on Power Systems, vol. 24, no. 1, pp. 347 –355, Feb. 2009.

[27] Y. H. Li, W. P. Yuan, K. W. Chan and M. B. Liu, "Coordinated preventive control of transient stability with multi-contingency in power systems using trajectory sensitivities", International Journal of Electrical Power & Energy Systems, vol. 33, no. 1, pp. 147–153, Jan. 2011.

Chapter 6.

Transient Stability Constrained-Optimal Power Flow Including Multiple Contingencies and Two-Axes Representation of Synchronous Generators

Abstract— Transient Stability Constrained-Optimal Power Flow (TSC-OPF) is a nonlinear optimization problem that considers both static and dynamic constraints. It is used to perform economic dispatches while ensuring transient stability. TSC-OPF models that retain the dynamics of all the generators usually apply classic synchronous generator models, due to the high nonlinearity of the system dynamics and the large number of constraints. This paper proposes a TSC-OPF model that includes a transient synchronous generator *dq*-axes model, making it possible to represent electromagnetic transients in the rotor. The proposed optimization model includes also an excitation system and a turbine governor, and can perform multi contingency analysis. The model is solved using a non-heuristic Interior Point algorithm on GAMS. Results of the application to several standard test systems are shown, including the IEEE 118 Bus test case with 20 generators.

Contents

6.1 Introduction

Transient Stability Constrained-Optimal Power Flow (TSC-OPF) is an optimization problem that simultaneously includes static and dynamic constraints in the formulation. TSC-OPF has received growing interest in the last decade as a tool for preventing transient instability, because of its combination of economic objectives, steady-state power flow equations and dynamic simulations in a single model [1]-[3].

To be a useful tool in dynamic security assessment, a TSC-OPF model must represent the dynamics of the network with sufficient accuracy, comparable to that of the dynamic simulations routinely performed by Transmission System Operators. It must also be able to include multiple contingencies (MC) in a single model.

The high nonlinearity of electromechanical oscillations in power systems makes TSC-OPF models difficult to solve. Some approaches apply iterative

algorithms, running the dynamic simulation of a fault and correcting the generation dispatch at each iteration [4]-[6]. These techniques have been applied to relatively large power systems, but only in single contingency studies. Other approaches make use of Direct Methods to reduce the size and complexity of the optimization model [7]-[12]. These works rely on reduced dynamic models such as the Single-Machine Equivalent (SIME). They usually apply several iterations to refine the heuristic constraints, and are applied to single fault studies with few exceptions [13]. Although these methods can be used on power systems of virtually any size, they can be reportedly not well suited for multi-swing unstable conditions [1] and may be prone to sub-optimal solutions [3].

Both MC studies and multi-swing instabilities can be addressed if fault and post-fault states of different contingencies are included in the optimization model, and the dynamics of all synchronous machines are preserved. As the corresponding programming model has a very large dimension and requires heavy computation, most of the efforts in this field have been centered on reducing the problem scale and improving computation efficiency. In [14], for example, a transformation of the original formulation to the Euclidean space is applied to analyze the stability of the system without representing the trajectories of the variables. This makes it difficult to evaluate the behavior of the variables after the fault. Similar approaches are followed in [15] and [16], where Lyapunov functions are used.

The application of the trapezoidal rule to the differential equations, and the inclusion of the resulting equations in the optimization model, makes it possible to represent the trajectories of the variables. To solve the resulting large, nonlinear problem, the equations are successively linearized in [17]. In [18] and [19] a specially tailored Interior Point algorithm is applied. In [18], the steady-state and the dynamic constraints are separated and the resulting problem is solved using an iterative procedure. Authors of [19] incorporate MC into the analysis. In [20], the steady-state and the dynamic constraints are included in a single nonlinear model that is applied to small isolated systems and then solved using a conventional solver. All these studies use the classical dynamic model of

the synchronous generators, consisting of a voltage source of fixed magnitude behind an impedance, and are applied to small systems containing no more than 10 generators.

This work proposes a new TSC-OPF model that includes a transient *dq*-axes dynamic model of the synchronous generator. Compared to the classical model, the transient model makes it possible to represent the electromagnetic transients in the rotor, and represents a major improvement in dynamic model accuracy. The proposed model is solved using an Interior Point algorithm on GAMS (General Algebraic Modeling System), which is a high-level, well-trusted modelling system. The solver takes into account all equations and stability constraints, making it possible the inclusion of MC.

The proposed TSC-OPF model also includes a turbine governor and an excitation system. Together, the features included in the model represent a significant advance in the application of TSC-OPF studies to real power systems. Results are shown on a number of systems, including the IEEE 118 Bus Test System with 20 generators.

6.2 Power system representation in the optimization model

Transient stability analysis involves three periods: a) pre-fault; b) fault; and c) post-fault. These periods are explicitly included in the TSC-OPF model as equality and inequality constraints. The pre-fault stage, as in any conventional Optimal Power Flow (OPF), is represented by equality constraints that represent power flow equations [21] and inequality constraints that represent limits on production of power plants, voltage at buses and current through lines and transformers [22]. During the fault and post-fault periods, loads are represented as constant admittances and Kron reduction is applied to the admittance matrix, retaining only the internal nodes of the generators. This is a typical approach in TSC-OPF and reduces the computational effort considerably [19].

6.2.1 Transient power plant model

The transient model consists of a voltage source $E'_{di} + jE'_{qi}$ behind an impedance $r_{ai} + jx'_{di}$. Although the model is well known [23], [24], the equations are included here for future references within the paper:

$$dE'_{di} / dt = \left(-E'_{di} + \left(x_{qi} - x'_{qi}\right) I_{qi}\right) / T'_{q0i} \tag{6.1}$$

$$dE'_{qi} / dt = \left(-E'_{qi} - \left(x_{di} - x'_{di}\right) I_{di} + E_{fdi}\right) / T'_{d0i} \tag{6.2}$$

$$d\Delta\omega_i / dt = \left(P_{mi} - P_{ei} - D_i \Delta\omega_i\right) / 2H_i \tag{6.3}$$

$$d\delta_i / dt = \omega_0 \Delta\omega_i \tag{6.4}$$

$$P_{ei} = E'_{di} I_{di} + E'_{qi} I_{qi} \tag{6.5}$$

where sub-index i refers to the i^{th} generator. Variables in (6.1), (6.2) and (6.5) are referred to a dq reference frame fixed to the rotor, while grid variables are usually referred to a common synchronous rotating $\alpha\beta$ reference frame. Fig. 6.1 shows both reference frames, together with internal voltage E'_i and output current I_i. A rotation is needed to change from one reference frame to the other:

$$\left.\begin{aligned} E'_{\alpha i} &= E'_{di} \sin\delta_i + E'_{qi} \cos\delta_i \\ E'_{\beta i} &= E'_{qi} \sin\delta_i - E'_{di} \cos\delta_i \end{aligned}\right\} \tag{6.6}$$

and similarly,

$$\left.\begin{aligned} I_{di} &= I_{\alpha i} \sin\delta_i - I_{\beta i} \cos\delta_i \\ I_{qi} &= I_{\beta i} \sin\delta_i + I_{\alpha i} \cos\delta_i \end{aligned}\right\} \tag{6.7}$$

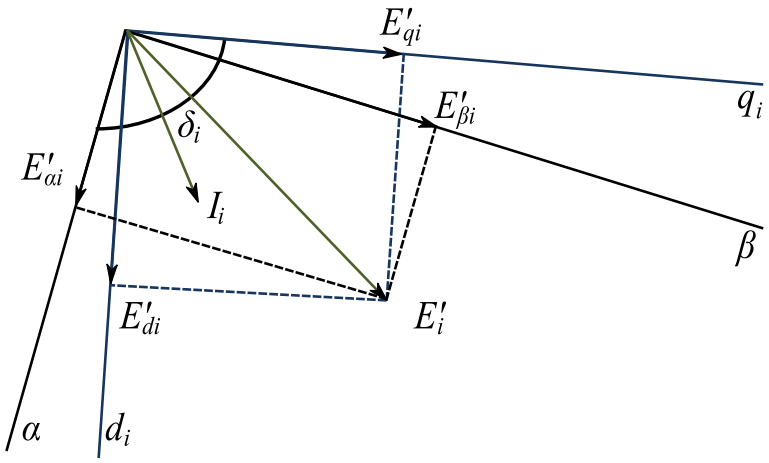

Fig. 6.1. Internal voltage, output current and reference frames for the i^{th} generator.

These rotations must be performed for every machine at every integration step because *dq* components are needed to solve machine models and *αβ* components are needed to solve grid equations. To avoid a large number of additional equality constraints in the optimization model, the formulation is modified to express all equations in terms of *dq* components [24]. The equation that relates internal voltages and output currents of all generators in the grid is:

$$I_{\alpha i} + jI_{\beta i} = \sum_{\forall j} \mathbf{Y}_{ij} \left(E'_{\alpha i} + jE'_{\beta i} \right) \tag{6.8}$$

where $\mathbf{Y}_{ij}$ is the *(i, j)* element of the reduced admittance matrix **Y**. If the admittance is expressed as $\mathbf{Y}_{ij} = Y_{ij}(\cos\theta_{ij} + j\sin\theta_{ij})$, then substituting (6.6) into (6.8), separating the real and imaginary parts and reordering the equations, yields:

$$\left.\begin{aligned} I_{\alpha i} &= \sum_{\forall j} Y_{ij} \left[E'_{dj} \sin\left(\delta_j + \theta_{ij}\right) + E'_{qj} \cos\left(\delta_j + \theta_{ij}\right) \right] \\ I_{\beta i} &= \sum_{\forall j} Y_{ij} \left[E'_{qj} \sin\left(\delta_j + \theta_{ij}\right) - E'_{dj} \cos\left(\delta_j + \theta_{ij}\right) \right] \end{aligned}\right\} \tag{6.9}$$

Replacing (6.9) in (6.7) and reordering:

$$\left.\begin{aligned} I_{di} &= \sum_{\forall j} Y_{ij} \left[E'_{dj} \cos\left(\delta_i - \delta_j - \theta_{ij}\right) + E'_{qj} \sin\left(\delta_i - \delta_j - \theta_{ij}\right) \right] \\ I_{qi} &= \sum_{\forall j} Y_{ij} \left[E'_{qj} \cos\left(\delta_i - \delta_j - \theta_{ij}\right) - E'_{dj} \sin\left(\delta_i - \delta_j - \theta_{ij}\right) \right] \end{aligned}\right\} \tag{6.10}$$

The equations in (6.10) calculate the *dq* components of the output current of the generators as a function of the *dq* components of the internal voltages. As a result, the TSC-OPF model is simplified because no *αβ* components appear, which allows the removal of all *αβ-dq* rotations and reduces the number of equality constraints in the optimization model.

In order to complete the model of the power plant, a voltage regulator and a turbine governor are included according to the following equations:

$$\frac{dE_{fdi}}{dt} = \frac{1}{T_{EXCi}}\left[-E_{fdi} + K_{EXCi}\left(V_{refi} - V_{termi}\right)\right] \tag{6.11}$$

$$\frac{d\Delta P_i}{dt} = -\frac{1}{T_{TGi}}\left(K_{TGi}\Delta\omega_i + \Delta P_i\right) \tag{6.12}$$

6.2.2 Transient stability constraint

Previous works on TSC-OPF implement the transient stability constraint as a limit on the angular deviations of the machine rotors. This constraint can be applied to small power systems, but it is not well suited for large ones because relatively large angular deviations may exist between parts of the system as a result of the pre-fault power flows, and not as a result of any instability. To solve this problem, the transient stability constraint is defined as a limit on the rotor speed deviation of every generator with respect to a common center of inertia (COI) speed deviation:

$$-\Delta\omega^{MAX} \le \Delta\omega_i^t - \Delta\omega_{COI}^t \le \Delta\omega^{MAX} \tag{6.13}$$

where the center of inertia speed deviation is calculated at each time step *t* as:

$$\Delta\omega_{COI}^t = \sum_{\forall i} H_i \Delta\omega_i^t \Big/ \sum_{\forall i} H_i \tag{6.14}$$

This ensures that the stability constraint is violated only if one or more machines lose synchronism with respect to the rest of the system. During the performed tests, a maximum deviation of approximately 0.01-0.05 p.u. has been found to be a good value to discriminate between stable and unstable cases.

6.3 Mathematical formulation

The proposed model is programmed on GAMS and solved using IPOPT [25], [26]. IPOPT is an open source software package for large-scale nonlinear optimization that implements an interior point line search filter method. This section provides the complete set of equations that constitute the model, in order to facilitate the replication of the results. The optimization model is:

$$\text{min.} \quad f(P_{Gi}) = \sum_{\forall i} \left(a_i P_{Gi}^2 + b_i P_{Gi} + c_i \right) \tag{6.15}$$

subject to:

$$\left.\begin{aligned} P_{Gi} - P_{Di} - V_i \sum_{\forall n} V_n Y_{in}^{Bus} \cos\left(\alpha_i - \alpha_n - \theta_{in}^{Bus}\right) = 0 \\ Q_{Gi} - Q_{Di} - V_i \sum_{\forall n} V_n Y_{in}^{Bus} \sin\left(\alpha_i - \alpha_n - \theta_{in}^{Bus}\right) = 0 \end{aligned}\right\} \tag{6.16}$$

$$\left.\begin{aligned} P_{Dl} + V_l \sum_{\forall n} V_n Y_{ln}^{Bus} \cos\left(\alpha_l - \alpha_n - \theta_{ln}^{Bus}\right) = 0 \\ Q_{Dl} + V_l \sum_{\forall n} V_n Y_{ln}^{Bus} \sin\left(\alpha_l - \alpha_n - \theta_{ln}^{Bus}\right) = 0 \end{aligned}\right\} \tag{6.17}$$

$$I_{mn}^2 - Y_{mn}^{Bus2} \left[\left(V_m \cos\alpha_m - V_n \cos\alpha_n\right)^2 + \left(V_m \sin\alpha_m - V_n \sin\alpha_n\right)^2 \right] = 0 \tag{6.18}$$

$$\left(I_{Gi} V_i\right)^2 - {P_{Gi}}^2 - {Q_{Gi}}^2 = 0 \tag{6.19}$$

$$\sin\varphi_i - Q_{Gi} / V_i I_{Gi} = 0 \tag{6.20}$$

$$\left.\begin{aligned} E_{di}'^0 - \left(x_{qi} - x_{qi}'\right) I_{Gi} \cos\left(\delta_i^0 - \alpha_i + \varphi_i\right) = 0 \\ E_{qi}'^0 + \left(x_{di} - x_{di}'\right) I_{Gi} \sin\left(\delta_i^0 - \alpha_i + \varphi_i\right) - E_{fdi}^0 = 0 \end{aligned}\right\} \tag{6.21}$$

$$\left.\begin{aligned} &V_i \sin\left(\delta_i^0 - \alpha_i\right) - E_{di}'^0 + \\ &I_{Gi}\left[r_{ai} \sin\left(\delta_i^0 - \alpha_i + \varphi_i\right) - x_{qi}' \cos\left(\delta_i^0 - \alpha_i + \varphi_i\right) \right] = 0 \\ &V_i \cos\left(\delta_i^0 - \alpha_i\right) - E_{qi}'^0 + \\ &I_{Gi}\left[r_{ai} \cos\left(\delta_i^0 - \alpha_i + \varphi_i\right) + x_{di}' \sin\left(\delta_i^0 - \alpha_i + \varphi_i\right) \right] = 0 \end{aligned}\right\} \tag{6.22}$$

$$\left.\begin{aligned} I_{di}^{0} - I_{Gi}\sin\left(\delta_i^0 - \alpha_i + \varphi_i\right) = 0 \\ I_{qi}^{0} - I_{Gi}\cos\left(\delta_i^0 - \alpha_i + \varphi_i\right) = 0 \end{aligned}\right\} \tag{6.23}$$

$$\left.\begin{aligned} K_{EXCi}\left(V_{refi} - V_{termi}^{0}\right) - E_{fdi}^{0} = 0 \\ \Delta P_i^0 = 0 \\ P_{ei}^{0} - P_{Gi} = 0 \\ \Delta\omega_i^0 = 0 \end{aligned}\right\} \tag{6.24}$$

$$E_{di}''^{t+1}\left(1 + \frac{\Delta t}{2}\frac{1}{T'_{q0i}}\right) - E_{di}''^{t}\left(1 - \frac{\Delta t}{2}\frac{1}{T'_{q0i}}\right) - \frac{\Delta t}{2}\frac{1}{T'_{q0i}}\left(x_{qi} - x'_{qi}\right)\left(I_{qi}^{t+1} + I_{qi}^{t}\right) = 0 \tag{6.25}$$

$$E_{qi}''^{t+1}\left(1 + \frac{\Delta t}{2}\frac{1}{T'_{d0i}}\right) - E_{qi}''^{t}\left(1 - \frac{\Delta t}{2}\frac{1}{T'_{d0i}}\right) - \frac{\Delta t}{2}\frac{1}{T'_{d0i}}\left[\left(E_{fdi}^{t+1} + E_{fdi}^{t}\right) - \left(x_{di} - x'_{di}\right)\left(I_{di}^{t+1} + I_{di}^{t}\right)\right] = 0 \tag{6.26}$$

$$\Delta\omega_i^{t+1}\left(1 + D_i\frac{\Delta t}{2}\frac{1}{2H_i}\right) - \Delta\omega_i^{t}\left(1 - D_i\frac{\Delta t}{2}\frac{1}{2H_i}\right) - \frac{\Delta t}{2}\frac{1}{2H_i}\left(2P_{mi} - P_{ei}^{t+1} - P_{ei}^{t}\right) = 0 \tag{6.27}$$

$$\delta_i^{t+1} - \delta_i^{t} - \frac{\Delta t}{2}\omega_0\left(\Delta\omega_i^{t+1} + \Delta\omega_i^{t}\right) = 0 \tag{6.28}$$

$$\Delta P_i^{t+1}\left(1 + \frac{\Delta t}{2}\frac{1}{T_{TGi}}\right) - \Delta P_i^{t}\left(1 - \frac{\Delta t}{2}\frac{1}{T_{TGi}}\right) + \frac{\Delta t}{2}\frac{K_{TGi}}{T_{TGi}}\left(\Delta\omega_i^{t+1} + \Delta\omega_i^{t}\right) = 0 \tag{6.29}$$

$$E_{fdi}^{t+1}\left(1 + \frac{\Delta t}{2}\frac{1}{T_{EXCi}}\right) - E_{fdi}^{t}\left(1 - \frac{\Delta t}{2}\frac{1}{T_{EXCi}}\right) - \frac{\Delta t}{2}\frac{K_{EXCi}}{T_{EXCi}}\left(2V_{refi} - V_{termi}^{t+1} - V_{termi}^{t}\right) = 0 \tag{6.30}$$

$$P_{ei}^{t} - E_{di}''^{t} I_{di}^{t} - E_{qi}''^{t} I_{qi}^{t} = 0 \tag{6.31}$$

$$\left.\begin{aligned} I_{di}^{t} - \sum_{\forall j} Y_{ij}\left(E_{d_j}''^{t}\cos\left(\delta_i^t - \delta_j^t - \theta_{ij}\right) + E_{qj}''^{t}\sin\left(\delta_i^t - \delta_j^t - \theta_{ij}\right)\right) = 0 \\ I_{qi}^{t} - \sum_{\forall j} Y_{ij}\left(E_{q_j}''^{t}\cos\left(\delta_i^t - \delta_j^t - \theta_{ij}\right) - E_{dj}''^{t}\sin\left(\delta_i^t - \delta_j^t - \theta_{ij}\right)\right) = 0 \end{aligned}\right\} \tag{6.32}$$

$$V_{termi}^{t2} - \left(E_{di}''^{t} + x_{di}' I_{qi}^{t}\right)^2 + \left(E_{qi}''^{t} - x_{di}' I_{di}^{t}\right)^2 = 0 \tag{6.33}$$

$$\Delta\omega_{COI}^{t} - \sum_{\forall i} H_i \Delta\omega_i^t \Big/ \sum_{\forall i} H_i = 0 \tag{6.34}$$

$$-\Delta\omega^{MAX} \le \Delta\omega_i^t - \Delta\omega_{COI}^t \le \Delta\omega^{MAX} \tag{6.35}$$

$$0 \le P_{Gi} \le P^{MAX}; 0 \le I_{Gi} \le I_{Gi}^{MAX} \tag{6.36}$$

$$V^{MIN} \le V_m \le V^{MAX}; -I_{mn}^{MAX} \le I_{mn} \le I_{mn}^{MAX}; E_{fd}^{MIN} \le E_{fdi}^{t} \le E_{fd}^{MAX} \tag{6.37}$$

$\forall i, j \in \{\mathcal{G}\}; \forall l \in \{\mathcal{L}\}; \forall m, n \in \{\mathcal{N}\}; \forall t \in \{\mathcal{T}\}$.

The objective function (6.15) is the cost of the energy calculated as a quadratic function, although other conventional cost functions can be used (to minimize deviation with respect to a schedule, minimize power losses, etc.).

Equations (6.16)-(6.24) correspond to the pre-fault stage. Equality constraints (6.16) and (6.17) represent the balance between input and output power in the generation and non-generation buses. Equation (6.18) calculates the current through the branches (lines and transformers). Equations (6.19)-(6.20) calculate the output current and power factor of the generators. Equations (6.21)-(6.24) calculate the initial conditions of the variables and the control outputs.

Equations (6.25)-(6.30) derive from the application of the trapezoidal rule to differential equations (6.1)-(6.4), (6.11) and (6.12). Equation (6.31) calculates the active power output of the generators at each time step. In (6.32), the current in the generators is calculated as a function of the reduced admittance matrix **Y** according to (6.10). Equation (6.33) calculates terminal voltage V_{term} that is an

input to the excitation system model. Equation (6.34) calculates the COI speed deviation, and (6.35) is the transient stability constraint, as explained in Section 6.2.

Equations (6.36) represent the capability limits of the generators. Equations (6.37) apply limits to bus voltages, branch currents and machine field voltages, respectively. The rest of the variables are also maintained within specified large limits, as is typical in constrained optimization.

MC analysis is provided replicating variables $\{E'_{di}, E'_{qi}, I_{di}, I_{qi}, \delta_i, \Delta\omega_i, \Delta\omega_{COI}, \Delta P_i, P_{ei}, E_{fdi}\}$ and (6.25)-(6.35) for each contingency, in the same optimization model. The solution of the TSC-OPF model applied to a MC study ensures that the system will remain in synchronism if any of the considered faults occurs.

6.4 Test cases

Section 6.5 shows the application of the proposed TSC-OPF model to two cases. The first case is the power system shown in Fig. 6.2 with 6 buses and 3 generators, which is described in [24]. A fault is applied at line 4-5, close to bus 4, and cleared after 300 ms by the removal of the affected line. The aim of this case is to show an example of the TSC-OPF where the small size of the system allows a clear view of the dynamics as calculated by the solver. The dynamic parameters of the power plants are shown in the Appendix.

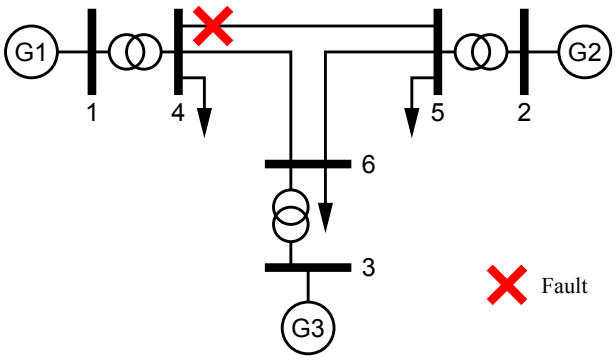

Fig. 6.2. 6 Bus Test System [24].

The second case is a version of the IEEE 118 Bus Test System containing 20 generators, as shown in Fig. 6.3. The size of this system is significantly larger than those of previously published TSC-OPF studies that retain the dynamics of all synchronous machines. The aim of this case is to show the application of the proposed model to a more realistic system and to evaluate the performance of the model depending on the size of the grid. Two different 3-phase short-circuits are analyzed: one at bus 19, cleared by the disconnection of line 19-34 after 300 ms, and another one at bus 49, cleared by the disconnection of line 49-54 after 300 ms. Buses 19 and 49 are selected for the following reasons: Firstly, they are connected to generators that operate at full load in the steady-state solution provided by the OPF and are therefore more prone to lose synchronism; and secondly, they are central buses with a relatively large number of incoming lines. IEEE 118 Bus System data can be found in [27].

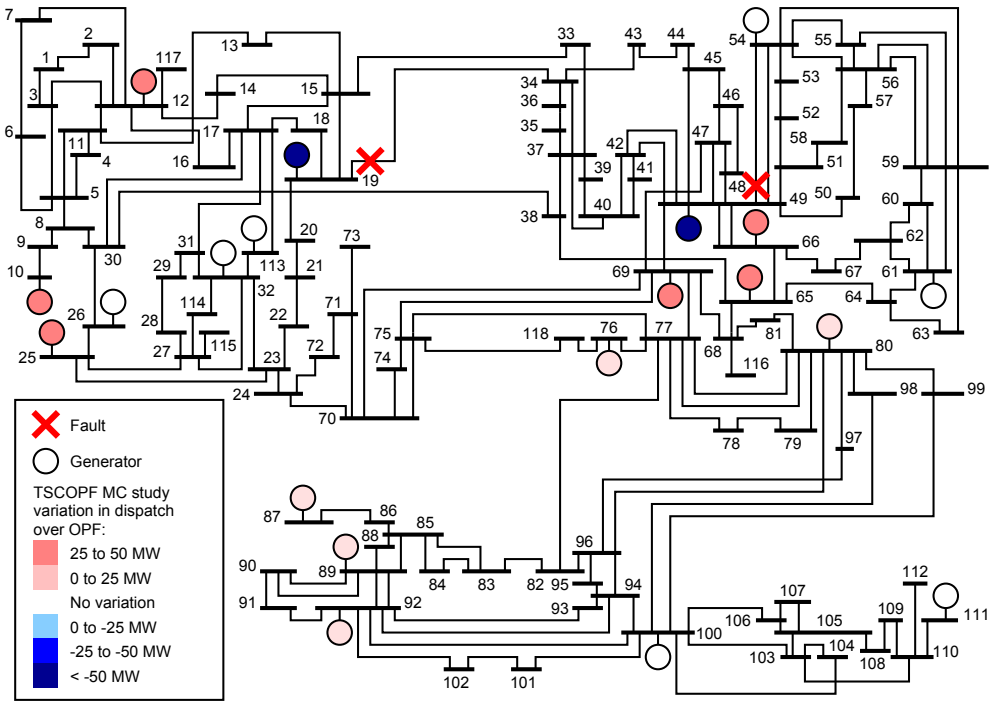

Fig. 6.3. IEEE 118 test power system.

The extension and complexity of the model formulated in Section 6.3 makes impractical its application to large systems and the systematic analysis of a set of faults. To overcome this problem, a program has been developed in the Python programming language that automatically builds the TSC-OPF model.

The program reads the power system data in standard PSS/E (Power System Simulator for Engineering) raw format and produces a file with the TSC-OPF model that can be fed into GAMS to be solved. Fig. 6.4 shows the relations between the input data and the different equations of the optimization model.

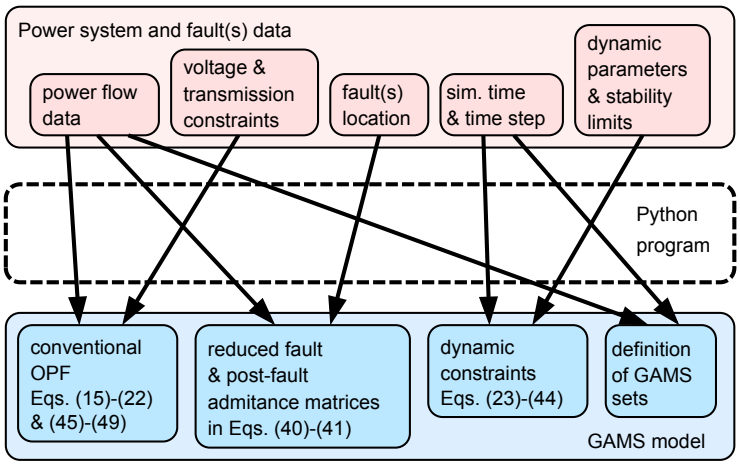

Fig. 6.4. Automatic building of the TSC-OPF model.

6.5 Results

6.5.1 Application to the 6 Bus System

The application of a conventional OPF to the 6 Bus system results in the dispatch shown in the first row of Table 6.1. However, when the specified fault is applied to this solution, generator 1 loses synchronism and the case is unstable.

TABLE 6.1: DISPATCH RESULTS FOR 6 BUS CASE; COST IN MONETARY UNITS (M.U.).

	P_1 [MW]	P_2 [MW]	P_3 [MW]	Cost [M.U.]
OPF	187.3	84.5	32.0	9260.4
TSC-OPF	158.0	81.3	63.6	9410.5

When the proposed TSC-OPF model is applied and the speed deviation of every generator is constrained to a band of 0.01 p.u. above or below the speed of the COI, the dispatch is modified to the values shown in the second row of Table 6.1. The analyzed time is 3 seconds and the time step is 0.02 s, which results in 150 time steps. Fig. 6.5 shows the evolution of some variables in the

TSC-OPF solution. It can be seen in Fig. 6.5 a) that the optimal solution is now stable because all the speeds remain within the limits. Fig. 6.5 b) shows the direct and quadrature components of the internal voltage, which are the state variables introduced by the transient synchronous generator model. Fig. 6.5 c) shows the variation in mechanical power provided by the turbine governors, as they respond to an increase in the system frequency as a result of the fault. Fig. 6.5 d) shows the variation in the field voltage provided by the excitation systems; it can be seen that the excitation systems increase the field voltage during the first 300 ms, responding to the voltage dip produced by the fault.

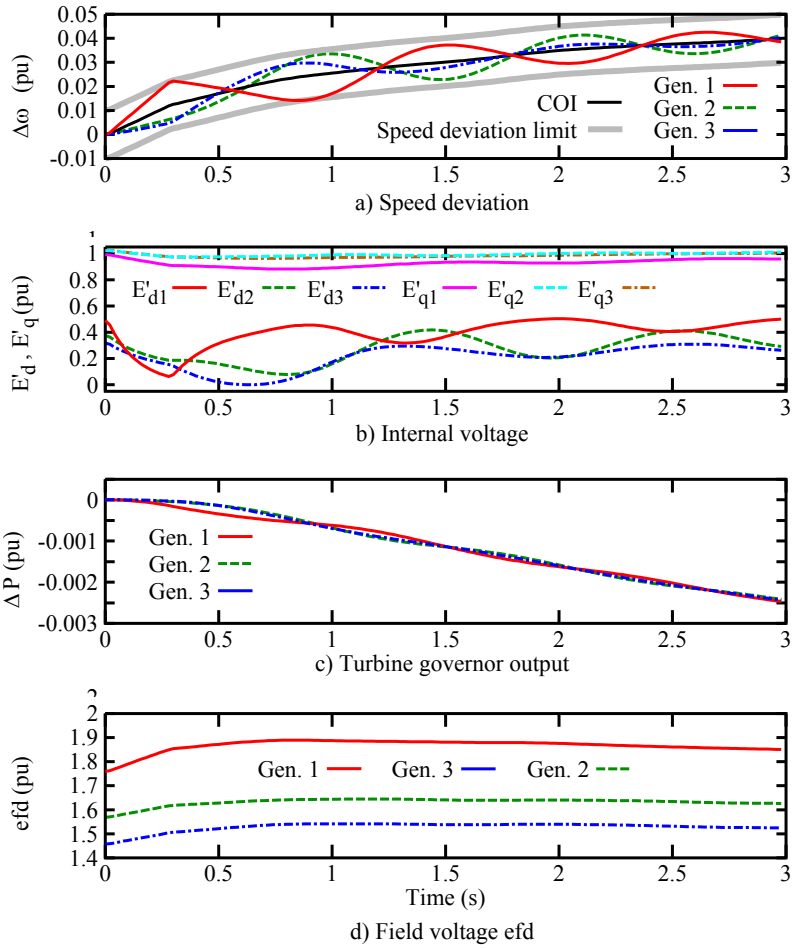

Fig. 6.5. Application of the TSC-OPF to the 6 Buses System.

6.5.2 Application to the IEEE 118 Bus system

The proposed TSC-OPF model is applied to the IEEE 118 Bus System and the two faults described in Section 6.4, with the speeds of the generators

constrained within a band of 0.02 p.u. above and below the speed of the COI. The results are shown for 1) conventional OPF, 2) fault at bus 19, 3) fault at bus 49 and 4) MC analysis with both faults.

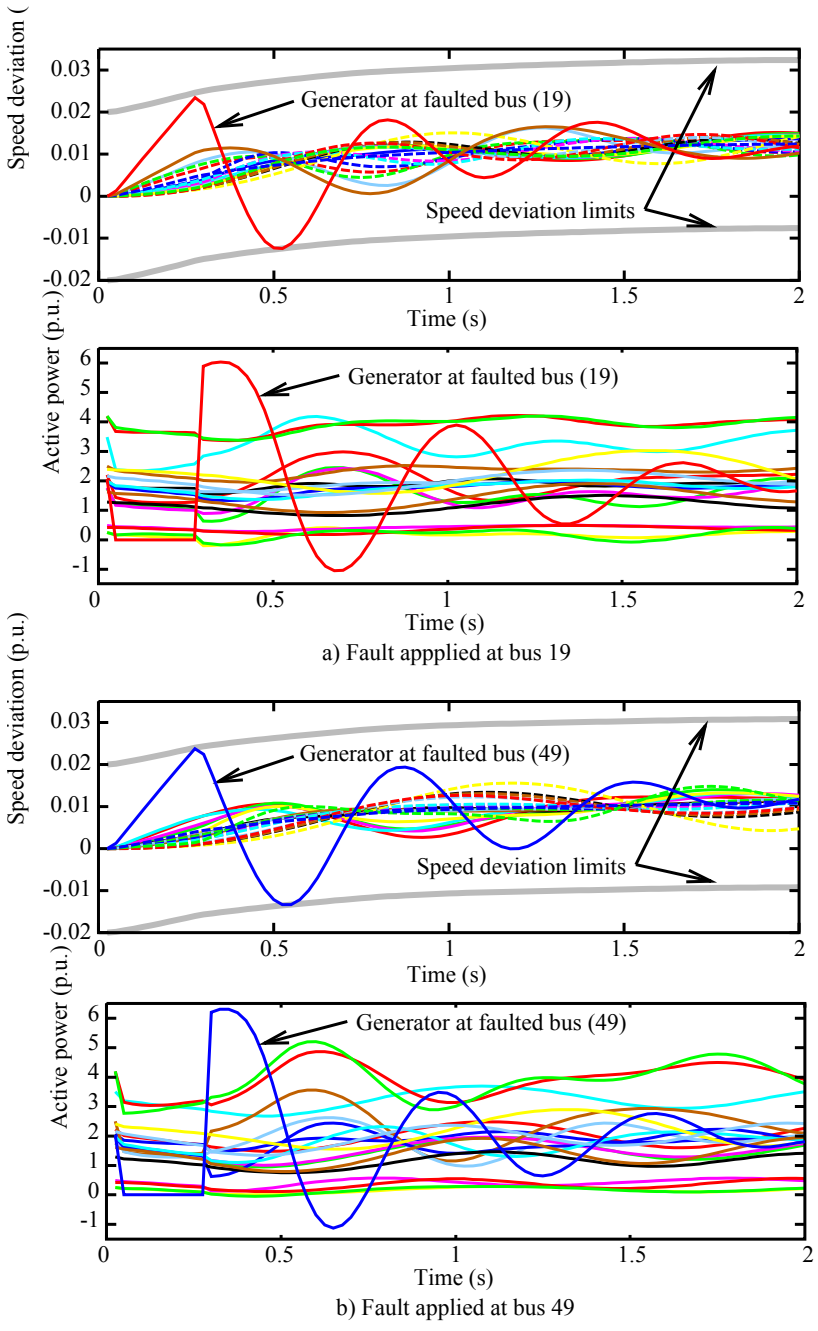

Fig. 6.6. Speed deviations and electrical power output.

Fig. 6.6 shows the speed deviations and active power productions provided by the optimal solution of the TSC-OPF when both faults are included in the MC model. The solution ensures that the system will remain stable if

either fault occurs. It can be seen that after any of the faults, the speed deviation is maintained inside the specified limits. The generator closest to the fault is the most affected by the fault in terms of speed deviation and active power oscillations. The effect on the dispatch can be observed in Fig. 6.3, in which the colors of the generators represent the variation in the dispatch provided by the TSC-OPF with respect to the dispatch of the OPF.

Fig. 6.7 shows the production of the different generators according to the optimal solutions of the OPF and TSC-OPF. It can be seen that the main effect of the TSC-OPF is the reduction of the production of the generators connected at the faulted buses. As these generators cannot maintain stability after the fault when operating at full load, the solution of the TSC-OPF reduces their production to comply with the stability constraints. When faults at buses 19 and 49 are studied separately, the optimal solution of the TSC-OPF results in a cost increase of 450.0 M.U. (Monetary Units) and 773.8 M.U. with respect to a conventional OPF. When both faults are simultaneously included in the MC model, the solution of the TSC-OPF results in a cost increase of 1294.7 M.U.

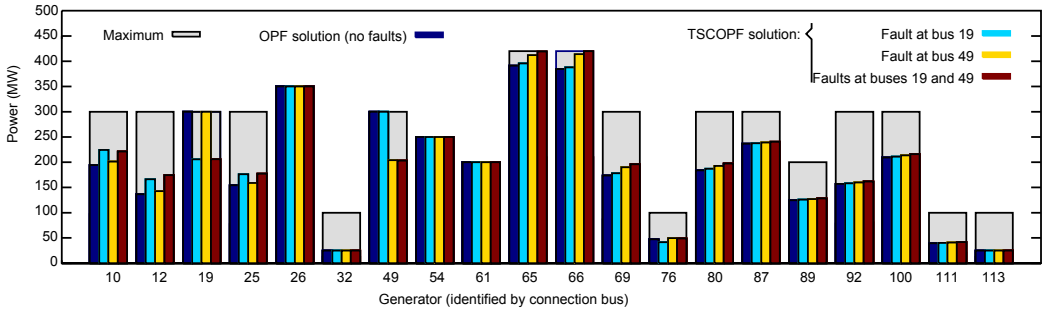

Fig. 6.7. Effect of the TSC-OPF on the dispatch of the IEEE 118 Bus System when both faults are included in the model.

6.5.3 Effect of the speed of the protections on the IEEE 118 system

An interesting application of the proposed model is as a tool to assess the selection of short-circuit protection devices. Faster protection can improve transient stability, but it is difficult to evaluate the economic impact of the investment that they require without using TSC-OPF. A systematic study of the effect of the protection speed has been performed, solving the TSC-OPF model with different fault clearing times from 200 ms to 300 ms.

The results are shown in Fig. 6.8. It can be seen that a reduction of the operating cost due to the transient constraints from 1294 to 536 M.U. (59 %) can be achieved if the fault clearing time is reduced from 300 ms to 220 ms at both faults. It also can be seen that the savings obtained by the reduction of the fault clearing time at bus 49 is 54 % larger than the savings obtained by the reduction at bus 19.

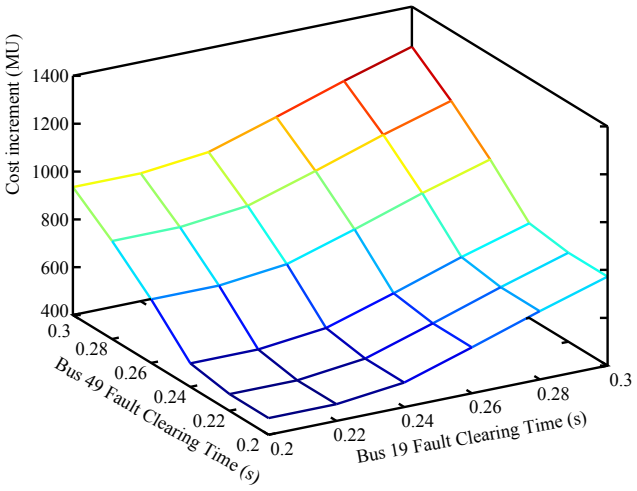

Fig. 6.8. Effect of the fault clearing time.

6.6 Performance of the solution of the TSC-OPF

The TSC-OPF model has been applied to other standard power systems in order to evaluate the computational cost of the solution. In addition to the 6 Bus and IEEE 118 Bus previously described, IEEE 30 Bus, IEEE 57 Bus and New England 39 Bus test cases were studied. Information about these systems can be found in [28] and [29].

The CPU time in the tables corresponds to the solution using GAMS and solver IPOPT on a computer with a single 2.5 GHz processor with a Linux operating system. The performance of the algorithm, when applied to one and two faults, is shown in Table 6.2 and Table 6.3, respectively. In all cases, no convergence problems are observed. To the knowledge of the authors, there are no similar reports of other TSC-OPF solutions to perform a consistent comparison.

It can be seen that the main factor affecting CPU time is the number of generators. The New England power system, for example, has more generators but fewer buses than the IEEE 57 Bus system, and the resulting CPU time is longer. The reason is that the size of the reduced admittance matrix **Y** is proportional to the square of the number of generators, and the number of dynamic constraints is proportional to the number of generators multiplied by the number of faults.

TABLE 6.2: SOLUTION OF THE TSC-OPF INCLUDING ONE FAULT.

	6 Bus	IEEE 30	IEEE 57	New Eng	IEEE 118
Size ($\mathcal{N}$ / $\mathcal{G}$)	6/3	30/6	57/7	39/10	118/20
N. variables	3127	4970	5829	8208	20436
N. constraints	3740	5955	6978	9849	24517
CPU time (s)	5	3	9	58	361

TABLE 6.3: SOLUTION OF THE TSC-OPF INCLUDING TWO FAULTS.

	6 Bus	IEEE 30	IEEE 57	New Eng	IEEE 118
Size ($\mathcal{N}$ / $\mathcal{G}$)	6/3	30/6	57/7	39/10	118/20
N. variables	6227	9850	11509	16288	40536
N. constraints	7449	11813	13799	19559	48677
CPU time (s)	21	10	34	133	530

6.7 Conclusions

A new formulation of a TSC-OPF model is proposed, including a two axes representation of the synchronous machine, an excitation system and a turbine governor. This is a major improvement with respect to the representation of synchronous generators by classical models, i.e., constant voltage sources behind impedances.

The proposed model, which is suitable for MC studies, is applied to several test cases and solved using GAMS and an interior-point solver. The size of IEEE 118 Bus System is significantly larger than those of most TSC-OPF studies retaining the dynamics of all synchronous generators. No convergence problems have been observed during the solution of the proposed model. A

practical application of the proposed model is given through the study of the economic impact of faster protection on the power dispatch. Given the nonlinear nature of the model it is not possible to guarantee that an obtained solution does not correspond to a local optimum of the problem. However, the consistency of the solutions over a wide range of cases suggests that global optima are obtained.

Although extensive work remains to be done in terms of system modelling in TSC-OPF (load modeling, non-conventional generation, magnetic saturation, etc.), it is expected that the proposed advances in model detail may help to increase the confidence of System Operators in TSC-OPF studies.

6.8 Nomenclature

Name	Variable	Units
E''^{t}_{d}, E''^{t}_{q}	Generator internal transient voltage components	p.u.
E^{t}_{fd}	Field voltage	p.u.
I^{t}_{d}, I^{t}_{q}	Generator output current components	p.u.
I_{G}	Magnitude of generator output current	p.u.
I_{mn}	Current between buses *m* and *n*	p.u.
P^{t}_{e}	Generator active power output	p.u.
P_{G}, Q_{G}	Generator active and reactive power output	p.u.
V	Bus voltage magnitude	p.u.
V^{t}_{term}	Voltage at the generator connection bus	p.u.
α	Bus voltage phase	rad.
δ^{t}	Generator angular deviation	rad.
ΔP^{t}	Turbine governor output	p.u.
$\Delta\omega^{t}_{COI}$	Center of inertia speed deviation	p.u.
$\Delta\omega^{t}$	Generator speed deviation	p.u.
φ	Bus angle between current and voltage	rad.

Name	Parameter	Units
D	Damping coefficient	p.u.
H	Inertia constant	s
K_{EXC}	Excitation system gain	p.u.
K_{TG}	Turbine governor gain	p.u.

r_a	Armature resistance	p.u.
P_D, Q_D	Active and reactive power demand	p.u.
T'_{d0}, T'_{q0}	Generator transient time constants	s
T_{EXC}	Excitation system time constant	s
T_{TG}	Turbine governor time constant	s
V_{ref}	Excitation system voltage reference	p.u.
x_d, x_q	*dq*-axes synchronous reactances	p.u.
$\mathbf{Y}$	Reduced admittance matrix	p.u.
$\mathbf{Y}^{bus}$	Bus admittance matrix	p.u.
Y_{ij}	Magnitude of the element (*i,j*) of $\mathbf{Y}$	p.u.
Y_{mn}^{Bus}	Magnitude of the element (*m,n*) of $\mathbf{Y}^{bus}$	p.u.
Δt	Time step	s
θ_{ij}	Phase of the element (*i,j*) of $\mathbf{Y}$	rad.
θ_{mn}^{Bus}	Phase of the element (*m,n*) of $\mathbf{Y}^{bus}$	rad.
ω_0	Frequency reference	rad./s

$()^{MAX}$ $()^{MIN}$ upper and lower limits of the variables.

Sets: $\mathcal{G}$, generators; $\mathcal{L}$, non-generator buses; $\mathcal{N}$, buses; $\mathcal{T}$, time steps.

6.9 Appendix

TABLE 6.4: DYNAMIC PARAMETERS OF GENERATORS AND CONTROLLERS.

H	D	r_a	x_d	x'_d	x_q	x'_q	T'_{d0}	T'_{q0}	K_{EXC}	T_{EXC}	K_{TG}	T_{TG}
3	2	0	1.5	0.3	1.5	0.3	6	0.5	100	1.0	50	1.0

Data in p.u. referred to the generator nominal power.

TABLE 6.5: IEEE 118 BUS SYSTEM GENERATOR COST DATA.

Gen.	Max P [MW]	a	b	c	Gen.	Max P [MW]	a	b	c
10	300	7	13	11	66	420	64	83	11
12	300	7	13	11	69	300	7	13	11
19	300	33	11	5	76	100	10	18	13
25	300	7	13	11	80	300	7	13	11
26	350	33	11	3	87	300	33	11	3
32	100	10	18	13	89	200	7	13	11
49	300	28	10	6	92	300	7	13	11
54	250	28	12	3	100	300	7	13	11
61	200	39	13	4	111	100	10	18	13
65	420	64	83	11	113	100	10	18	13

Where a is in M.U.; b in M.U./MW; c in 10^{-3}M.U./MW².

6.10 References

[1] Y. Xu, Z. Y. Dong, Z. Xu, R. Zhang and K. P. Wong, "Power system transient stability-constrained optimal power flow: A comprehensive review," in 2012 IEEE Power and Energy Society General Meeting, 2012, pp. 1–7.

[2] C. F. Moyano and E. Castronuovo, "Non-Linear Mathematical Programming Applied to Electric Power Systems Stability," in Optimization advances in electric power systems, Nova Science Publishers, Inc, 2009.

[3] F. Capitanescu, J. L. Martinez Ramos, P. Panciatici, D. Kirschen, A. Marano Marcolini, L. Platbrood and L. Wehenkel, "State-of-the-art, challenges and future trends in security constrained optimal power flow," Electric Power Systems Research, vol. 81, no. 8, pp. 1731–1741, Aug. 2011.

[4] M. La Scala, M. Trovato and C. Antonelli, "On-line dynamic preventive control: an algorithm for transient security dispatch," IEEE Transactions on Power Systems, vol. 13, no. 2, pp. 601–610, May 1998.

[5] E. De Tuglie, M. La Scala and P. Scarpellini, "Real-time preventive actions for the enhancement of voltage-degraded trajectories," IEEE Transactions on Power Systems, vol. 14, no. 2, pp. 561–568, May 1999.

[6] E. De Tuglie, M. Dicorato, M. La Scala and P. Scarpellini, "A corrective control for angle and voltage stability enhancement on the transient time-scale," IEEE Transactions on Power Systems, vol. 15, no. 4, pp. 1345–1353, Nov. 2000.

[7] R. Zarate-Minano, T. Van Cutsem, F. Milano and A. J. Conejo, "Securing Transient Stability Using Time-Domain Simulations Within an Optimal Power Flow," IEEE Transactions on Power Systems, vol. 25, no. 1, pp. 243–253, 2010.

[8] D. Ruiz-Vega and M. Pavella, "A comprehensive approach to transient stability control. I. Near optimal preventive control," IEEE Transactions on Power Systems, vol. 18, no. 4, pp. 1446–1453, 2003.

[9] A. Pizano-Martianez, C. R. Fuerte-Esquivel and D. Ruiz-Vega, "Global Transient Stability-Constrained Optimal Power Flow Using an OMIB Reference

Trajectory," IEEE Transactions on Power Systems, vol. 25, no. 1, pp. 392–403, 2010.

[10] S. W. Xia, B. Zhou, K. W. Chan and Z. Z. Guo, "An improved GSO method for discontinuous non-convex transient stability constrained optimal power flow with complex system model," International Journal of Electrical Power & Energy Systems, vol. 64, pp. 483–492, Jan. 2015.

[11] A. Pizano-Martínez, C. R. Fuerte-Esquivel, E. Zamora-Cárdenas and D. Ruiz-Vega, "Selective transient stability-constrained optimal power flow using a SIME and trajectory sensitivity unified analysis," Electric Power Systems Research, vol. 109, pp. 32–44, Apr. 2014.

[12] H. Ahmadi, H. Ghasemi, A. M. Haddadi and H. Lesani, "Two approaches to transient stability-constrained optimal power flow," International Journal of Electrical Power & Energy Systems, vol. 47, pp. 181–192, May 2013.

[13] S. Xia, K. W. Chan and Z. Guo, "A novel margin sensitivity based method for transient stability constrained optimal power flow," Electric Power Systems Research, vol. 108, pp. 93–102, Mar. 2014.

[14] L. Chen, Y. Taka, H. Okamoto, R. Tanabe and A. Ono, "Optimal operation solutions of power systems with transient stability constraints," IEEE Transactions on Circuits and Systems I: Fundamental Theory and Applications, vol. 48, no. 3, pp. 327–339, 2001.

[15] Y. Xia, K. W. Chan and M. Liu, "Direct nonlinear primal-dual interior-point method for transient stability constrained optimal power flow," IEE Proceedings-Generation, Transmission and Distribution, vol. 152, no. 1, pp. 11–16, 2005.

[16] Y. Sun, Y. Xinlin and H. F. Wang, "Approach for optimal power flow with transient stability constraints," IEE Proceedings-Generation, Transmission and Distribution, vol. 151, no. 1, pp. 8–18, 2004.

[17] D. Gan, R. J. Thomas and R. D. Zimmerman, "Stability-constrained optimal power flow," IEEE Transactions on Power Systems, vol. 15, no. 2, pp. 535–540, 2000.

[18] D. Layden and B. Jeyasurya, "Integrating security constraints in optimal power flow studies," in IEEE Power Engineering Society General Meeting, 2004., 2004, pp. 125–129 Vol.1.

[19] Yue Yuan, J. Kubokawa and H. Sasaki, "A solution of optimal power flow with multicontingency transient stability constraints," IEEE Transactions on Power Systems, vol. 18, no. 3, pp. 1094–1102, 2003.

[20] I. A. Calle, E. D. Castronuovo and P. Ledesma, "Optimal re-dispatch of an isolated system considering transient stability constraints," International Journal of Electrical Power & Energy Systems, vol. 44, no. 1, pp. 728–735, Jan. 2013.

[21] J. J. Grainger and W. D. Stevenson Jr., Power System Analysis, 1 edition. New York: McGraw-Hill Science/Engineering/Math, 1994.

[22] J. Zhu, Optimization of Power System Operation. John Wiley & Sons, 2009.

[23] P. Kundur, Power System Stability and Control. McGraw-Hill Professional, 1994.

[24] P. M. Anderson and A. A. Fouad, Power System Control and Stability, 2nd ed. Wiley-IEEE Press, 2002.

[25] "Computational Infrastructure for Operations Research COINOR, Interior Point Optimizer IPOPT." Available: https://projects.coin-or.org/Ipopt.

[26] A. Wächter, "An Interior Point Algorithm for Large-Scale Nonlinear Optimization with Applications in Process Engineering," PhD Thesis, Carnegie Mellon University, Pittsburgh, Pennsylvania, 2002.

[27] "IEEE 118 bus test case data," Electrical and Computer Engineering Department, Illinois Institute of Technology. Available: http://motor.ece.iit.edu/data/JEAS_IEEE118.doc.

[28] "Power Cases - Illinois Center for a Smarter Electric Grid (ICSEG)." Available: http://publish.illinois.edu/smartergrid/power-cases/.

[29] "TEST SYSTEM REPORT Development of a Comprehensive Power System Simulation Laboratory." Available: http://www.itee.uq.edu.au/pssl/drupal7_with_innTheme/?q=node/374.

Chapter 7.

Conclusions

In this chapter, the final conclusions and contributions obtained from the development of this work are presented. The list of publications derived from this research is included. Possible future works to enhance and to improve the topic of study are also presented here.

Contents

7.1 General conclusions

The OPF has been, and remains, an appropriate tool to define control corrective actions and optimal operational points, necessary to ensure an adequate level of safety in the operation of the power system. Furthermore, the demanding operating conditions of current electric power systems reveal a growing necessity of having OPF models that incorporate security constraints, with accuracy comparable to that of the simulations performed routinely by the system operators. The TSC-OPF seems to be the right tool to address this problem because it includes, in the same optimization problem, economic and security objectives and both static and dynamic technical constraints. The TSC-OPF also makes possible a more rational and smart utilization of the equipment, integrating different functionalities of the system towards the same objective: a more secure and economic operation of the system.

The TSC-OPF has had a great development in recent years, with different approaches to represent and to solve the transient stability problem. Most of these studies use simple models to represent the electrical system components (e.g., the classic model to represent the dynamics of the generators), and they do not include dynamic models of other devices (HVDC, FACTS, wind farms, etc.) to analyze their effects on the transient stability of the power system. Until now, efforts have been focused on reducing the computational burden of the problem, losing sight of the need for more realistic models, necessary to make the TSC-OPF a useful tool in dynamic security assessment.

Some final conclusions from the work developed in this thesis are:

- After application of the proposed TSC-OPF to the study systems, it has been observed that the computational burden of the algorithm does not pose a significant problem in the test systems used. Each case is solved in a few minutes using a medium-cost laptop. No convergence problems have been observed in the solution of the proposed model.

  Given the nonlinear nature of the model, it is not possible to guarantee that the obtained solutions do not correspond to a local optimum of the problem. However, the consistency of the solutions over a wide range of cases suggests that global optima are obtained. The proposed models are applied to several test cases and are solved with conventional tools, such as MATLAB and GAMS.

- In the case of optimal re-dispatch, results show that the proposed optimisation problem adequately calculates the optimal dispatch of the system for different load levels, in an efficient way. The innovative application of the proposed algorithm to several operation points and fault clearance times serves as an assessment tool for the transmission system operator, to estimate the cost of assuring the transient stability of the system.

- A novel study of the maximum loadability of a system with both steady-state and transient stability constraints, is performed. The model is applied to a variety of cases with a large number of restrictions (maximum and minimum capability of generators, maximum current through the lines, voltage limits and transient stability constraints, among others) whose impose different limits to the solution for each study case.

  The effect of the transient stability constraints on the maximum loadability is quantified by comparing the results with those calculated with a classical optimization problem, with only steady-state constraints. The results show that in many cases the transient

stability constraints significantly reduce the loadability margins. Moreover, the maximum loadability of a system is a function of the specified stability limit.

In the study, the effect of the rotor angle deviation limit on the maximum loadability is evaluated by performing the analyses over a wide range of angle limits. This study provides a useful resource to assist in the selection of the maximum angle limit for the operation.

- The inclusion of the model of a HVDC-LCC link in the formulation, with a control of power injection, makes possible the study of the economic impact of different dynamic behaviours of the link, facing the most demanding contingency.

  The HVDC interconnection shows a clear beneficial economic impact on the system, reducing the energy price with and without dynamic considerations. For the off-peak load case, to ensure the transient stability of the system results in an overprice of 25 %, for a delay of 0 ms and a power injection in form of step, when compared with the result of a conventional OPF. With a delay of 200 ms and increasing power injection in ramp (1.0 s), a reduction of 11.5 % is obtained. Therefore, optimizing the dynamic features of the equipments has a significant impact in real operation price, also justifying TSC-OPF studies.

- The inclusion of a transient *dq*-axes synchronous generator dynamic model, an excitation system and a turbine governor in a TSC-OPF model, retaining the dynamics trajectories of all generators, is a major improvement with respect to the representation of synchronous generators made hitherto, because makes it possible to represent the electromagnetic transients in the rotor and represents a major improvement in dynamic model accuracy. Also, the novel application of the *dq*-axes dynamic model in TSC-OPF studies opens the door to

more detailed representations of control loops in generators for further researches.

- An interesting and practical application of the proposed model is as a tool for the study of the economic impact of faster protections on the power dispatch.

  The results of the TSC-OPF show that the reduction of the clearance time in some protections from 300 to 250 ms reduces the generation cost in the Balearic power system (at off-peak load) by 8.84 %. When the study is applied to the IEEE 118 bus system, a reduction of 59 % in the operating cost due to the transient constraints can be achieved if the fault clearing time is reduced from 300 to 220 ms. Multiple contingencies have been included in this study.

7.2 Contributions

The main contributions of this thesis are summarized below:

1. New formulations of TSC-OPF, including steady-state and transient stability constraints, are developed. In the proposed models, the dynamic representation of the time-domain simulations for all the generators is discretized by the trapezoidal rule, and included into the OPF, which is solved as a whole.
2. The TSC-OPF is used to obtain the maximum loadability of a system, taking into account both steady-state and transient stability constraints. To the author's knowledge, this is the first application of TSC-OPF with this aiming.
3. The TSC-OPF is used to study the economic impact of faster protection on the power dispatch. This is a novelty on the field.
4. A two axes representation of the synchronous machine, an excitation system and a turbine governor are included in the TSC-OPF. This makes it possible to represent the electromagnetic transient in the rotor, which affect transient stability.

5. A mathematical simplification is developed, to avoid the numerous *αβ-dq* rotations when two axes models are used. This simplification reduces the number of equality constraints in the TSC-OPF model, without decreasing the accuracy of the models.
6. A representation of a real HVDC-LCC link is included in the formulation of the TSC-OPF. The HVDC-LCC model includes a power injection control, with different reconnection delays and recovery ramps.
7. The research results in four papers, submitted to relevant indexed journals in the area. Two of them are still in revision steps.

7.3 Publications

As a result of this research work, were obtained results that have been reported in various forums. The developed publications are listed below.

Indexed journals:

- I. A. Calle, E. D. Castronuovo and P. Ledesma, "Optimal re-dispatch of an isolated system considering transient stability constraints", *International Journal of Electrical Power & Energy Systems*, vol. 44, no. 1, pp. 728–735, Jan. 2013.
- I. A. Calle, E. D. Castronuovo and P. Ledesma, "Maximum loadability of an isolated system considering steady-state and dynamic constraints", *International Journal of Electrical Power & Energy Systems*, vol. 53, pp. 774–781, Dec. 2013.
- I. A. Calle, P. Ledesma and E. D. Castronuovo, "Application of Transient Stability Constrained-Optimal Power Flow to a Transmission System Including a HVDC-LCC Link", submitted.
- P. Ledesma, I. A. Calle and E. D. Castronuovo, "Transient Stability Constrained Optimal Power Flow Including Multiple Contingencies

and Two-Axes Representation of Synchronous Generators", submitted.

National conferences:

- I. A. Calle and E. D. Castronuovo, 'Optimal Power Flow with Transient Stability Constraints', in *MIXGENERA 2011 Options for the future*, University Carlos III de Madrid, Leganés, Madrid, Spain., 2011. ISBN: 978-84-614-9978-6. Available: http://electrica.uc3m.es/geste/Anteriores/MixGenera2011es.html

7.4 Future works

For possible future researches, it is suggested:

1. To apply efficient techniques, such as parallel computation, to reduce the computational burden of the proposed TSC-OPF problem.
2. To explore the effect of alternative objective functions in the optimization problem.
3. To perform analysis of real cases, in collaboration with the System Operators.
4. To analyze the implementation of other implicit integration methods.
5. To apply TSC-OPF to microgrids in island mode operation.